DATE ISSUED AUG 14 1975

ORNL-TM-4504

ORNL
MASTER COPY

Graphitization Kinetics of Fluidized-Bed Pyrolytic Carbons

Ronald Lee Beatty

OAK RIDGE NATIONAL LABORATORY
OPERATED BY UNION CARBIDE CORPORATION • FOR THE U.S. ATOMIC ENERGY COMMISSION

This report was prepared as an account of work sponsored by the United States Government. Neither the United States nor the Energy Research and Development Administration, nor any of their employees, nor any of their contractors, subcontractors, or their employees, makes any warranty, express or implied, or assumes any legal liability or responsibility for the accuracy, completeness or usefulness of any information, apparatus, product or process disclosed, or represents that its use would not infringe privately owned rights.

ORNL-TM-4504

Contract No. W-7405-eng-26

METALS AND CERAMICS DIVISION

GRAPHITIZATION KINETICS OF FLUIDIZED-BED PYROLYTIC CARBONS

Ronald Lee Beatty

A Dissertation
Presented to
the Graduate Council of
The University of Washington

In Partial Fulfillment
of the Requirements for the Degree
Doctor of Philosophy

AUGUST 1975

OAK RIDGE NATIONAL LABORATORY
Oak Ridge, Tennessee 37830
operated by
UNION CARBIDE CORPORATION
for the
U.S. ENERGY RESERRCH AND DEVELOPMENT ADMINISTRATION

ACKNOWLEDGMENTS

The author gratefully acknowledges his thesis advisor, Dr. D. B. Fischbach, for continued support and innumerable helpful discussions throughout the course of this work and manuscript preparation.

Special thanks are extended to the following:

J. L. Scott for continued support and encouragement;

C. B. Pollock for preparation of glassy carbon microspheres and other assistance;

H. Keating for preparation of flat-plate x-ray specimens;

B. C. Leslie, M. D. Allen, and H. R. Gaddis for metallography and photomicrographs;

W. J. Mason and E. V. Davis for microradiography;

J. L. Botts for hydrogen analyses; and

Patricia Viles for typing this manuscript.

Last but far from least, appreciation must be expressed to the author's wife Barbara for undaunting support without which this work could not have been done.

This research was sponsored by the U.S. Energy Research and Development Administration under contract with Union Carbide Corporation, and by NASA under grant to the University of Washington.

ABSTRACT

The graphitization behavior of twelve fluidized-bed pyrocarbons was studied as a function of heat-treatment time and temperature over the range 1350 to 3000°C to investigate the influence of initial microstructure on the graphitization process. The term "graphitization" implies development of the thermodynamically stable hexagonal graphite structure, but is defined more broadly in this work to include any thermally induced structural change whether or not any layer stacking order is attained. A broad range of chemically vapor-deposited microstructures was prepared by spanning a range of deposition conditions including temperatures from 1150 to 1900°C and a variety of propylene and methane concentrations. All-carbon substrates, including glassy carbon microspheres and thin graphite plates, were employed to avoid introduction of impurities which might catalyze graphitization of the coatings during deposition or subsequent heat treatment. Structural development of the deposits resulting from heat treatment was monitored by room temperature measurement of immersion density, mean diamagnetic susceptibility ($\overline{\chi}$), apparent crystallite diameter (L_a), and mean interlayer spacing ($\overline{d}$). L_a and $\overline{d}$ were determined by x-ray diffraction methods. The twelve carbons studied were found to span a wide range of graphitizabilities, primarily as a function of deposition temperature. Hydrocarbon concentration was of much less importance except for deposition at 1900°C. The most graphitizable carbons of the group were those deposited at

the lowest temperature (1150°C) from various propylene concentrations, and one deposited at 1900°C from very low methane concentration. Hydrogen content of the as-deposited carbons decreased with increasing temperature of deposition, and initial graphitization behavior of the low-temperature carbons appeared to be related to hydrogen content and evolution. Rates of change in the parameters measured varied widely throughout the range of heat-treatment times (HTt) and temperatures (HTT) for the different carbons and showed trends clearly distinguishing the more graphitizable or "soft" carbons from the essentially nongraphitizing or "hard" carbons. These trends were apparent from the earliest stages and produced a sort of "graphitization signature" relating to ultimate graphitizability. Effective activation energies (ΔH) determined by superposition analysis of density and $\overline{X}$ data showed a spectrum of values ranging from 160 to 350 kcal/mole. The ΔH values obtained for nongraphitizing carbons fell in the range 175 ± 15 kcal below 1950°C, 240 ± 35 kcal at 1950 to 2700°C, and 330 ± 20 kcal above 2700°C. For graphitizing carbons deposited at 1150°C, values near 245 kcal were obtained from $\overline{X}$ data for the HTT range 1350 to 1650°C, while densification data yielded values of about 160 kcal in the same range. This difference was related to a rate limitation imposed by hydrogen evolution on $\overline{X}$ increase but not on densification. Structural development of the 1150°C deposits proceeded in the 1650 to 1950°C range with activation energies obtained from $\overline{X}$ data near 200 kcal/mole; densification data for these deposits in this and higher ranges were not

analyzable. The $\overline{X}$ changes above 1950°C showed ΔH values near 240 kcal, but above 2400 to 2700°C changes were too small to allow analysis. However, the graphitizable 1900°C deposit showed a single-valued ΔH for $\overline{X}$ change of about 240 kcal from 2100 to 3000°C. Thus, the behaviors observed for graphitizable carbons above 2000°C, the area in which most graphitization kinetic studies have been concentrated, are consistent with the bulk of evidence reported in the literature. Different kinetic behaviors below 2000°C were shown due to different initial microstructures as well as to different parameters measured. The very high activation energies shown by the nongraphitizing carbons above 2700°C have not been previously reported except in one study of creep in glassy carbon.

TABLE OF CONTENTS

	Page
Chapter I. Introduction	1
Chapter II. Literature Review	9
X-Ray Diffraction Parameters	10
Diamagnetism of Carbon and Graphite	23
Kinetics of Graphitization	35
Chapter III. Experimental Procedure	41
Specimen Preparation	41
Heat Treatment	48
Magnetic Susceptibility	52
Density	57
X-Ray Diffraction	63
Hydrogen Analysis	68
Metallography	69
Microradiography	69
Chapter IV. Experimental Results	71
As-Deposited Properties	71
Microstructures (As-Deposited)	72
Effect of Heat Treatment	86
Effect of Heat Treatment on Properties	89
Density	89
X-Ray Parameters	112
Mean Diamagnetic Susceptibility	118
Activation Energy for Graphitization	123
Chapter V. Discussion	141
Chapter VI. Summary and Conclusions	165

Page

References 169

Appendix I 183

Appendix II 187

Appendix III 191

Appendix IV 197

Appendix V 201

LIST OF TABLES

		Page
Table I.	Deposition Conditions Employed in Preparing Pyrocarbon Specimens	47
Table II.	Deposition Conditions and As-Deposited Properties of Experimental Carbons	58
Table III.	Densification of Carbons Due to Heat Treatment for 18 min at 1800°C and 18 min at 3000°C	108

LIST OF FIGURES

		Page
Fig. 1.	Heat Treatment Furnace	49
Fig. 2.	Electromagnet and Recording Balance	53
Fig. 3.	Density Gradient Column	59
Fig. 4.	(a–l) Microstructures of Specimens As-Deposited and After Heat Treatment for 18 min at 3000°C	73
Fig. 5.	Radiographs (75×) of Coated Microspheres After Heat Treatment for 18 min at 3000°C. .	88
Fig. 6.	(a–l) Effect of Heat Treatment Temperature on Isochronal (18-min) Changes in: Density, ρ; Diamagnetic Susceptibility, $\overline{X}$; Crystallite Diameter, L_a; Interlayer Spacing, $\overline{d}$	90
Fig. 7.	Effect of Time on Isothermal Densification .	101
Fig. 8.	(a,b) Effect of Time on Isothermal Change in Mean Diamagnetic Susceptibility ($\overline{X}$) . . .	102
Fig. 9.	Effect of Heat Treatment Temperature on Isochronal (18-min) Densification	105
Fig. 10.	Effect of Initial Hydrogen Content on Densification After 18 min at 1800°C	110
Fig. 11.	Correlation of Crystallite Diameter (L_a) with Mean Interlayer Spacing ($\overline{d}$)	116
Fig. 12.	Effect of Heat Treatment Temperature on Isochronal (18-min) Change in Mean Diamagnetic Susceptibility ($\overline{X}$)	121

Page

Fig. 13. Correlation of Crystallite Diameter (L_a) with Mean Diamagnetic Susceptibility ($\bar{X}$) . . 122

Fig. 14. (a,b) Master Curves Formed by Superimposing Isothermal Diamagnetic Susceptibility ($\bar{X}$) Data 127

Fig. 15. (a,b) Master Curves Formed by Superimposing Isothermal Density (ρ) Data 130

Fig. 16. Arrhenius Plots of Relative Rate Constants Showing Activation Energies (kcal/mole) for Change in Mean Diamagnetic Susceptibility ($\bar{X}$) 133

Fig. 17. Arrhenius Plots of Relative Rate Constants Showing Activation Energies (kcal/mole) for Densification 134

Fig. 18. Effect of Temperature on Activation Energies for Densification and Diamagnetic Suceptibility ($\bar{X}$) Change for Twelve Carbons . . . 136

CHAPTER I

INTRODUCTION

The thermodynamically stable form of carbon, at ordinary pressures and temperatures, is generally held to be hexagonal graphite. This structure was proposed by Hull in 1917 [1] and verified by Bernal in 1924 [2]. It exhibits a regular ABABAB stacking of plane layers of carbon atoms which are arrayed in a fused benzene ring structure within the layers. The bonding within layers comprises a localized trigonal sp^2 covalent bond with the fourth electron forming a delocalized Π bond. The carbon to carbon distance within a layer is about 1.42 Å, indicative of a one-third double-bond character. While a layer structure of uniform bond lengths and angles (120°) is generally accepted, recent x-ray work by Ergun [3] provides some evidence that one-third of the bonds are shorter than the others (i.e., the layers have a quinoid structure). In either case the unit cell is hexagonal and the interlayer distance in perfect graphite is 3.354 Å with the interlayer interaction being of the relatively weak van der Waals type. This structure of tightly bound layers loosely held together clearly accounts for the characteristic anisotropy of graphitic materials.

Graphitization is usually defined as evolution of the hexagonal graphite structure due to heat treatment of non-equilibrium forms of carbon. These may include other allotropic forms such as diamond, chaoite, lonsdaleite, and rhombohedral graphite as well as disordered or so-called

amorphous carbons. The above forms are metastable at atmospheric pressure and will transform to hexagonal graphite if heated at ordinary pressures. Rhombohedral graphite comprises layers identical with those of hexagonal graphite but exhibits an ABCABC stacking sequence rather than the ABAB sequence characteristic of the equilibrium form. This appears to be a strain-induced stacking fault rather than a true allotropic form. At high temperature these faults anneal out and the rhombohedral form transforms to the hexagonal structure. The term "amorphous" as applied to carbons is misleading in that all common forms of carbon (other than diamond) possess the two-dimensional hexagonal layered structure to some extent. References to "amorphous" carbon usually refer to materials having very small, probably very imperfect aromatic layers randomly stacked.

Graphitization of poorly crystalline carbons should be considered in terms of a progressive improvement of an initially very imperfect structure. Heat treatment of such carbons effects removal of defects within and between layers and may allow growth of layers across crystallite boundaries as well as crystallite rearrangement. The rate and extent of structural improvement resulting from a particular thermal treatment is greatly dependent on the initial structure which is determined by the chemical and thermal history of the carbonization or pyrolysis process.

The present work is concerned with microstructural development including the disorder-order transformation of

nongraphitic pyrolytic carbons, and the term "graphitization" will be applied broadly to any thermally induced structural change whether or not any three-dimensional periodicity is evidenced. The subject pyrolytic carbons which are vapor deposited onto hot substrates by thermal decomposition of hydrocarbons in a fluidized bed are disordered carbons (i.e., totally lacking in triperiodicity, as deposited). They comprise structural units, commonly referred to as crystallites, of varying size, perfection, and relative orientation. Each crystallite is a cluster of small, imperfect aromatic layers or "molecules" stacked nearly parallel but not otherwise ordered with respect to one another. The layer stacks or crystallites which individually must be very anisotropic in all properties may have an overall random arrangement in the body or they may exhibit some degree of preferred orientation depending on the deposition conditions.

Essentially all properties, mechanical, thermal, electronic, or x-ray structure of such materials are highly structure sensitive. Properties depend on the size, perfection, and relative orientation of the individual crystallites. This structure sensitivity allows nearly any property to be used for monitoring structural development or "graphitization," though graphitization of disordered carbons is an extremely complex process and is not well understood at present. For example, some carbons are "soft" or easily graphitized, while others are "hard" or cannot be graphitized by thermal treatment alone (i.e., without use of catalysts). However, even hard

carbons which probably owe their nongraphitizability to an extensive system of cross-link or nontrigonal bonds developed within and between crystallites early in the carbonization process undergo considerable structural change at high temperatures. While these changes may not include development of layer stacking, they are nevertheless manifested in measurable property changes. Measurement of the rate of change of a structure-sensitive property as a function of temperature thus provides information on the kinetic nature of the "graphitization" of hard as well as soft carbons, even when knowledge of the detailed mechanisms involved is very incomplete.

Kinetic analysis is a valuable tool in seeking fundamental understanding of the graphitization process as well as a useful source of practicable property change rate information. While kinetic data do not explicitly elucidate detailed mechanisms, they can be related by inference to single or multiple mechanisms on the basis of theoretical energy considerations.

The treatment of graphitization as a thermally activated, kinetic process has received attention only recently. Characteristics of commercial graphites have traditionally been specified in terms of heat-treatment temperatures without particular concern for treatment times, and sometimes without much attention to the actual structures involved. The kinetic nature of graphitization is now well established, though specific mechanisms involved are not well understood.

Literature on the subject contains a great diversity of information on graphitization rates, activation energies, and conclusions about the processes involved. These differences are the result of many factors including different types of carbons studied, varying amounts of impurities in the starting materials, various heat-treatment ranges employed, and the use of different kinetic parameters and methods of analysis.

The present study was undertaken to explore the effects on graphitization behavior of a broad range of initial microstructures and a wide range of heat-treatment temperatures. Fluidized-bed deposition was selected as the method of preparing experimental materials because of the extensive range of processing conditions and resulting microstructures possible [4]. When carbon substrates are employed, the vapor deposition process gives no significant impurities other than hydrogen. The density, preferred orientation, and crystallite size of vapor deposited carbons can be varied by appropriately regulating the deposition temperature and concentration of reactant hydrocarbon. Further it has been shown [4] that the range of microstructures which can be obtained by fluidized-bed deposition includes carbon of varying degrees of graphitizability.

Kinetic parameters used in the present work to monitor graphitization were diamagnetic susceptibility and densification. These parameters were chosen for their respective sensitivities to changes in electronic band structure and microstructural compactness and for the relatively large

changes which can be effected in these properties. Use of two parameters having different structure sensitivities provides some check on the rate limiting involvement of mechanisms which may contribute more to changes in one property than the other. Both diamagnetic susceptibility and density are multiply structure dependent, but this does not impede their use as kinetic parameters. For example, $\bar{\chi}$ increases with increasing layer size and perfection, but decreases with increasing layer order (decreased $\bar{d}$). As long as $\bar{\chi}$ is changing, however, kinetic analysis of the data will yield an effective activation energy characteristic of the mechanism or mechanisms involved. Densification may be effected by removal of intralayer defects, improvement of layer stacking order, or removal of intercrystallite porosity by crystallite growth or rearrangement, but the effective activation energy is still characteristic of the mechanism(s) responsible. Detailed interpretation of the microstructural changes occurring is aided by x-ray diffraction measurements of crystallite sizes and interlayer spacings.

In addition to the available variety of fluidized-bed pyrocarbons which makes them ideal for kinetic study, these deposits are representative of materials having considerable technological importance. The exploitation of this class of carbons for fuel containment in high-temperature gas-cooled nuclear reactors [5,6] and for human prosthetic applications [7,8] gives added interest to understanding their behavior. Pyrocarbons of similar characteristics deposited

on stationary substrates also find application as matrix-impregnant material in carbon-carbon composites.

CHAPTER II

LITERATURE REVIEW

The graphitization process has been reviewed extensively by Maire and Méring [9], by Pacault [10], and by Fischbach [11] in survey papers to which the interested reader may refer. These papers provide abundant evidence that graphitization is a thermally activated kinetic process, the details of which have received attention only in recent years. It is further shown that graphitization of disordered carbons entails a gradual structural improvement fundamentally unlike the recrystallization of metals. Fischbach [11] points out that the term "graphitization" has been widely misused in the carbon products industry to imply that a carbon material is "graphite" simply by virtue of heat treatment to a specified temperature (usually above 2500°C) without regard to the structure actually developed. Characterizing a carbon material as graphite on the basis of heat-treatment temperature alone implies incorrectly that time at temperature makes no difference in the structure evolved and all carbons heated to the same temperature develop the same structure. Franklin [12] showed clearly in 1950 that the latter implication is untrue; carbons can be broadly classified as graphitizing or non-graphitizing, soft or hard, depending on the extent to which they develop the graphite structure during heat treatment. Because of strong structure sensitivity the graphitization process can be followed experimentally by measuring essentially

any mechanical, dimensional, thermal, optical, chemical, electronic, or magnetic property as a function of heat-treatment time (HTt) and temperature (HTT).

X-Ray Diffraction Parameters

The most widely used tools for studying graphitization include x-ray diffraction techniques to determine interlayer spacings ($\bar{d}$), crystallite heights (L_c), and diameters (L_a), preferred orientations, and other characteristics. X-ray techniques are commonly employed as the primary experimental tool and are nearly always used to provide supplementary structural information to other primary methods. Extensive reviews of x-ray studies of carbon have been conducted by Ergun [13] and by Ruland [14].

Nearly all x-ray diffraction studies of the graphitization process have been conducted after the specimen is cooled to room temperature for experimental convenience. This, however, raises the question of whether room temperature measurements are truly representative of microstructural changes occurring at high temperatures. To examine the effects of internal stresses due to anisotropic crystallite shrinkage during cooling, Fitzer and Weisenburger [15–17] have recently studied the graphitization of cokes by *in situ* x-ray measurements at temperatures up to 2500°C. They have concluded that rapid cooling from the treatment temperature to room temperature does not affect basic diffraction profile shapes. The only differences observed in the high-temperature

patterns were reduced intensity and slightly increased half maximum breadths due to diffuse scattering.

The application of x-ray diffraction methods to carbon materials goes back to Bragg's [18] work in determining the structure of diamond and to Bernal's [2] work on the graphite structure. However, most carbons of practical interest do not possess these ideal crystallographic structures, and understanding of the nature and diversity of disordered carbons was greatly advanced by Warren's [19] work with random layer lattices and Franklin's [12] observations of variations in graphitizabilities.

Warren [20] established the existence of graphite-like layers in carbon black in 1934. While Warren was not the first to apply x-ray diffraction methods to carbon blacks, his work did much to dispel the concept of this class of materials as amorphous and/or very finely crystalline graphite. Warren subsequently [19] developed the diffraction theory for random layer lattices and Biscoe and Warren [21] coined the term "turbostratic" as a name for disordered carbons. Since the x-ray patterns consisted of crystalline reflections (001) and two-dimensional lattice reflections (hk), the structure was explained as comprising true graphite layers arranged roughly parallel and equidistant but randomly stacked.

Biscoe and Warren analyzed the dimensions of the "parallel layer groups" or "crystallites" by use of the Scherrer equation. The dimension in the plane of the layers or the crystallite diameter thus becomes

$$L_a = 1.84\lambda/\beta \cos\theta ,$$

determined from the widths of the (10) and (11) reflections and the layer stack or crystallite height becomes

$$L_c = 0.89\lambda/\beta \cos\theta ,$$

from the width of the (002) and (004), when present, reflections. In these expressions λ is the wavelength (Å), θ is the Bragg angle, and β is the corrected width (radians) at half maximum intensity. Warren [19] had shown earlier that the peak of a two-dimensional lattice reflection (hk) is displaced toward larger angle from the position of the crystalline reflection (hk0) by an amount $\Delta(\sin\theta) = 0.16\lambda/L_a$. Failure to take this shift into account when calculating interatomic distances from two-dimensional reflections would lead to false conclusions about lattice contractions. By employing this correction Biscoe and Warren concluded that there was no appreciable difference in the a-axis dimensions of the lattice in carbon black and graphite.

In determining average interlayer spacings in carbon blacks Biscoe and Warren found that values obtained from the (002) peaks were slightly larger than values obtained from the (004) peaks. The discrepancy was attributed to the influence of small angle scattering on the (002) peaks and they concluded that the (004) should be used where possible. Franklin [22] later showed that in nongraphitic carbons the (002) takes the form of a diffuse band with a maximum displaced

toward smaller angles relative to the (002) line of graphite and developed a correction procedure. Franklin further explained the observed scattering intensities in diffuse diagrams as due to the presence of a disorganized phase which makes only a gas-like contribution to the scattering and the existence of a large number of single misaligned layers. Stevens, in determining interlayer spacings for low-temperature pyrolytic carbons [23], developed a computerized treatment to apply Lorentz and polarization factor corrections to the (002) diffraction profile. He found the uncorrected peak displacement to be a function of crystallite size, with a shift to lower angle as large as 0.2° θ for L_c about 20 Å.

Franklin [12] investigated the structure of carbons of different origin treated at temperatures between 1000 and 3000°C and found that most carbons could be characterized as belonging to one of two distinct classes, graphitizing or nongraphitizing. The differences in structure, which were apparent from the earliest stages of carbonization, were attributed to the formation at low temperature of a strong system of cross-linking between crystallites in the nongraphitizing carbons. Franklin noted that the non-graphitizing carbons were characterized by low density due to a system of fine-structure porosity of up to 50% of the carbon volume. By low-angle x-ray scattering measurements she showed the size of these fine pores to be on the order of a few tens of angstroms, the same order of size as the crystallites.

More recent x-ray small-angle scattering work has been directed at analyzing the pore structure of nongraphitizable carbons. Rothwell [24], in analyzing glassy carbons, found initially a large range of small voids which grew and coalesced with heat treatment to attain a fairly uniform spherical size near 50 Å after heating at 3000°C. Fitzer, Schaefer, and Yamada [25] found pore diameters of 25 Å in glassy carbons heated to 500 or 1200°C. The diameter increased to 35 Å after heating to 3000°C. Perret and Ruland [26] found a micropore system with diameters in the 10 to 30 Å range for a polyacrylonitrile-derived carbon. The size of these pores increased linearly with heat-treatment temperature from 2000 to 3000°C and the volume fraction of micropores varied from 0.17 to 0.25. It was concluded that the pores were irregular polyhedra bounded by graphitic layer planes. In a further analysis of the micropore system of glassy carbons, Perret and Ruland [27] concluded that the pore shape is needle-like with sharp edges and that the pore structure stems from a felt-like entanglement of stacks of ribbon-shaped carbon layers.

Franklin [12] considered a rigid intercrystallite cross-linking system in nongraphitizing carbons as responsible for forming the fine pores and for preserving them on heating to high temperatures. The cross-link system was pictured as holding neighboring crystallites apart and in random orientation with respect to each other, thus hindering the coalescence which would be a prerequisite for graphitization.

She concluded that in the graphitizing carbons the cross-linking is much weaker, the structure is more compact, and that neighboring crystallites exhibit a strong tendency to lie in nearly parallel orientation. She further concluded that crystallite growth occurs by movement of entire layers or groups of layers thereby explaining the enchancement of growth by the preorientation existing in graphitizable carbons and the impeding of growth by the cross-linking between crystallites and the random crystallite orientation in nongraphitizable carbons.

Franklin observed that the formation of a dense, graphitizing carbon is favored by the presence of an excess of hydrogen in the starting material. Higher hydrogen content of the pyrolysis products during the early stages of carbonization would provide greater mobility for the continual destruction of cross-links, thereby preventing the carbon from "setting" at low temperatures. On the other hand a deficiency of hydrogen, or the presence of oxygen, favors the formation of a highly cross-linked, nongraphitizing structure.

From work on the structure of graphitic carbons Franklin [28] proposed a method of determining the degree of graphitization of soft carbons from the relation

$$\bar{d} = 3.440 - 0.086\ (1 - p^2)\ ,$$

where $\bar{d}$ is the mean interlayer spacing and p is the fraction of disordered layers. This relation was subsequently modified by Bacon [29] to the form

$$\bar{d} = 3.440 - 0.086\ (1 - p) - 0.064\ p(1 - p)\ ,$$

to give better agreement with experiment when p is small (i.e., when the material is nearly completely graphitized). The basis for this analysis is the concept of a discrete and well defined $\bar{d}$ value (3.44 Å) characteristic of completely disordered (turbostratic) stacking of perfect aromatic layers in graphitizable carbons. A further premise of the degree of graphitization analysis is that $\bar{d}$ is not a true measure of a uniform interlayer spacing but rather a mean value indicative of the probability p that a random disorientation occurs between any two given neighboring layers. Achievement of ordered stacking is assumed to occur in a discontinuous manner (i.e., entire layers or groups of layers shift so that the interlayer spacing attains the graphite value of 3.354 Å at each orientation leaving the 3.44 Å spacing at each disorientation). A random distribution of oriented and disoriented layers would thus imply a random distribution of these two spacings and would produce an apparent value equal to the mean spacing. There would then be a linear relationship between $\bar{d}$ and p. Since the linear relationship was not observed experimentally, Franklin [28] accounted for the deviation from linearity by including intermediate $\bar{d}$ values for first and second neighbor layers to oriented groups.

Houska and Warren [30] applied the method of Warren and Averbach [31,32] for separating strain broadening from small-particle size broadening to a study of carbon black

graphitization. They found that the (001) peaks must be corrected for the distortion broadening resulting from the distribution of 3.354 and 3.44 Å spacings to obtain what they considered to be a true stacking height. Further work in separating distortion and size broadening was done by Warren [33], Guentert [34], and Bowman [35].

Bacon [36,37] noted that comparison of spacings deduced from (001) and (hkl) lines could be used for direct determination of the different spacings between oriented and disoriented layers. Bowman [35], in studying ordering and crystallite growth during graphitization of coke, concluded that high-temperature annealing produces a systematic growth in crystallite height, but that growth in the a-axis direction is a function of crystallite size and indicative of a nucleation process. He further concluded that the individual layers do not contain appreciable distortion and that the high-temperature annealing removes the interlayer strain without causing the growth of crystals by actual mass transfer.

While early work on the structure of disordered carbons was based largely on carbon blacks and ungraphitized cokes, the development of pyrolytic carbons (often incorrectly termed pyrolytic graphites in the literature) since about 1950 has provided a new and interesting class of carbons for theoretical and experimental analysis. Pyrolytic carbon (PC) was actually produced as early as 1880 [27] by thermally decomposing a carbonaceous gas on a hot surface, but it was not until the work of Brown and Watt [28–30] and Brown, Clark,

and Eastabrook [31] in the 1950's that details of PC structures became known. Their x-ray work showed PC to have high preferred orientation, but to exhibit a total lack of stacking order. Extensive and detailed x-ray studies of PC carried out by Guentert [43] and by Guentert and Cvikevich [44] confirmed these observations. Guentert analyzed PC's deposited under various conditions at temperatures ranging from 1700 to 2500°C for preferred orientation, layer order, and crystallite sizes and strains. He found high preferred orientations, with ratios of basal planes parallel:perpendicular to the deposition plane increasing from about 10:1 for 1700°C deposits to values as high as 10^4:1 for deposits formed above 1900°C. Typical crystallite dimensions were $\bar{L}_c$ = 200 Å and $\bar{L}_a$ = 260 Å with layer order being nearly random over the entire range of deposition temperatures, and c-direction strains decreasing only slightly with increasing deposition temperature. Guentert and Cvikevich [44] studied the effects of heat treatment on similar materials and noted that the degree of graphitization with increasing HTT (heat-treatment temperature) could be readily followed by the development of modulations in the (hk) reflections and by the decrease in interlayer spacing. Heat treatment also effected large increases in preferred orientation and increases in $\bar{L}_c$ and $\bar{L}_a$ to 830 and 1000 Å, respectively. It should be noted that the pyrolytic carbons discussed here were all deposited on stationary substrates as distinguished from PC deposited in fluidized beds, the subject material of the present work.

The discussion of disordered carbon structures thus far has been based primarily on the turbostratic model of Biscoe and Warren [21]. While this model has undoubtedly been of great value in illuminating the characteristics of disordered carbons and is still the most widely held concept of these materials, its basic premise of nearly perfect layers must be regarded as an oversimplification.

An alternative model for the structure of disordered carbons has been developed by Méring and Maire [45,9]. They propose imperfect layers, or more specifically, layers having interstitial carbon atoms attached to one or both sides as the basis for the observed characteristics of disordered carbons. They have accumulated considerable evidence that only in this way can certain chemical affinities of the layers be explained. However, this model, which attempts to explain all the details of disordered carbon structures on the basis of a single specific layer defect, is also likely to be an oversimplification. Undoubtedly the greatest contribution of this model has been in calling attention to the importance of layer defects and thus to the inadequacy of the turbostratic or perfect-layer model which had previously been rather generally accepted.

A more generalized approach to x-ray analysis of disordered carbons has been taken by Ruland [14,46–49]. He has emphasized the importance of many types of layer defects, and thereby the inadequacy of the turbostratic model. The probably important defects include interstitial atoms or

layers, vacancies or holes in layers, layer curvature, dislocations, cross-link bonding, etc. Ruland has characterized carbon structures on the basis of four parameters: the rms displacement of adjacent layers parallel to the layers (σ_{12}); the rms displacement of adjacent layers normal to the layers (σ_3); the mean interlayer spacing ($\bar{a}_3$, identical with $\bar{d}$); and the fraction of rhombohedral stacking sequences (α). He found a good linear relationship between $\bar{a}_3$ and σ_{12}^2 and a somewhat less well-defined relationship between $\bar{a}_3$ and σ_3. He showed that α may be large for $\bar{a}_3$ values above 3.38 Å (i.e., the preference for ABA rather than ABC stacking is not effective until the first layer pair achieves the AB order). This model attaches no fundamental significance to the $\bar{a}_3$ ($\bar{d}$) value of 3.44 Å traditionally attributed to random layer stacking, an obvious advantage in considering certain disordered carbons which have $\bar{d}$ values appreciably greater than 3.44 Å.

Ruland has criticized the concepts of totally disorganized carbon and single layers as not being physically reasonable. He points out that a gas-like distribution of particles in a solid system is virtually impossible and that scattering attributed by Franklin [22] and others to a disorganized phase can be more satisfactorily explained by variations in layer sizes and interlayer spacings. This interpretation suggests that the boundaries of the stacking domains or crystallites may not be as neatly defined and will not have the same physical significance as the crystallite

dimensions in ordinary polycrystalline materials. Ruland attributes this difference to the extreme anisotropy of the graphite lattice and points out that there is no reason to assume that during carbonization the growth of one layer has any relation to growth of the weakly attached adjacent layers. From this viewpoint uniform crystallite boundaries perpendicular to the layer planes would be unlikely and schematic representations of crystallites as stacks of plane uniform layers commonly found in the literature may be misleading.

A further consequence of the concept of nonuniform imperfect layers is clarification of the significance of the commonly employed parameters L_c and L_a. These parameters are usually determined from broadening of the (001) and (hk) or (hk0) lines, respectively. As discussed earlier, it has been established that determination of L_c requires a correction for distortion broadening due to the presence of more than one actual interlayer spacing and the method of Warren and Averbach [31] has been the usual one applied. However, Ruland [14] has plotted $\bar{d}$ vs L_c for the results of several workers and found the scatter very large. He concludes that the contribution of lattice imperfections to line broadening is significant and that there is in fact no simple way of separating size and disorder effects. The usual interpretation of L_a as an apparent layer diameter is of particular interest because of the extensive correlations observed by many workers between L_a and other properties or structural features. It now seems clear that L_a values determined from

line broadening are effectively a measure of the average size of planar, defect-free layer regions and that the actual layer dimensions may be much larger. Despite these uncertainties in interpreting parameters like L_c and L_a, Ruland emphasizes that the use of apparent L_c and L_a values obtained from the widths of (001) and (hk0) lines to characterize carbons can be considered entirely valid, as long as it is remembered that these parameters depend in a complex way on crystallite imperfections as well as dimensions, and that the actual sizes may be much larger than the apparent values. The widely employed $\overline{d}$ is in itself also a very useful parameter, but since it probably represents only the mean of a broad distribution of interlayer spacings, fundamental significance should not be attached to its use in calculating a "degree of graphitization."

Perret and Ruland [50] have applied Ruland's theory [48] of profile analysis for random-layer lines to a heat-treatment series of nongraphitizing carbons and shown that size and disorder effects can be separated. Their results indicate that in nongraphitizing carbons lattice defects are reduced at high temperatures, but that layer growth is inhibited so that even after heating to 3000°C the average layer size is only about 60 Å. They conclude that layer growth must occur at temperatures below 2000°C in graphitizing carbons and that high-temperature elimination of imperfections in the layer structure leads to three-dimensional ordering only when the layer size exceeds a critical limit.

Diamagnetism of Carbon and Graphite

Though all pure carbons are characteristically diamagnetic, the magnitude of the diamagnetic susceptibility is highly structure sensitive. Thus, susceptibility is a very useful parameter for studying the graphitization process.

The susceptibility of large single crystals of graphite was first measured by Krishnan and Ganguli [51–54]. They found the specific susceptibility at room temperature of the crystal perperdicular to the hexagonal axis, $\chi_{\perp}$, to be about -0.5×10^{-6} emu/g, which is close to the value for diamond. The susceptibility parallel to the hexagonal axis, $\chi_{||}$, was determined to be about -21.5×10^{-6} emu/g.* More recent measurements by Poquet *et al.* [55] on purified single crystals have produced values of 0.3 and 21.0 for $\chi_{\perp}$ and $\chi_{||}$, respectively. Soule and Nezbeda [56] obtained similar values by very careful evaluation of single crystal susceptibilities including consideration of twinning, bending, and small crystallite inclusions. The $\chi_{\perp}$ value is the ion core contribution and should be the same for each direction of measurement and essentially independent of structure. The very large anisotropic component, $\Delta\chi = \chi_{||} - \chi_{\perp}$, is predominantly a free charge carrier contribution of the

---

*All values of susceptibility will subsequently be expressed in units of -10^{-6} emu/g.

Landau-Peierls [57–59] type and arises from the position of the Fermi level in a region of the electronic energy band where the density of states changes rapidly with energy. Therefore, its magnitude is affected by any factor which changes the carrier concentration or the band structure of the material. This is the source of the structure sensitivity of more or less graphitic carbons.

Since the structure sensitivity of the diamagnetism is almost entirely due to the anisotropic component, it is obvious that a value measured in any given direction on a polycrystalline carbon will be a function of preferred orientation. This in fact provides a means of measuring preferred orientation by determining $\chi_{||}/\chi_{\perp}$, which may be related to macroscopic properties such as thermal expansion [60]. However, in characterizing the structural development of a carbon, a more useful parameter is the total (tensor trace) susceptibility defined as $\chi_T = \chi_{||} + 2\chi_{\perp} = \sum_{i=1}^{3} \chi_i$, where the χ_i are measured in three orthogonal directions. The validity of this method of determining χ_T for a polycrystalline material without regard for anisotropy has been shown analytically by Eatherly and McClelland [61]. They verified their analysis experimentally by making measurements on various commercial petroleum base, natural flake, and lampblack base graphites. For the highly graphitic Atcheson graphites they found χ_T values of 20.5 to 21.2 in excellent agreement with single crystal values after a minor correction for intercrystalline carbon or crystallites too

small to develop a crystalline field. They further pointed out that a single measurement on a powdered randomly packed graphite should yield an average susceptibility, $\bar{\chi} = \chi_T/3$. Thus, $\bar{\chi}$ is a valid and convenient parameter to measure in systems of random crystallite orientation.

The large Landau-Peierls contribution to $\chi_{||}$ discussed above is characteristic of carbons comprising large crystallites. Experimentally when the crystallite diameter L_a falls below about 200 Å the diamagnetic susceptibility is markedly reduced. Miwa [62] in 1934 observed the crystallite size dependence of susceptibility for a series of carbon blacks. He found $\bar{\chi}$ to increase roughly linearly with crystallite height L_c. However, in view of the now-recognized fundamental dependence of susceptibility on L_a rather than L_c, this dependence probably accrued fortuitously due to the usual proportionality of L_a and L_c [28,63]. The fundamental relationship of L_a to magnetic susceptibility was noted by Pinnick [64] in a study of carbon blacks and baked carbon rods. After producing specimens with L_a values ranging from 50 to 3000 Å, he measured $\bar{\chi}$ values ranging from 1.7 for the smallest crystallites to 7.8 for the larger crystallites. Interestingly the entire increase in $\bar{\chi}$ occurred in the L_a range 50 to 150 Å. On the basis of the susceptibility data as well as changes in Hall effect and thermoelectric power, Pinnick concluded that the susceptibility increase was due to an increase in filling of the π band which brings the Fermi level into a region of higher curvature of the constant energy surfaces.

Pinnick noted, however, that the susceptibilities of his specimens having 50 Å crystallites were not far above values for large aromatic molecules. The anisotropic component of susceptibility, $\Delta\chi = \chi_{||} - \chi_{\perp}$, for small aromatic systems up to four rings, had been calculated quantum mechanically by London [65] and by Brooks [66] and shown experimentally by Lonsdale [67] to be proportional to the number of benzene rings in the system. The anisotropic component $\Delta\chi$ for benzene is about -54×10^{-6} emu/mole (about -0.7×10^{-6} emu/g) and for molecules of roughly linearly connected rings approximately a proportionate multiple of this. Mrozowski [68,69] interpreted the proportionality of the diamagnetism to the number of rings or to molar volume as a consequence of the π electrons forming closed shells and filling exactly a Brillouin zone. Experimentally a further increase in $\bar{\chi}$ has been noted for molecules large in two dimensions; ovalene with ten rings has a $\Delta\chi$ of about -0.9×10^{-6} emu/g which has been attributed by Dorfman [70] to a further delocalization of the π electrons (i.e., the π electrons are concentrated at the periphery of the molecule rather than being confined to single-ring orbits). Pinnick [64], assuming that results from small aromatic systems could be extrapolated to larger systems, concluded that in the limiting case of very large crystallites the London-type of closed shell diamagnetism plus the ion core values could lead to a $\bar{\chi}$ of about -2.0×10^{-6} emu/g. Accordingly he subtracted this value from his measured $\bar{\chi}$ values

and attributed the difference to the free carrier or Landau-Peierls diamagnetism. On this basis he showed the Landau-Peierls contribution to be a factor only for L_a values larger than about 75 Å.

On the assumption that the London susceptibility is roughly proportional to the number of benzene rings plus a contribution from delocalization, Kiive and Mrozowski [71] obtained a $\overline{\chi}$ of 1.2 as the limit for very large condensed ring planes; this value includes the ion core contribution. They explain the further increase in χ with heat treatment as due to the appearance of excess free carriers in the form of holes in the full energy band, increasing in number up to HTT of 1300°C and subsequently decreasing slowly towards a limiting value for a large graphite crystal. The conclusion that the free carrier concentration first increases then decreases came from observations of points at which the Hall constant changes sign. The continued increase in χ even with decreasing carrier concentration was attributed to a decreasing carrier effective mass with increasing crystallite size.

Pinnick and Kiive studied the change in susceptibility of carbons of varying crystallite sizes resulting from shifting of the Fermi level [72]. They moved the Fermi level experimentally by forming compounds of carbons with bisulfate ions and found the susceptibility decrease to be greater for larger crystallites. It was concluded that the Landau-Peierls theory was inadequate to explain all the findings.

The magnetic behavior of several carbons has been examined as a function of source and pretreatment temperature. Honda studied the susceptibility development of coal and found a minimum at about 700°C HTT which he attributed to a paramagnetic contribution of unpaired electrons [73]. He found that $\bar{\chi}$ increased rapidly for treatment temperatures above 1400°C. Adamson and Blayden also found a maximum in the paramagnetism of carbons prepared between 500 and 700°C [74].

A number of theoretical analyses have been made of the magnetic susceptibilities of carbons and graphite. Pacault and Marchand [72,75] assumed a London-type anisotropic component and calculated $\bar{\chi}$ including the ion core and London contributions to be about 0.85 for large layers. Pacault, Marchand, and Lumbroso [72,75,76] developed a two-dimensional electron gas model to explain the additional large diamagnetism of graphite. On the other hand McClure [77] showed that the London theory of the diamagnetism of aromatic molecules can be extended to give the same results for graphite as are derived from solid-state theory, including the correct temperature dependence. McClure assumes that the susceptibility of small molecules does not depend on temperature because the energy gap between the levels in the absence of a magnetic field is much greater than thermal energies; the energy level spacing decreases with increasing molecular size, and for very large molecules the mean occupation of the levels changes with temperature causing the susceptibility to be temperature dependent. A further difference noted in

extending the London theory to graphite is that all of the anisotropic susceptibility of graphite is contributed by states very near the band degeneracy, while that of a small molecule comes more or less uniformly from all the π electrons. McClure suggests that the transition between the two types of behavior may account for the very rapid increase of susceptibility found experimentally when particle diameters increase from 50 to 150 Å.

Solid-state band theoretical calculations of the diamagnetism of graphite have been made employing both two- and three-dimensional models. Qualitatively the basis for the diamagnetism considered here is that in the absence of a magnetic field the lower energy levels in each group of states are preferentially occupied; when the field is applied the groups of states which were originally distributed in energy combine to the original average energy of the groups so that the total energy of the electrons is raised. McClure [78] has formulated a two-dimensional model, based on the two-dimensional band structure calculated by Wallace [79], which assumes that all of the π-electron diamagnetism is due to band-to-band transitions. This model which assumes no interlayer interactions yields a theoretical trace susceptibility of 39. The two-dimensional calculations have been extended to three dimensions (i.e., to include interlayer interactions) by Haering and Wallace [80] and by McClure [81]. These calculations have been made to show good agreement with the single-crystal experimental trace susceptibility of

-22×10^{-6} emu/g when appropriate values are taken for the interlayer interaction parameter.

Understanding of the structure sensitivity of the diamagnetism of carbons has been significantly advanced in the past decade by work on pyrolytic carbons. These materials, which are deposited from gaseous hydrocarbons onto hot substrates in the temperature range 1600 to 2400°C, provide a variety of structures which are not available in the more conventional carbons. In particular, PC characteristically exhibits a relatively high degree of preferred orientation and large crystallite diameter. In the as-deposited condition these large layers show little or no stacking order so that electronic properties approaching those of the theoretical two-dimensional graphite might be expected if the model is valid. Fischbach [82–84] was the first to experimentally observe the large room temperature susceptibility of PC. He studied specimens deposited at 2100 to 2300°C and found χ_T values as high as 33.2, about 50% larger than the single crystal value of 22.0, for the as-deposited materials.

Wagoner and Eckstein [85] measured the susceptibilities of a series of PC's deposited in the range 1600 to 2500°C and found a maximum χ_T of 33.5 for the 2400°C deposit. Their results showed χ_T increasing with increasing deposition temperature from 13.2 for the 1600°C specimen to the 33.5 maximum of the 2400°C deposit and then falling to 27.5 for the sample formed at 2500°C. These observations of total susceptibilities up to about 50% larger than single crystal

values provide reasonable confirmation of the validity of McClure's two-dimensional model which predicts a χ_T of 39 for no interlayer interaction.

The effect of deposition temperature in the range 1600 to 2400°C on the diamagnetism of pyrolytic carbon has also been studied by Chang [86]. He found a maximum χ_T of about 23 for a deposition temperature of 2000°C. Chang also proposed the use of magnetic susceptibility for evaluating fluidized-bed pyrocarbon coatings, but his experiments were confined to materials deposited on stationary substrates.

Fischbach [83] reasoned that if the enhanced diamagnetism of pyrolytic carbon is a result of reduced interlayer interaction due to lack of stacking order, the susceptibility should decrease on heat treatment as the layer disorder anneals out. He showed this to be the case in annealing the 2100 to 2300°C deposits to temperatures as high as 3600°C. At heat-treatment temperatures above 2400°C the susceptibilities fell rapidly from the as-deposited values to a minimum near HTT 2900°C, rose again to about the single-crystal value at HTT 3200°C, and remained essentially constant at this value. The decrease in χ with HTT above 2400°C was correlated directly with x-ray diffraction data which showed increasing layer ordering as expected. The minimum in the χ versus HTT curve is apparently related to a transition, discussed by Fischbach in a subsequent paper [87], between different stages of the graphitization process. During the initial stage (for PC deposited above 2000°C) of graphitization a large increase

in layer ordering occurs with little change in other structural parameters; hence the rapid drop in χ. Subsequent stages are characterized by large increases in crystallite diameter, L_a, and preferred orientation. The susceptibility minimum thus suggests the development of relatively small, well-ordered "graphite" crystallites which subsequently grow in diameter with further heat treatment. This causes χ to increase toward the single-crystal graphite value.

The existence of a minimum in the room temperature χ_T versus HTT curve has also been observed by Poquet [88] for a group of pyrolytic carbons deposited at 2100°C. Poquet found a maximum as-deposited χ_T of 30.4 and noted minimum χ_T values similar to Fischbach's [87] at HTT about 2700°C. Further annealing at 2900°C increased χ_T again, but not quite up to the single-crystal value.

The effects of thermal treatment on the diamagnetism of carbons discussed thus far has been based on more or less graphitizing or "soft" materials. Until recently little information was available on the magnetic behavior of "hard" nongraphitizing carbons, though the characteristic retention of a highly disordered structure even after prolonged heat treatment at very high temperature should provide an interesting contrast to the behavior of graphitizing carbons. Glassy carbon produced by controlled pyrolysis of thermosetting polymer resins is a classic example of nongraphitizing carbon. This material is hard, vitreous-appearing, nearly impervious to gases and has a bulk density of about 1.5 g/cm^3

(only about 66% of the theoretical density of graphite). The structure comprises tangled ribbon-like crystallites with very little internal stacking order and considerable lattice distortion. The distortion is associated with extensive cross-link bonding between crystallites which holds them in the tangled, random array and inhibits development of a compact structure. These cross-link bonds between crystallite edges are apparently very stable and cannot be entirely removed by thermal treatment alone.

Fischbach [89] has studied the magnetic behavior of two glassy carbons, one originally processed at 3000°C and the other at 2000°C. Both materials were heat treated at temperature intervals up to 3200°C and examined after each treatment for changes in χ, L_a, and $\bar{d}$. As expected, no changes occurred at HTT up to the original processing temperature. The GC-2000 material showed a steady increase in χ_T from HTT 2200°C up to 3000°C where it achieved a $\chi_T \simeq 16.5$, essentially the same as the as-received value for the GC-3000. The x-ray parameters L_a and $\bar{d}$, however, did not change smoothly over the same range. L_a, which was initially about 40 Å, did not start increasing until HTT above 2600°C. It then increased to about 75 Å after treatment at 3200°C. The initial $\bar{d}$ of 3.50 Å decreased to about 3.42 Å after treatment at 3200°C, but most of the decrease occurred in the 2000 to 2400°C range in which L_a remained constant. There was no change in χ_T with the initial decrease in $\bar{d}$ resulting from the 2200°C heat treatment. This is of particular interest

because the diamagnetism of graphitizing carbons is known to decrease with decreasing $\bar{d}$ at constant L_a as a result of the increase in layer stacking order. Fischbach noted that the decrease in $\bar{d}$ in glassy carbon may result more from changes in lattice distortion than from increased layer ordering since the x-ray diffraction results indicated very little layer stacking order even after the 3200°C heat treatment.

The strong L_a dependence of susceptibility observed for this glassy carbon is similar to results found on other nongraphitizing carbons. However, for nongraphitizing carbons χ increases much more rapidly with L_a than is the case for graphitizing carbons. Fischbach noted that for given $\bar{d}$ and χ_T values, the L_a values observed for glassy carbon are only about half those measured on high-temperature pyrolytic carbons. The reason for this discrepancy is not entirely clear but may be related to the significance of the L_a determinations for these two different types of carbon. Warren's [19] peak displacement method of measuring L_a assumes no distortion within the layers, and it is always difficult to separate distortion broadening from the crystallite size effect in x-ray line broadening measurements. Thus it seems possible that cross-link bonding distortions in nongraphitizing carbons may result in serious underestimation of crystallite sizes by x-ray methods.

Kinetics of Graphitization

Graphitization of disordered carbons is an evolutionary process which occurs by the gradual elimination of intralayer defects and stacking faults. There is no evidence for a distinct graphite phase (except where a molten carbide phase is present) growing out of the disordered phase. Graphitization, without catalysts, therefore is not directly comparable to recrystallization which occurs in metals, nor can it be analyzed by the classical concepts of chemical kinetics which require quantitative statements relating the amounts of reactant and product species to progress of the reaction. However, since graphitization does entail the evolution of a limiting, ideal structure from an initial imperfect structure, any parameter which provides a relative measure of structural perfection can be used to determine a rate of graphitization. As shown earlier most of the commonly employed parameters leave some ambiguity with regard to unique interpretation of detailed structure; L_a and $\bar{d}$ may not have the same significance for graphitizing and nongraphitizing carbons and χ_T has the dual dependence on L_a and layer order. Nevertheless, these parameters, and others, may be meaningfully used on a relative basis to measure extent of graphitization for a given carbon. The limitation to be kept in mind is that accurately measured values of a given parameter do not necessarily uniquely describe a structure, and care must be

taken in comparing values of any parameter for carbons of different types on an absolute basis.

Graphitization has actually been treated as a kinetic process only recently. In fact, prior to the early 1960's, it was generally believed to be relatively insensitive to heat-treatment time and dependent primarily on the maximum heat-treatment temperature. Hence, it was common practice (and sometimes still is) to specify the structure of a graphitizing carbon in terms of a maximum processing temperature without regard for treatment time. The concept of a limiting structure characteristic of the maximum treatment temperature was probably a result of the very high activation energy for graphitization which obscures the kinetic nature of the process unless careful measurements are made as functions of time.

Fair and Collins [90] were among the first to show the time dependence of graphitization and to attempt a kinetic analysis. For a commercial grade of baked carbon they found that the rate of graphitization, determined from measurements of interlayer spacing and electrical resistivity, decreased very rapidly with heat-treatment time at any temperature although a zero rate was never attained in times up to 20 hr. Fair and Collins also noted that the rate of graphitization increased with increasing temperature and decreased more rapidly with time at higher temperature. From these results they concluded a distribution of activation energies was involved and that the activation energy was a function of

the extent of transformation, increasing as graphitization progressed. A distribution of activation energies was also obtained by Mizushima [91] in a study of molded petroleum cokes. Mizushima heated specimens for various times over the temperature range 900 to 2500°C and determined graphitization rate from measurements of electrical and thermal conductivities and crystallite size. He obtained activation energies ranging from about 80 to 210 kcal/mole with peaks in the distribution of about 100 and 200 kcal/mole at 1400 and 2200°C, respectively.

Fischbach, on the other hand, obtained single-valued activation energies in graphitization studies of petroleum coke [92] and pyrolytic carbon [93]. He determined a single effective activation energy (ΔH) of 250 kcal/mole from measurements of interlayer spacing on petroleum coke heated isothermally for different times in the temperature range 2300 to 2700°C. An effective ΔH of 260 kcal/mole, in excellent agreement with the petroleum coke value, was obtained for the pyrolytic carbon in the heat-treatment temperature range 2500 to 3000°C. Extent of transformation of the PC was followed by measurements of interlayer spacing and magnetic susceptibility. Fischbach further showed that graphitization of both coke and PC can be adequately described by a superposition of first-order rate processes with a distribution of rate constants. His method of analysis, which is now widely used, has been discussed in detail [87,94].

Graphitization of several carbons has been shown to exhibit the general characteristics of a thermally activated process (i.e., properties change as a function of isothermal heat-treatment time, and the rate of change increases rapidly with increasing treatment temperature). Accordingly the process can be described by an Arrhenius-type dependence on treatment temperature through a Boltzmann factor K(T) so that the rate constant $k = k_o K(T)$, where k_o is the temperature-independent preexponential or frequency factor and $K(T) = \exp(-\Delta H/RT)$ is the temperature-dependent Boltzmann factor; ΔH is the activation energy, R is the gas constant, and T is absolute temperature. In principle, the rate constant k at any given temperature for a simple first-order process should be obtainable from the slope of a plot of the logarithm of fractional change in any measured property against treatment time. In fact, Fischbach [87,94] has shown this method to work for individual stages in the graphitization of certain pyrolytic carbons. However, he noted that the method is not generally applicable and is not valid where a distribution of unresolved rate processes is involved.

An alternative technique proposed by Fischbach [87,94] for determining the activation energy of graphitization involves the superposition of isothermal property change curves. This method is widely applicable in that it is not dependent on first-order form and does not assume a single-valued preexponential. The superposition technique can be

applied where there is a broad distribution of rate constants provided that the distribution is not a function of temperature. Its application is based on determination of a temperature-compensated time scale which places property versus time data for a given carbon at various isothermal temperatures on a single master curve. This method of analysis has been successfully applied by Fischbach [11] to much of the early high-temperature data of other workers and shown to give activation energies near 250 kcal/mole where much lower values had been obtained by other analytical techniques.

The superposition method of determining graphitization activation energies has been extensively employed by Pacault, Marchand, and co-workers at the University of Bordeaux [10, 95–99] in studies on several types of carbons. For the heat-treatment temperature range above 2000°C their results are in fair agreement with those of Fischbach. Noda [100,101] has compiled activation energies obtained by several workers by superposition and noted that values obtained can be related to the preheat-treatment temperature. Values ranged from 260 kcal/mole for pyrolytic carbons formed at 2000°C down to 164 kcal/mole for a pitch coke prebaked at 1100°C.

Extensive analyses of different types have been carried out for three petroleum cokes by Murty, Biederman, and Heintz [102,103]. They conclude from the agreement of different methods that for the HTT range 2300 to 2700°C, ΔH is single valued at about 230 kcal/mole for all three cokes

despite large differences in graphitization rate. They attribute the varying graphitization rates of the cokes to different preexponential factors which were considered to reflect the structural configurations of the starting materials. Of the various properties measured, the macroscopic anisotropy factors, as determined by x-ray methods, gave the best correlation with rate; it was thus concluded that more anisotropic cokes have a higher preexponential factor and a corresponding higher rate or ease of graphitization.

High-temperature deformation of carbon has been shown by several workers to enhance the graphitization rate. The kinetic aspects of this enhancement have been considered by Fischbach [104] to involve "two components: (1) An immediate and direct influence of the deformation process, and (2) a residual effect due to deformation-induced microstructural changes." He concludes that stress-assisted bond breaking is the principal mechanism involved.

CHAPTER III

EXPERIMENTAL PROCEDURE

Specimen Preparation

Twelve different pyrolytic carbons were prepared for this work by deposition onto substrate carbon microspheres in a fluidized bed. The carbon substrate was necessary to avoid contamination of the pyrolytic carbon during deposition or subsequent heat treatment. The original source material used for the substrate microspheres was Dowex* 50W-X8 cation exchange resin, a sulfonated styrene-divinylbenzene copolymer with the X8 indicating 8% divinylbenzene cross-linkage [105]. The resin was further designated as 20 to 50 mesh hydrogen form. In the as-received condition this resin contains about 50 to 56% by weight of water and the actual wet mesh size range (U.S. Std) is 16 to 40 (1190 to 420 μm). After drying at 100°C in air for 16 hr most of the water is removed and the resin particles are shrunk to a 20 to 50 mesh (841 to 297 μm) size range. The particles were then carbonized by heating in inert atmosphere in a fluidized bed to 1000°C at a heating rate of 200°C/hr. A final heat treatment at 3000°C for 15 min was provided to stabilize the structure against dimensional or other changes on further experimental treatment, and to volatilize impurities, particularly sulfur,

---

*Dowex is a registered trademark of the Dow Chemical Co.

which might be present. A spectrographic analysis of the product showed the only remaining measurable impurities to be 0.04% oxygen and 0.74% sulfur. The product was then screened into narrow size fractions and the largest size fraction, 30 to 35 mesh (595 to 500 μm), available in sufficient quantity was taken for coating. Most of these particles were nearly perfect spheres and the small content of nonspherical pieces was rejected by shape separation on a vibrating tray.

The structure of the substrate microspheres was typical of other glassy carbons derived from thermosetting resins. Particle density was 1.25 g/cm^3, and x-ray diffraction patterns showed no modulation of the (hk) lines even though the material had been heat treated at 3000°C for 15 min.

While the glassy carbon kernels provided the primary base for the PC deposition, some thin graphite plates were also included in each deposition run and fluidized along with the microspheres so that they could receive the same coating. The plates were to be used for evaluation techniques for which the microspheres were inappropriate, in particular, for determination of preferred orientation or anisotropy by an x-ray method. The technique of fluidizing plates or discs along with small particles was developed by Bokros [106,107] in order to apply Bacon's [108] method of graphite anisotropy measurement to fluidized bed PC's. Of course, the flat specimens thus obtained can and have been used extensively by other workers for evaluations such as

mechanical properties [4,109,110], thermal and electrical conductivities [109,111,112], and dimensional change [113–116]. The basic requirement of substrate plates for this purpose is that they be of suitable geometry and mass to mix well with the fluidized bed in order to acquire a coating representative of that on the particles. The plates used successfully in the present work were 6 × 6 mm^2 and 0.25 mm thick. Similar plates 0.9 mm thick were also included in initial coating runs but these stayed near the bottom of the bed and did not obtain representative coatings; they apparently could not be adequately suspended by fluidizing conditions suitable for the low-density microspheres. The plates were made by first machining 6 mm^2 bars of graphite and then slicing the bars with a thin, high-speed, silicon carbide abrasive wheel. The graphite used was POCO* grade AXF-5Q, a fine-grained, unimpregnated grade which had been baked at 2500°C. Cutting with the high-speed abrasive wheel produced plates of uniform thickness with a fairly good polish on the flat surfaces.

The pyrolytic carbon coatings were deposited in a fluidized-bed furnace which had been developed at the Oak Ridge National Laboratory for the coating of nuclear fuel particles. The design and operation of the coating system has been discussed in detail elsewhere [117]. Basically the system comprises a vertical graphite reaction tube which is heated by a 25-kW graphite resistance furnace. The

---

*Manufactured by UNION POCO, Decatur, Texas.

reaction chamber used in this work was 3.5 cm ID with a conical bottom of 36° included angle. Two types of coating tubes were used for the present work; a low-temperature tube, used for deposition temperatures up to 1350°C, allowed for some preheating of the fluidizing gas through the final 10 cm of passage into the coating chamber, and a high-temperature tube, used at temperatures above 1550°C, provided a water-cooled passage for the gas to within about 2 cm of the coating chamber. The two designs are necessary to accommodate the range of hydrocarbon reaction rates encountered in the deposition temperature range employed. In both the low- and high-temperature designs the fluidizing-coating gas mixture enters the reaction chamber through a single orifice after the component flow rates are individually set with a bank of rotameters.

The total gas flow rate for a coating run is limited to some range by the fluidizing requirements of the particles of given size and density in the coating chamber diameter employed. Gas flow rates too low will not provide adequate bed agitation and particles may even fall out the bottom, while flow rates too high can blow particles completely out of the coating chamber. For the 550-μm average diameter particles of 1.25 g/cm^3 density in the 3.5-cm-diam tube used in the work, optimum bed action appeared to require a flow rate of about 3 liters/min of propylene or equivalent. Fluidization prior to coating required 5 liters/min of helium. These flow rates, however, apply only to the beginning of

coating since large coating thicknesses were to be built up and the fluidizing flow rate requirement increases roughly linearly with particle diameter (if overall density is not being changed) and with particle density. In these coating runs the average particle diameter was being increased from 550 μm to about 850 μm, and the coating deposited was slightly denser than the original kernels. Accordingly, the total gas flow rate was changed incrementally during each run until twice the initial flow rate was reached for the final stage. As the total gas flow rate was increased, the concentration of reactant hydrocarbon in helium carrier gas was maintained constant, thereby providing an increase in reactant supply roughly proportional to the increase in surface area of the fluidized bed.

The selection of uniform charge size for all coating runs was based on the maximum total gas flow rate for the system and the maximum hydrocarbon flux desired for any run. The maximum practicable hydrocarbon flux was 2.0 cm^3 propylene per minute per square centimeter of bed surface area. With a maximum total flow rate of 3.0 liters/min of undiluted propylene, this fixed the bed surface area at 1500 cm^2. The geometrical surface area of the glassy carbon microspheres was calculated at about 90 cm^2/g before coating; the mean value during deposition of a 40-μm increment of coating, the increment at which the flow rate would be increased, was about 105 cm^2/initial g. Allowing 100 cm^2 for about 35 graphite plates and the coating tube walls thus fixed the

microsphere charge at 1400 cm^2/105 cm^2/g $\simeq$ 13.5 g (17.7 cm^3 tapped volume) for each run.

Within the gas flow rate limitations discussed, conditions for deposition of the PC specimens were selected on the basis of previous studies [117–119] to produce carbons with a wide range of properties. Since methane and propylene had been the most widely studied hydrocarbons in fluidized-bed PC development, these gases (C.P.) were employed exclusively in this work. Further, essentially the complete range of dense (not porous, sooty) PC structures known to be obtainable in fluidized beds can be deposited from methane or propylene by selecting suitable concentrations and temperatures. The coating deposition conditions employed and the process results are shown in Table I.

The integral coated microsphere was the specimen form of primary interest for kinetic study, so no further specimen preparation was necessary for the bulk of each PC. However, certain evaluation techniques required coatings removed from the kernels, and the flat-plate specimens are of use only when removed from the graphite substrate. The microsphere coatings were fractured by compressing microspheres individually between glassy carbon anvils in a small vise equipped with a receptable to catch the debris. Care was taken to produce coating fragments as large as possible. This operation was greatly facilitated by using a vacuum tweezer to position each microsphere prior to crushing and, with a small particle-collecting attachment, to gather the

Table I. Deposition Conditions Employed in Preparing Pyrocarbon Specimens

Specimen	Deposition Conditions				Process Results	
	Temperature (°C)	Reactant in He (%)	Reactant Flux ($cm^3/min\text{-}cm^2$)	Time[a] (hr)	Efficiency[b] (%)	Coating[c] Weight (%)
C-12	1150	C_3H_6 100	2.0	0.57	36	85.1
C-13	1150	C_3H_6 16.7	0.5	2.27	36	83.1
C-7	1150	C_3H_6 3.2	0.1	8.00	31	77.0
C-1	1250	C_3H_6 100	2.0	0.32	57	82.1
C-3	1250	C_3H_6 16.7	0.5	1.07	54	79.9
C-4	1250	C_3H_6 3.2	0.1	5.33	59	81.1
C-8	1300	CH_4 3.2	0.1	21.00	38	78.7
C-5	1350	CH_4 19.4	0.6	2.67	55	78.4
C-6	1350	CH_4 6.5	0.2	8.00	51	78.7
C-9	1550	C_3H_6 40	1.0	0.35	68	76.4
C-10	1900	CH_4 40	1.0	1.07	71	77.5
C-11	1900	CH_4 3.2	0.1	5.25	77	59.2

[a]Approximate deposition rate in μm/hr can be obtained by dividing the time into 150.

[b]$\frac{\text{Weight of carbon deposited}}{\text{Weight of carbon supplied}} \times 100.$

[c]$\frac{\text{Weight of coating deposited}}{\text{Weight of coating + GC kernels}} \times 100.$

usable coating fragments after crushing. The plate coatings were removed by first mounting the coated plates on a support block and trimming off the edges with a diamond saw, then demounting and grinding away one side of the coating and the substrate. In this way only one coating square was recovered from each plate, but the substrate was too thin (0.25 mm) to permit its removal in a manner affording salvage of both coating sides.

Heat Treatment

All heat treatments were done in a small, horizontal, manually controlled, graphite resistance furnace shown schematically in Fig. 1. The furnace was designed to operate at temperatures up to 3000°C in atmospheric pressure of argon. Maximum furnace power was 7.5 kW (at approximately 6 V) which limited the working hot zone size. Inside dimensions of the heating element tube were 20 cm length and 1.6 cm diameter. A heating element designed to flatten the axial temperature profile by increasing power dissipation (decreasing cross section) near the ends provided a uniform hot zone length of more than 4 cm at temperatures up to 2700°C. At higher temperatures the limited power necessitated use of a uniform-cross-section element which provided only a 2-cm-long uniform hot zone. Element life at 3000°C was only a little more than 1 hr.

Temperatures were measured with a Pyro Micro Optical Pyrometer sighting on appropriately positioned graphite

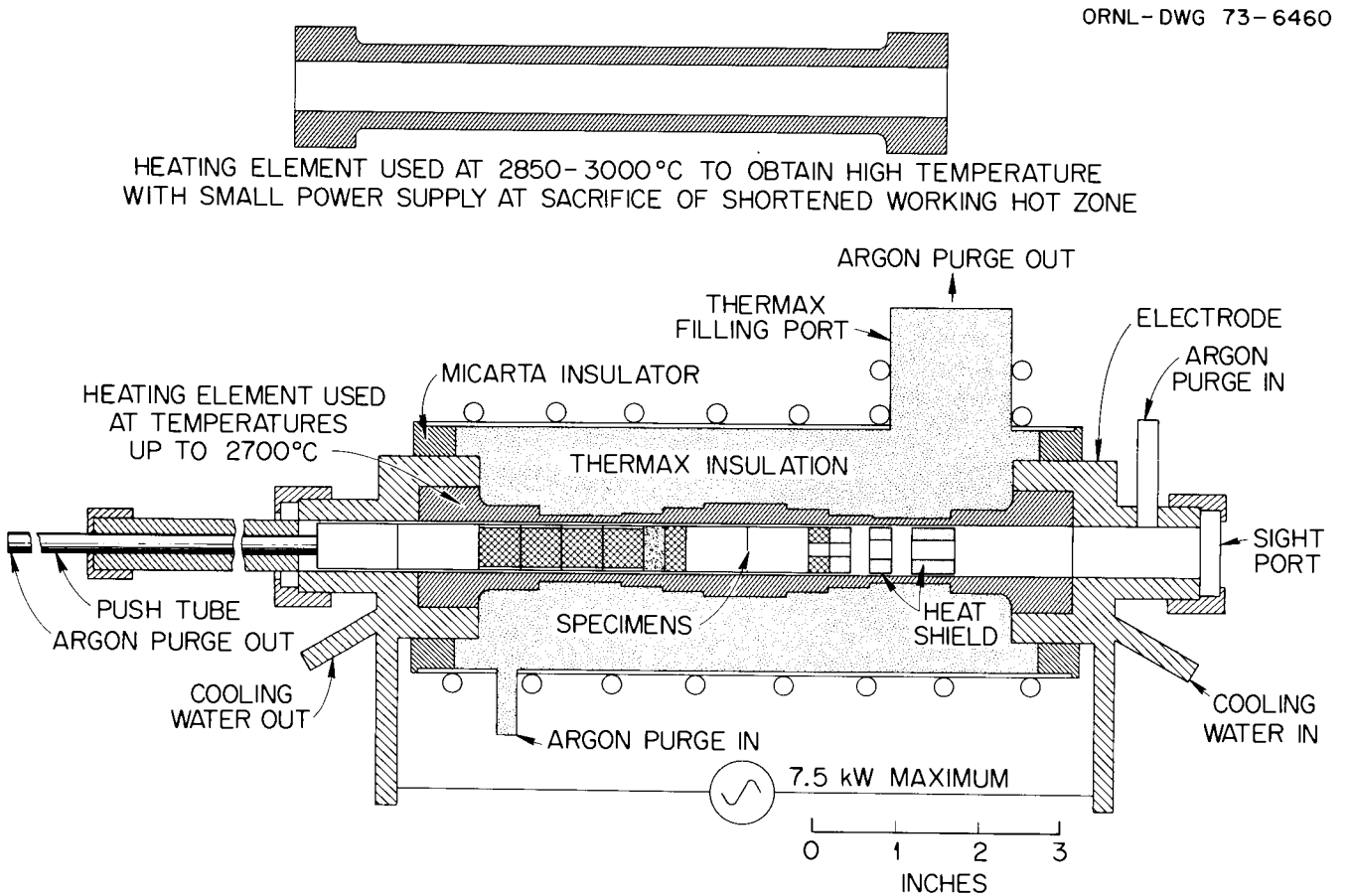

Fig. 1. Heat Treatment Furnace.

insulating spacers or on the specimen crucibles. Since a graphite furnace of the type used provides nearly ideal blackbody conditions, no emittance correction was necessary. However, a correction was made for the silica-glass window; the correction factor was determined by observing the apparent temperature drop imposed by addition of an identical window to the optical path at different temperatures.

With the manual power control, and some practice, specimen temperature could be raised very quickly to the desired level and held within ±10°C, the accuracy with which the optical pyrometer could be read. The technique involved preheating the hot zone to about 50°C above the desired HTT while the specimens resided near the end of the heating element at a temperature about 800°C below the hot zone temperature. The specimens were then pushed into the hot zone and the power appropriately controlled to heat the specimens to the desired HTT in about 30 sec without overshooting the target temperature. The power then had to be reduced gradually until the furnace stabilized at the desired temperature; this required about 30 min. After this point small adjustments were necessary only to compensate for fluctuations in line voltage. At the end of the prescribed time the specimens were cooled very rapidly by pushing them out of the hot zone.

Both isochronal and isothermal heat treating procedures were employed in this work. While isothermal data provide the more convenient basis for kinetic analysis, isochronal

data can be obtained much more quickly. Therefore, a preliminary series of isochronal heat treatments was done on all specimens to obtain a preview of the property response to be expected. The specimen in each case was approximately 0.2 g of integral coated particles. Temperatures employed were 200°C increments from 1600 to 3000°C and the time was 30 min. Magnetic susceptibility measurements, which will be discussed later, were made after each heat-treatment step. The subsequent isothermal treatments were carried out at 150°C intervals from 1350 to 3000°C. Of course, only HTT's above the deposition temperature were run for each lot. The shortest time run at each temperature was 2 min with each succeeding run adding twice the previous cumulative time up to 486 min total time at HTT up to 1950°C. At higher temperatures the longer times were eliminated until a total of only 18 min was accumulated at 3000°C by each specimen. The total time was reduced at high temperature partly because of the limited heating element life and partly because property changes were occurring so rapidly that longer times were not necessary to complete the study. The sample used in all isothermal treatments comprised approximately 0.2 g of integral coated particles plus a few coating fragments removed from the kernels. No flat-plate specimens were heat treated. After each heat-treatment step a magnetic susceptibility measurement was made on the entire 0.2 g of microspheres, and a few integral particles and coating fragments were set aside for density and x-ray measurements.

Magnetic Susceptibility

Magnetic susceptibility measurements were made at room temperature by the Faraday technique [120,121] using a 4-in. electromagnet* with constant force pole caps and a recording semimicro analytical balance† as shown in Fig. 2. The equipment as used was designed by Scott and its operation has been discussed previously [122]. The quantity measured is the force exerted on a specimen by a magnetic field gradient. This force F is related to the change in energy induced by the magnetic field, and for a diamagnetic material is in the direction of decreasing field strength. If the z-direction is the axis of the magnet pole pieces, the x-axis is the direction of motion (vertical), and H is the field strength expressed as

$$H^2 = H_x^2 + H_y^2 + H_z^2 ,$$

then for a specimen of mass M and mass susceptibility χ

$$F_x = \frac{M\chi}{2}\left(\frac{dH_x^2}{dx} + \frac{dH_y^2}{dx} + \frac{dH_z^2}{dx}\right) .$$

The pole pieces are designed such that H_x and H_y are negligibly small so that

---

*Alpha Scientific Model AL 7500 electromagnet and Model AL 7500PS power supply.

†Ainsworth Model FV electrobalance with Bristol Type AU-2 recorder unit.

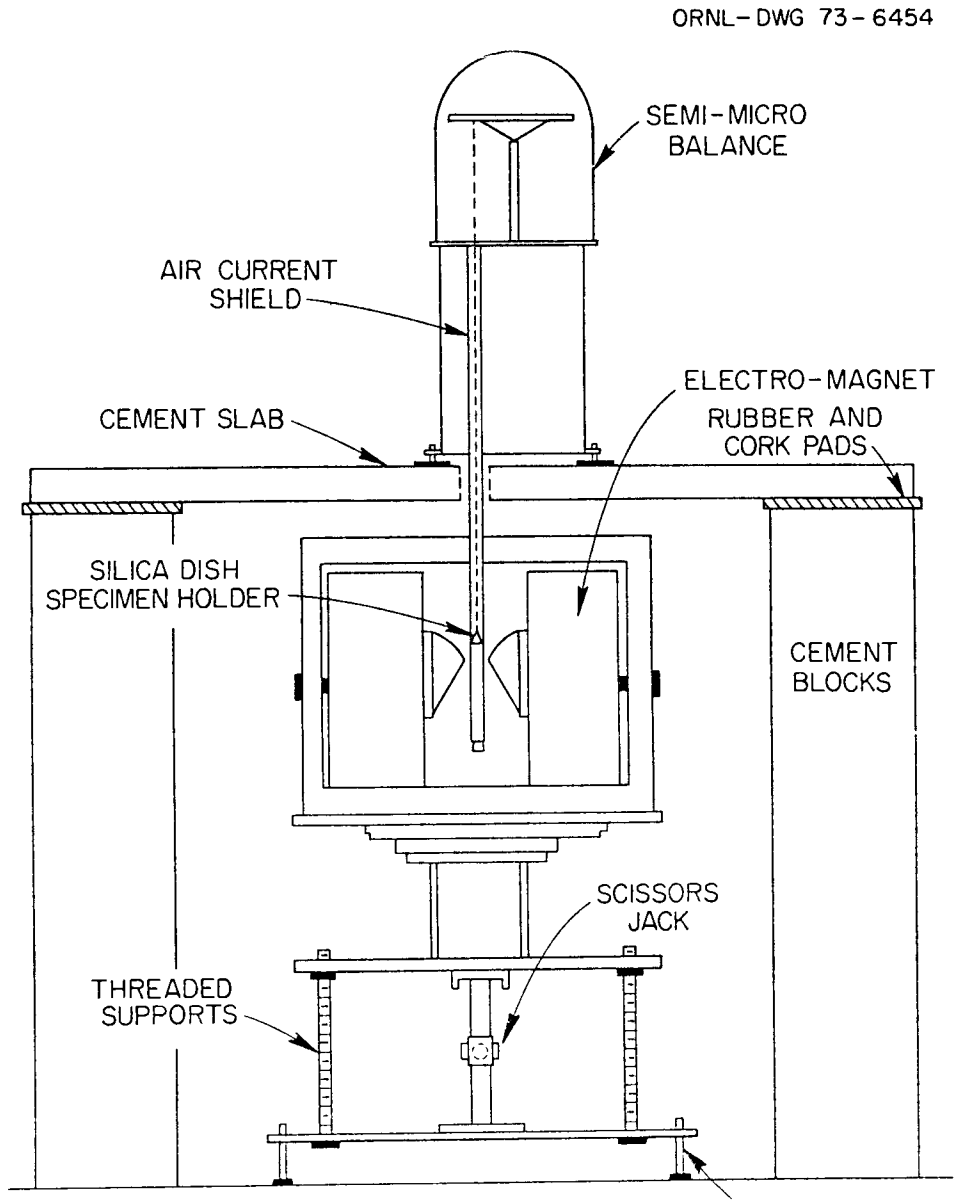

Fig. 2. Electromagnet and Recording Balance.

$$F_x = M\chi/2(dH_z^2/dx) = g\Delta W ,$$

where dH_z^2/dx is the force constant, g is the acceleration of gravity, and ΔW is the apparent weight change of the sample of mass M in the horizontal magnetic field H_z with a vertical gradient. The mass susceptibility is then

$$\chi = 2g\Delta W/M(dH_z^2/dx)$$

In cgs electromagnetic units H is in oersteds and χ is usually expressed in emu/g.

The term dH_z^2/dx is made constant over a distance large enough to accommodate the sample volume by appropriate design of the pole cap profile [123,124]. The region of constant force for the magnet used here was determined [122] to extend from 13.8 to 16.0 mm above the pole peak and to be independent of operating current (field strength). The force profile was obtained by plotting weight change of a susceptibility standard at constant operating current as a function of vertical distance above the pole peak. The specimen-pole peak distance was varied by means of a scissors jack and leveling screws supporting the magnet and measured with a cathetometer placed 1.5 m away.

The value of the force constant was determined experimentally in this work from measurements on susceptibility standards including palladium, cane sugar, and distilled water. A silica-glass dish suspended from the balance by an aluminum chain was used as a sample holder for

all standard and experimental measurements. The dish was diamagnetic and each measurement was corrected for its contribution. With each calibration specimen suspended in the region of constant force, five measurements were made of the apparent weight change induced by the magnetic field at an operating current of 9 amps. The force constant was then calculated from the average of these measurements and the literature values of χ for these standards by

$$dH_z^2/dx = 2g\Delta W/\chi M \ .$$

Data and results are given in Appendix I. A force constant of 2.25×10^7 G^2/cm* was obtained from each standard at the 9 amp operating current and this value was used in all the carbon susceptibility calculations.

While spectrographic analysis of the glassy carbon microspheres had shown no impurities but oxygen and sulfur, and there was no reason to expect contamination of the vapor-deposited coatings, significant error in the measured susceptibility could be introduced by an extremely small

---

*The gauss is the cgs unit of magnetic flux density B which is related to field intensity H in oersteds by $B = \mu H$. In free space μ is unity so that B and H are numerically equal. While not strictly correct in other media, units of gausses and oersteds are commonly used interchangeably in the literature.

concentration of ferromagnetic impurity. With the Faraday technique an extrapolation method due to Honda and Owen and described by Bates [125] can be used to show the absence of ferromagnetic impurities or to correct for their presence. In this method susceptibility is measured as a function of field strength and $\chi_{apparent}$ is plotted against 1/H. Extrapolation of this plot to infinite field strength or 1/H = 0 gives the true susceptibility. If the plot is a horizontal straight line, susceptibility is not a function of field strength and there is no ferromagnetic contribution. Honda-Owen plots of all specimens used in this work are given in Appendix II. No field strength dependences were evident so no impurity corrections were necessary. The Honda-Owen plots, of course, give no information about paramagnetic or diamagnetic impurities, but these are unimportant in small concentrations.

As indicated previously all carbon susceptibility measurements in this work were made on integral coated particles (approx 0.2-g samples). Since the glassy carbon kernels were known to be essentially isotropic, and any preferred orientation in the coating would be averaged by the radial symmetry, each coated microsphere as a whole can be assumed magnetically isotropic. Thus the mean susceptibility $\overline{\chi}$ which is determined for an anisotropic block by taking one-third of χ_T, the total of measurements in three orthogonal directions, is obtained by a single measurement on the microspheres.

The actual weight change induced by the magnetic field in each measurement, after correction for the sample holder, was corrected for the contribution of the glassy carbon kernels. The kernel weight fraction (obtained from coating weight fractions shown in Table I) of each lot was known from the charge and product weights observed in specimen preparation, and kernel susceptibility, shown in Table II, was measured independently and shown to be invariant with further heat treatment.

Density

Density measurements were made on microsphere coating fragments by a gradient column technique [126–129]. The basic apparatus, depicted schematically in Fig. 3, includes a glass column and a mixing system which can fill it with a liquid mixture increasing linearly in density from top to bottom. The density scale is obtained from the positions of density standards. In this system 50-ml burets were used to contain the gradient columns. The buret graduations were used directly for reading specimen and standard positions, thereby avoiding the time consuming task of aligning a cathetometer for each reading. Two burets were used for each set of measurements to cover the density range involved. With standards at approximately 0.1 g/cm^3 intervals, the low-density column covered the range 1.4 to 1.8 g/cm^3 and the high-density column overlapped slightly with the range 1.8 to 2.2 g/cm^3. With the 50-ml scale (approx 50 cm) the

Table II. Deposition Conditions and As-Deposited Properties of Experimental Carbons

Specimen	Deposition Conditions				As-Deposited Properties					
	Temperature (°C)	Hydrocarbon in He (%)		Hydrocarbon Flux ($cm^3/min\text{-}cm^2$)	Density (g/cm^3)	$\bar{\chi}$ (-10^{-6} emu/g)	$\bar{d}_{(004)}$ (Å)	$L_{a(10)}$ (Å)	BAF[a]	Hydrogen Content (ppm)
C-12	1150	C_3H_6	100	2.0	1.992	1.33	3.47	33	1.01	1590
C-13	1150	C_3H_6	16.7	0.5	2.041	1.34	3.46	32	1.02	1110
C-7	1150	C_3H_6	3.2	0.1	2.072	1.42	3.46	33	1.53	700
C-1	1250	C_3H_6	100	2.0	1.960	1.48	3.46	36	1.03	850
C-3	1250	C_3H_6	16.7	0.5	1.886	1.57	3.46	35	1.06	640
C-4	1250	C_3H_6	3.2	0.1	1.708	1.74	b	36	1.14	440
C-8	1300	CH_4	3.2	0.1	1.422	2.28	3.51[c]	39	1.62	280
C-5	1350	CH_4	19.4	0.6	1.571	2.21	3.50[c]	40	1.12	380
C-6	1350	CH_4	6.5	0.2	1.406	2.62	3.50[c]	43	1.16	290
C-9	1550	C_3H_6	40	1.0	1.467	2.95	3.44	51	1.04	180
C-10	1900	CH_4	40	1.0	1.681	6.27	3.43	82	1.00	b
C-11	1900	CH_4	3.2	0.1	2.094	8.13	3.43	87	1.24	b
GC Kernels	HTT 3000				1.25	4.99	3.42	60		

[a]Average of two measurements (see Appendix III).

[b]Not measured.

[c]Measured on (002) because (004) was not sufficiently developed.

ORNL-DWG 73-6458

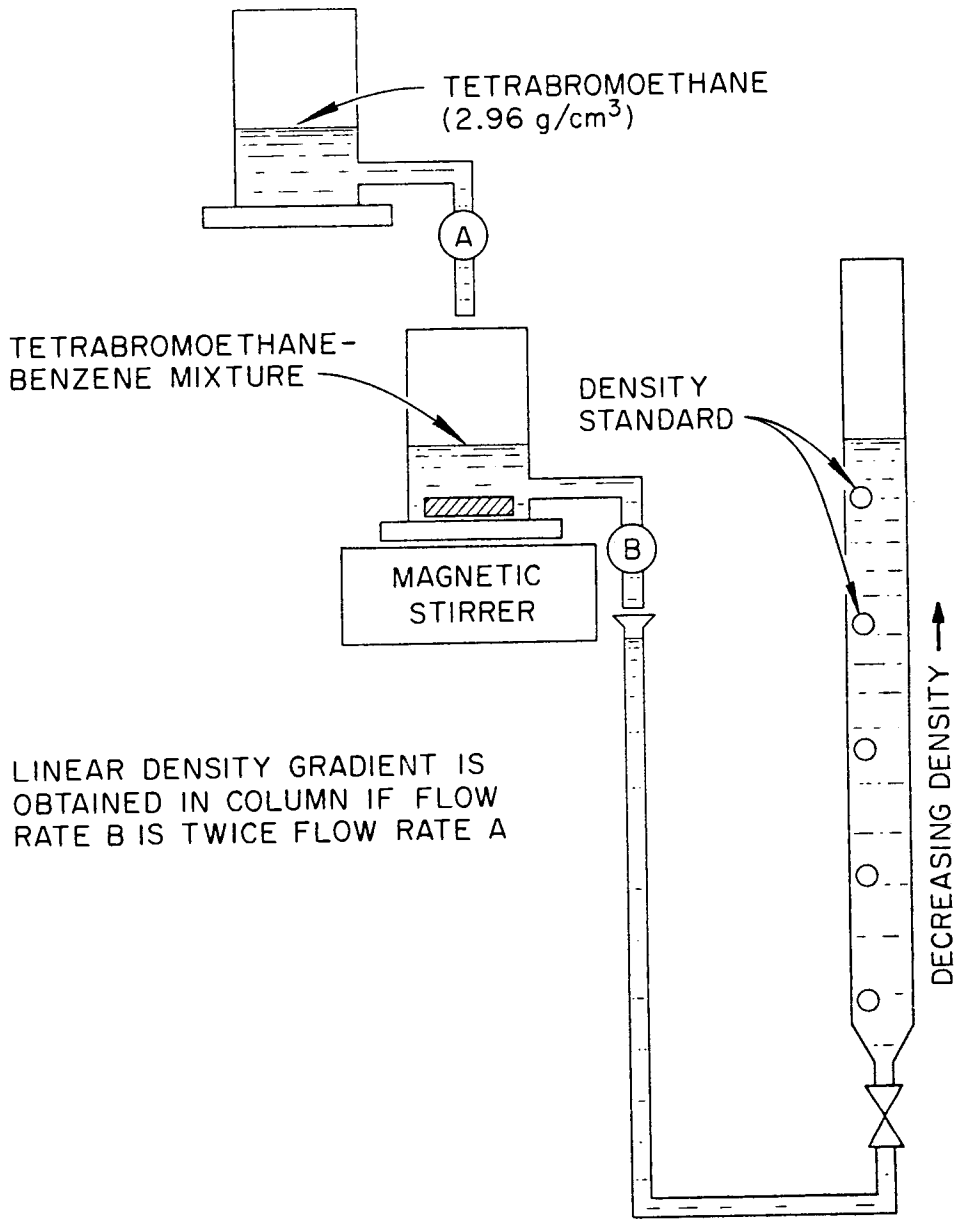

Fig. 3. Density Gradient Column.

density gradient was about 0.01 g cm^{-3} cm^{-1} if the standards were arranged to linearly cover the full scale length, and each scale division represented about 0.001 g/cm^3. On this scale the third density figure after the decimal can be read with ease and a fourth estimated. Practice in column filling technique did allow building nearly linear gradients and positioning the standards appropriately to take advantage of the full buret scale length. A further advantage of the burets was that they could be filled directly through the bottom thus avoiding the need to disturb the column by withdrawing a fill tube.

The filling technique involves flowing a heavy liquid into a stirred reservoir of low-density liquid which is being drained into the column. In principle the effluent from the stirred reservoir will increase linearly in density with time if its flow rate is exactly twice the inflow of heavy liquid [126]. In practice this is difficult to achieve, but was approximated in this work by use of an adjustable orifice to set the heavy-liquid flow at about half the mixture flow rate into the column. No adjustments were made during the filling of a column. The preset orifices, however, did not maintain constant flow rates. The heavy-liquid flow rate varied with hydrostatic head and the mixture flow, while essentially independent of head due to the action of the stirrer, decreased with increasing density (viscosity). Fortunately these changes were in the same direction so that the ratio did not change greatly.

The liquids used in this work were tetrabromoethane (2.96 g/cm^3) and benzene (0.78 g/cm^3). The tetrabromoethane, which was used undiluted as the heavy liquid, was repeatedly recycled by evaporating out the benzene. Incomplete elimination of the benzene resulted in a slightly reduced heavy-liquid density (approx 2.88 g/cm^3) after recycling, but this was unimportant since all specimen densities were less than 2.2 g/cm^3. The light-liquid reservoir in each case was filled with a mixture having a density 0.1 g/cm^3 lower than the lowest density standard in the column to provide the appropriate range. The standards were placed in the buret prior to filling so that their positions could be observed during filling and the flow could be stopped at the proper point. This also avoided disturbing the column by dropping in standards after filling.

The "standards" used were glass spheroids purchased from a commercial source* which had calibrated their densities to five significant figures. However, some of the calibrations were found to be in error; one was wrong by nearly 0.4%. Accordingly, all standards were carefully recalibrated by the sink-float method, and results are tabulated in Appendix IV. This entailed matching the density of a liquid mixture to that of the standard and then measuring the liquid density by the pycnometric method. A crystal of NaCl was

---

*Tecam density floats for density gradient column, manufactured by Techne, Inc., 661 Brunswick Pike, Princeton, N.J.

also measured to check the accuracy of this technique and the density obtained was within 0.005% of the handbook value. Absolute densities determined by the gradient column technique can, of course, be no better than the standards.

Specimens used for all density measurements were microsphere coating fragments. Measurements were made on coatings removed from the kernels after heat treatment in selected cases as a check on the constraint effects of the rigid kernel and spherical geometry, but all other coatings measured had been removed from the kernels prior to heat treatment. Some of the coatings had porosity near the outer surface which could trap air bubbles and lead to apparent densities lower than the true values. Therefore, all specimens were evacuated in a test tube and immersed in a liquid mixture of approximately the coating density prior to being introduced into the gradient column. The coating fragments used could be observed easily with the unaided eye and sank in the column to nearly their equilibrium density levels within about 10 min. However, in all cases at least 1 hr was allowed for settling before readings were taken. The position of each specimen was taken as the average of five pieces. Readings of all specimens and standards were made in sequence from top to bottom for each column to minimize error due to temperature fluctuations.

X-Ray Diffraction

Structural parameters except preferred orientation were examined by the standard Debye-Scherrer diffraction method using nickel-filtered copper radiation. The small, 57.3-mm-diam Norelco cameras with the Straumanis film arrangement were used throughout. These small cameras were deemed to provide adequate precision for this work and reduced the long exposure times required on the very poorly graphitic carbons to half that needed with the 114.6-mm camera. Even so, exposure times ranged up to 8 hr for the as-deposited materials. The film used was Kodak industrial x-ray film, type AA which is a fine-grain, high-contrast film of intermediate speed. The specimens were single pieces of microsphere coating glued to the end of a glass fiber which did not intercept the x-ray beam and rotated during exposure. As in the density measurements, most of the coatings studied had been removed from the kernels prior to heat treatment.

The principal parameters sought from the Debye-Scherrer films were average interlayer spacing $\overline{d}$ and crystallite size L_a. The films were examined with a direct manual reader to obtain the position of the (004) line for $\overline{d}$ determination and the (10) or (100) when resolved for computing L_a by the Warren displacement method [20]. A film dimensional change correction was made from the positions of a pair of fiducial marks placed 158.90 mm apart on the film before processing. The accuracy of the fiducial mark correction was verified by

comparison with a Straumanis correction on a graphite pattern which had readable back-reflection lines. The Straumanis correction could not be applied directly to the PC films because of the poor development of back-reflection lines. Only a few as-deposited and low-HTT specimens failed to provide a readable (004) line, in which case the (002) was read, and $\bar{d}$ values were obtained using the Bragg equation $n\lambda = 2d \sin \theta$. Since the (004) is a second-order reflection $\bar{d} = \lambda/\sin \theta$, where $\lambda = 1.542$ Å, the weighted average Cu K_α wavelength. The (004), which is the highest angle basal reflection readable for these materials, affords better precision than the much stronger (002) peak.

The L_a values determined from the (10) or (100) positions by Warren's formula

$$L_{a(10)} = 0.16\lambda/\Delta(\sin \theta) ,$$

where $\Delta(\sin \theta)$ refers to the shift from the graphite (100) line position, seemed to vary erratically. The films were then scanned with a recording microdensitometer* to obtain patterns which could be used for line broadening measurements. Such traces can be analyzed quantitatively because film density is a linear function of exposure (within a suitable range) and the densitometer scale is linear with optical density. Apparent crystallite diameter L_a values were

---

*Joyce-Loebl MKIIICS double-beam recording microdensitometer.

determined by the method discussed by Klug and Alexander [130] from the densitometer traces. This involved applying the Scherrer equation $L_a = K\lambda/\beta \cos \theta$, where λ is the x-radiation wavelength, β is the corrected half-height width of the (10) peak in 2θ radians, θ is the Bragg angle, and K is a shape factor constant shown by Warren [20] to be 1.84 for the case of two-dimensional layer diameters. The pure diffraction broadening β was obtained from the relationship $\beta^2 = B^2 - b^2$, where B is the total measured line broadening and b is the instrumental broadening, determined in this study from the (100) line width of a well-graphitized, high-temperature PC of very large crystallite size. The instrumental broadening thus determined was about 1° 2θ. This correction ranged from essentially no change in the smallest to about 10 Å in the largest L_a values measured. Strictly speaking, this correction is valid only for a Gaussian peak, which the (10) peak is not, but the correct was small or negligible in each case and should not introduce significant relative error. No attempt was made to correct for strain broadening, and the polarization error due to the large breadth has been shown to be unimportant [130].

The half-height width was determined for the (10) peak of all specimens which showed no modulation of the two-dimensional reflections. At HTT above 2250°C, (10) modulation, indicative of the onset of layer ordering, was observed in some specimens and meaningful width measurement of this peak could not be made. The (100) line was not sufficiently

resolved for measurement in any of these cases, and the (110) was too narrow for even roughly accurate separation of instrumental broadening. For the (10) broadening measurements, peak height was determined with respect to a straight-line estimate of the background. The half-height breadth was taken as the horizontal projection of a line drawn parallel to the base line at half the peak height.

Preferred orientation measurements were made on the as-deposited flat-plate specimens by a modified Bacon technique [108] using a monochromatic-pinhole camera and nickel-filtered copper radiation. This method for determining the Bacon anisotropy factor (BAF) is based on the work of several investigators. The original method developed by Bacon [108] for bulk graphites is based on the orientation dependence of individual crystallite contributions to an averageable property coefficient (e.g., thermal expansion). Then the value of the property in any arbitrary direction inclined at the angle ϕ to the z-axis direction is

$$\sigma(\phi) = \sigma_a \sin^2 \phi + \sigma_c \cos^2 \phi ,$$

where σ_a and σ_c are the property coefficients in the crystallite a- and c-directions, respectively. After obtaining suitable expressions for the property coefficient in the z- and xy-directions, and assuming that $\sigma_a = 0$, Bacon derived an anisotropy factor

$$BAF = \frac{\sigma_z}{\sigma_{xy}} = \frac{2\int_0^{\Pi/2} I(\phi)\cos^2\phi\sin\phi\, d\phi}{\int_0^{\Pi/2} I(\phi)\sin^3\phi\, d\phi},$$

where $I(\phi)$ is the density of crystallite c-axes per unit solid angle that makes an angle ϕ with the normal to a reference plane. Bokros [106] showed that the cylindrical symmetry of pyrolytic carbons allowed this technique to be applied conveniently to flat-plate specimens prepared in a fluidized bed. Tassone [131] further modified the technique to avoid the time-consuming $I(\phi)$ distribution analysis and showed empirically that accurate BAF determinations could be made with only two $I(\phi)$ measurements. He obtained the maximum intensity $I(0°)$ and the minimum $I(90°)$ and plotted the ratio $I(90°):I(0°)$ against BAF's determined by complete $I(\phi)$ curve analysis. This produced an empirical curve requiring only measurement of the ratio $I(90°):I(0°)$ for further BAF determination. Ergun and Schehl [132] have verified Tassone's empirical curve on a theoretical basis.

In the present work the specimen plate was positioned immediately in front of a 0.4-mm beam collimator and oriented at the Bragg angle for the (002) reflection, approximately 13°, to the x-ray beam. Each specimen was x-rayed in two positions, with the beam striking the outer surface first and with the beam striking the substrate side first. This was done to check for anisotropy gradients since the relative absorptions from front to back of the specimen are not the same at 0 and 90°. Bokros has shown [107] that the

absorption with this technique is maximum at 62°, but that absorption at 0 and 90° is negligibly different. However, this assumes that the specimen is homogeneous. BAF values determined for both irradiation positions are shown in Appendix III. The values in Table II are the average of these two values.

A specimen-to-film distance of 7.5 cm provided a diffraction circle of appropriate size. The exposure was made on Kodak no-screen medical x-ray film, a high-speed, medium contrast film, in 2 to 6 hr depending on specimen type. The (002) diffraction ring obtained on each film was then scanned radially at 0 and 90° with a microdensitometer to plot intensity profiles which could be used for determination of a BAF by Tassone's method. The integrated intensity was obtained from each plot by cutting out and weighing the paper between the densitometer plot and a straight-line estimate of background. BAF values were determined from the I(90°):I(0°) ratios obtained and Tassone's BAF curve as verified by Ergun and Schehl. The curve is reproduced in Appendix III.

Hydrogen Analysis

Hydrogen content was determined by heating 2- to 4-g samples of the coated microspheres under vacuum and collecting the evolved hydrogen in a calibrated volume. Specimens were held in an inductively heated graphite crucible for 90 min at 800°C to outgas both specimen and crucible, then heated to

2000°C with 30-min holds at 1300, 1600, and 2000°C. All gas collected after the 800°C outgassing was assumed to be hydrogen since no measurable release was observed for any specimen until it was heated to approximately its deposition temperature. Hydrogen content was calculated from the coating specimen weight and the measured gas pressure accumulated in the calibrated volume after 30 min at 2000°C.

Metallography

Specimens of the coated microspheres in the as-deposited condition and after heat treatment at 3000°C for 18 min were sectioned and polished and photographed under bright-field illumination and polarized light. Techniques used were similar to standard metallographic methods but have been developed extensively for examination of coated nuclear fuel particles [133].

Microradiography

X-radiographs were made of certain heat-treated (3000°C for 18 min) microspheres to check for the presence of voids formed between the kernels and coatings. This technique of contact microradiography also has been developed for examining coated nuclear fuel particles [134]. The x-ray source was a tungsten tube operated at 6 kV and 14 mA at a distance of 57 cm from the high-resolution photographic plate on which the microspheres rested. A helium-purged tube was used to minimize x-ray absorption over the large source-to-specimen distance.

CHAPTER IV

EXPERIMENTAL RESULTS

As-Deposited Properties

Characteristics of the twelve carbons produced by the fluidized-bed deposition process are shown in Table II along with the deposition conditions for reference. The as-deposited properties cover a very broad range which provides the basis for many comparisons of their graphitization behavior. Initial densities range from 1.406 to 2.096 g/cm^3, approximately 62 to 93% of the theoretical graphite density, respectively. Mean diamagnetic susceptibilities range from 1.33 in units of -10^{-6} emu/g, little more than the value for large aromatic molecules, to 8.13, well above the graphite single-crystal value of 7.33, and appear to be largely a function of deposition temperature. Two of the specimens, C-7 and C-8, have moderately high preferred orientations while having other properties comparable to certain other specimens. The other carbons all have low degrees of preferred orientation though only one, C-10, is totally isotropic. Apparent crystallite diameters range from 32 to 87 Å, with size largely a function of deposition temperature. Mean interlayer spacings range from 3.43 Å for the 1900°C deposits to 3.51 Å for C-8. However, the largest $\overline{d}$ value measured on an (004) line was 3.47 Å. For the 1300 to 1350°C methane deposits C-8, C-5, and C-6 the (004) was so poorly

developed that no measurements were possible. The $\bar{d}$ values of 3.50 to 3.51 Å were, therefore, obtained from the (002) without correction for low-angle scattering and may be slightly high.

Microstructures (As-Deposited)

Polished sections of the as-deposited microsphere coatings photographed under both bright-field and polarized light are shown in Fig. 4(a) through (l), along with corresponding photomicrographs of the particles after heat treatment for 18 min at 3000°C. Many differences in microstructure may be noted among the twelve as-deposited carbons. The high preferred orientations determined by x-ray technique on flat-plate specimens of C-7 and C-8 are clearly evident in the Maltese cross effect shown in the polarized light photomicrographs of the microspheres [Fig. 4(e) and (g)]. Qualitative determinations of anisotropy are commonly made from such photographs [118] and several studies have been directed at making the method quantitative [135–140]. Much lower anisotropies can be seen in the polarized light photomicrographs of C-13, C-4, C-5, and C-6 [Fig. 4(b), (f), (h), and (i)], while the other specimens appear essentially isotropic. It should be noted that the Maltese cross-like extinction under polarized light is indicative of macroscopic (if one may use this term with regard to millimeter-size bodies) or overall preferred orientation, which corresponds to the x-ray anisotropy, and is

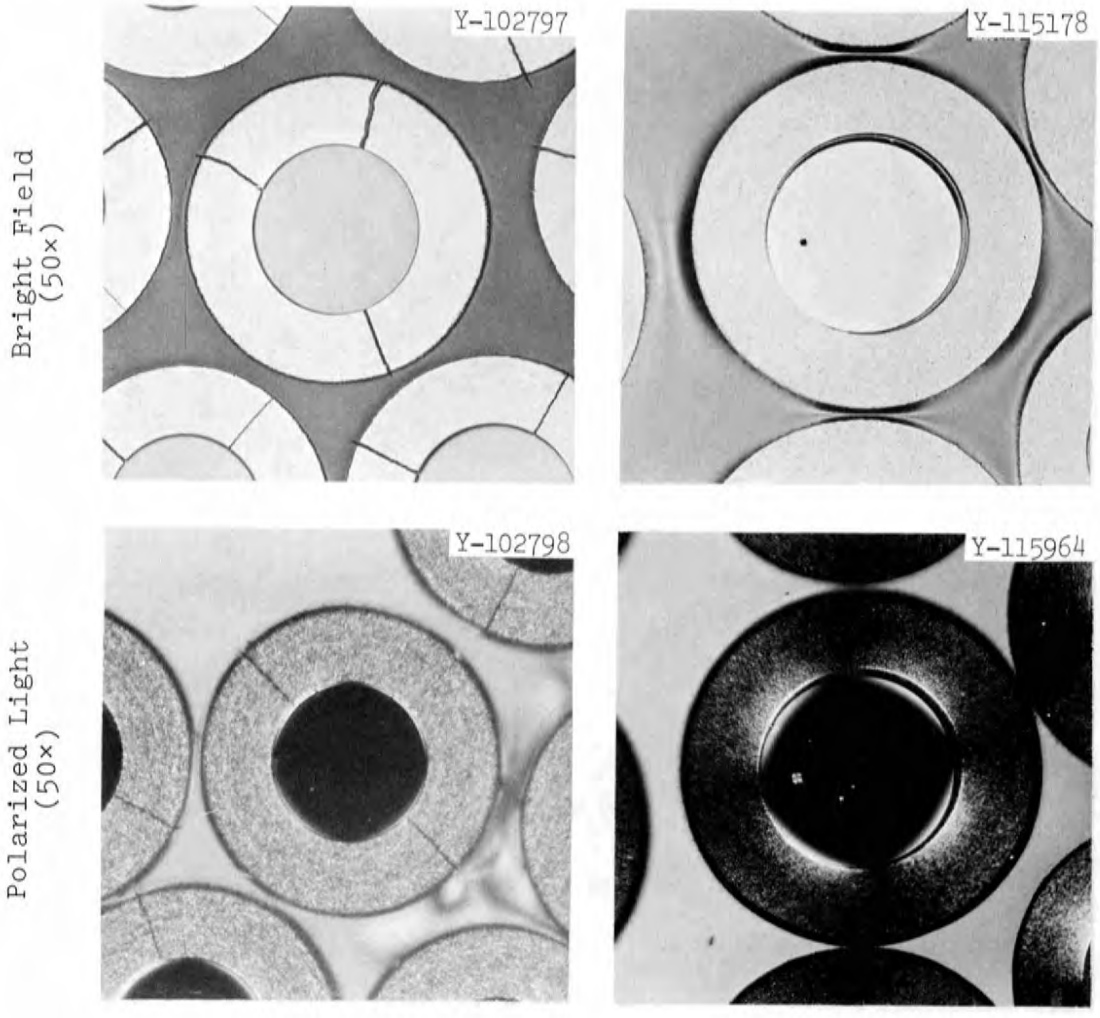

As-Deposited After 18 min at 3000°C

Fig. 4(a). Microstructure of Specimen C-12 As-Deposited and After Heat Treatment for 18 min at 3000°C.

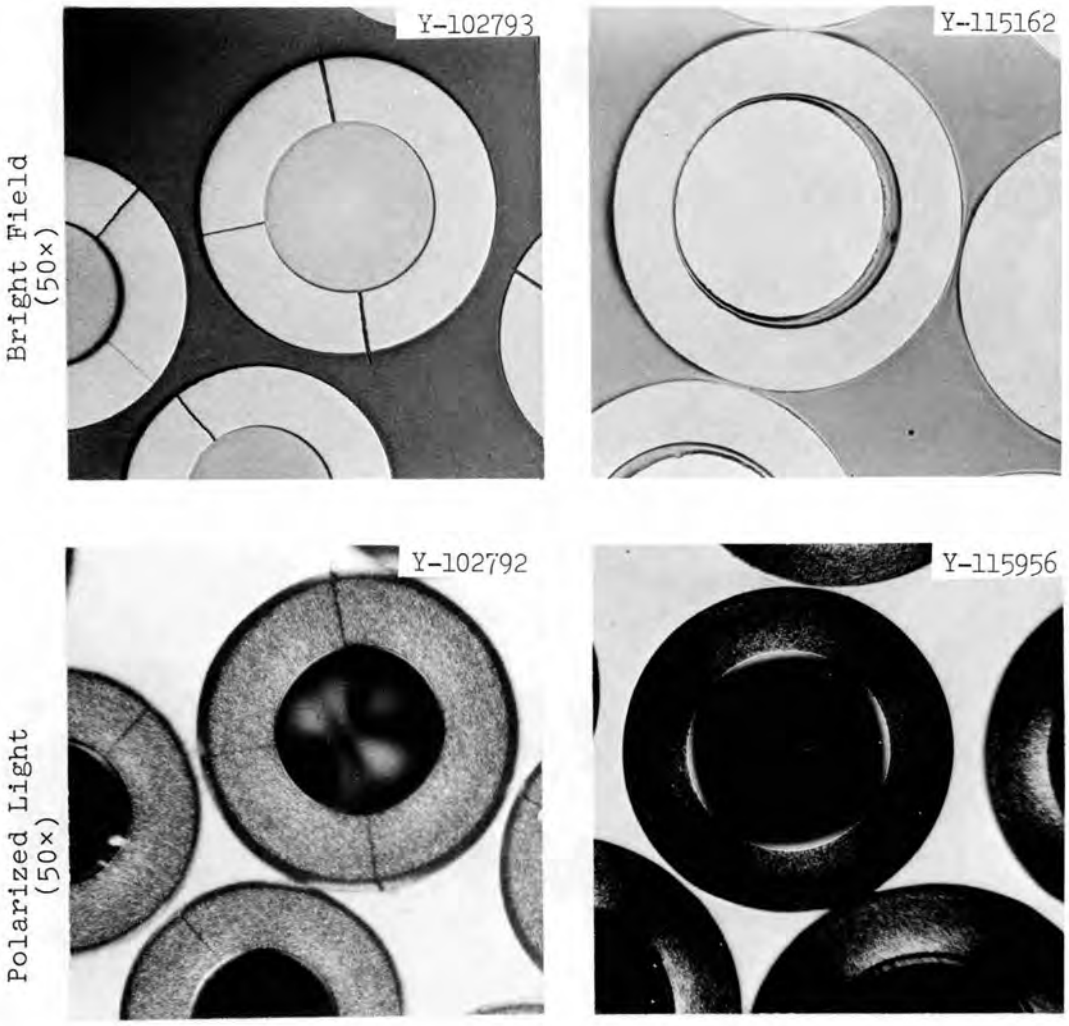

As-Deposited After 18 min at 3000°C

Fig. 4(b). Microstructure of Specimen C-13 As-Deposited and After Heat Hreatment for 18 min at 3000°C.

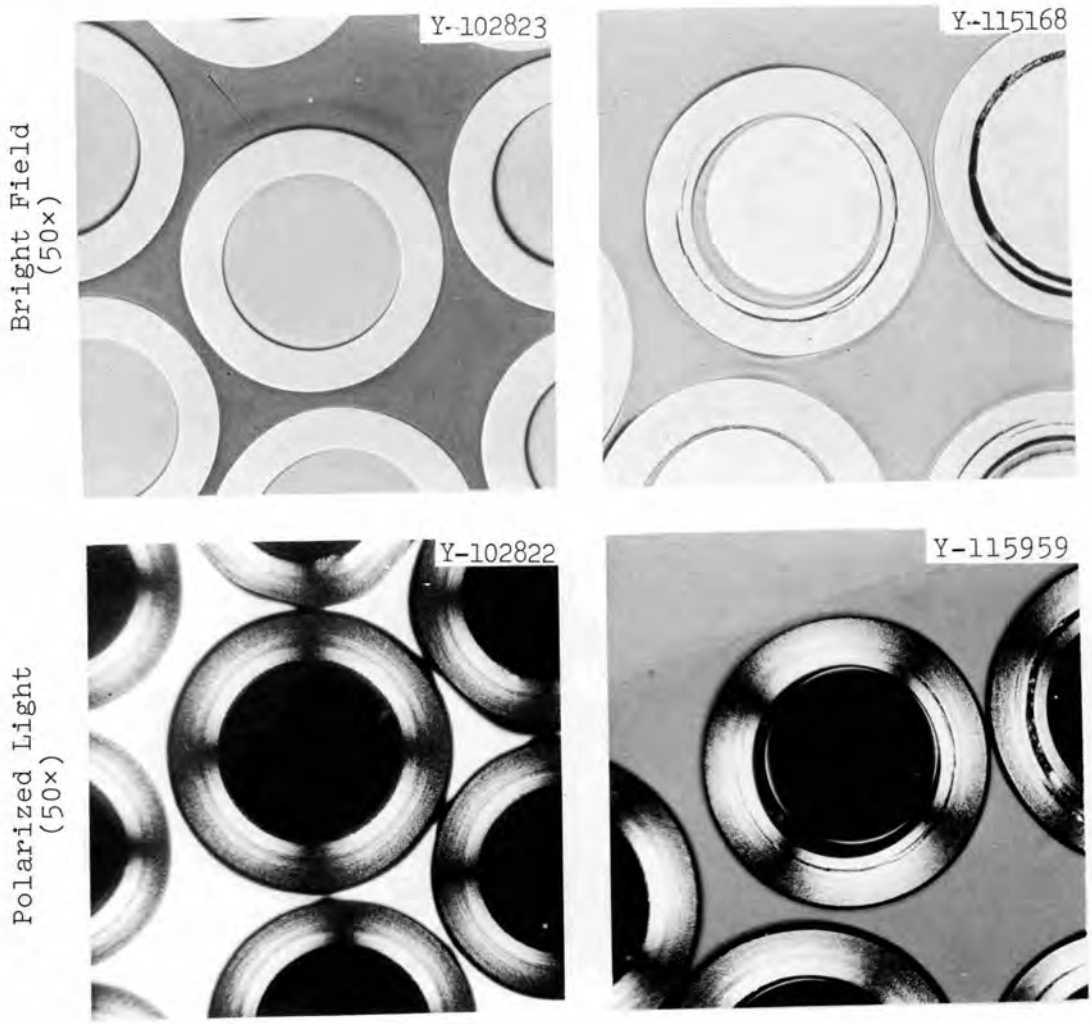

As-Deposited After 18 min at 3000°C

Fig. 4(c). Microstructure of Specimen C-7 As-Deposited and After Heat Treatment for 18 min at 3000°C.

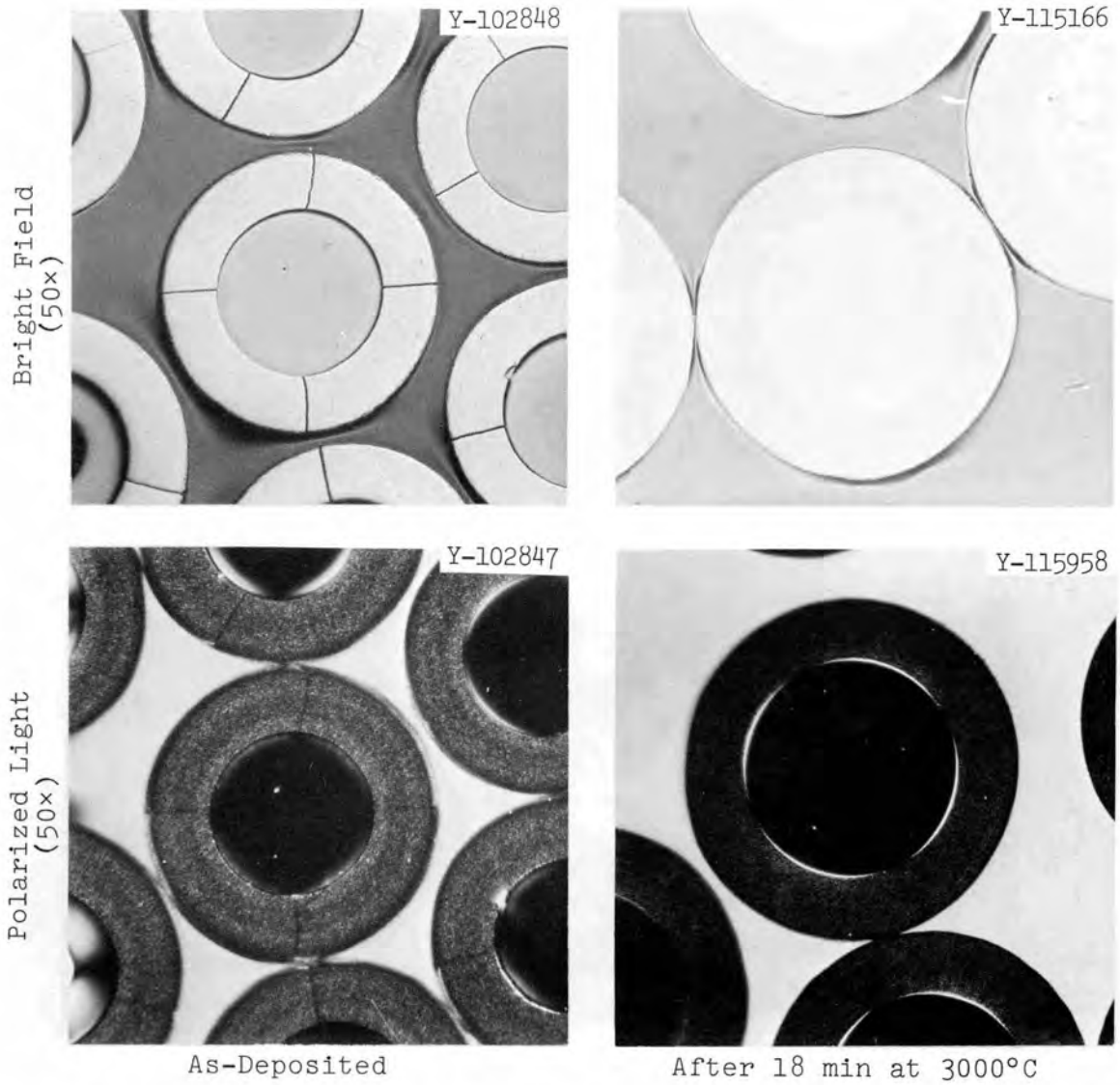

Fig. 4(d). Microstructure of Specimen C-1 As-Deposited and After Heat Treatment for 18 min at 3000°C.

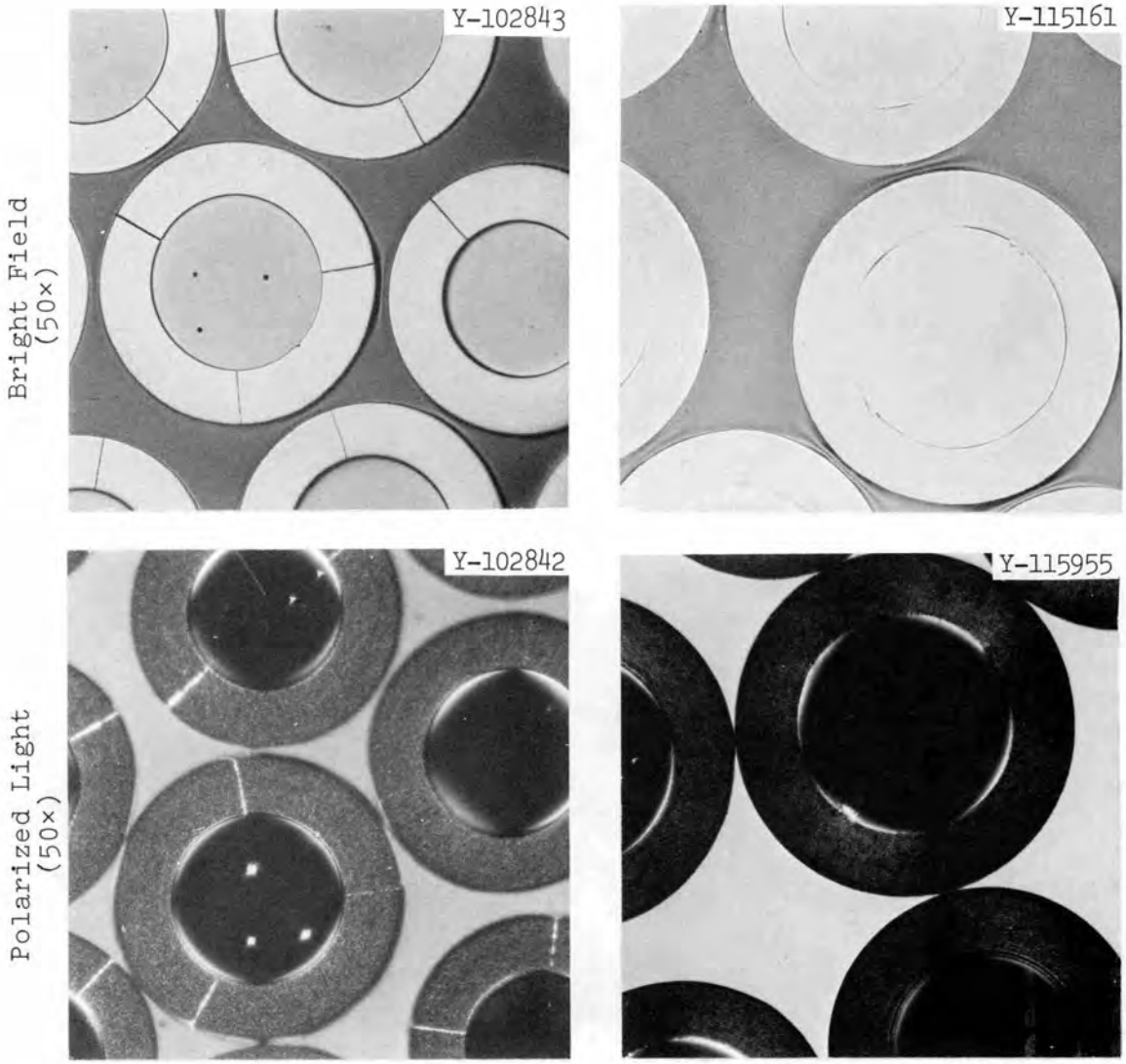

As-Deposited After 18 min at 3000°C

Fig. 4(e). Microstructure of Specimen C-3 As-Deposited and After Heat Treatment for 18 min at 3000°C.

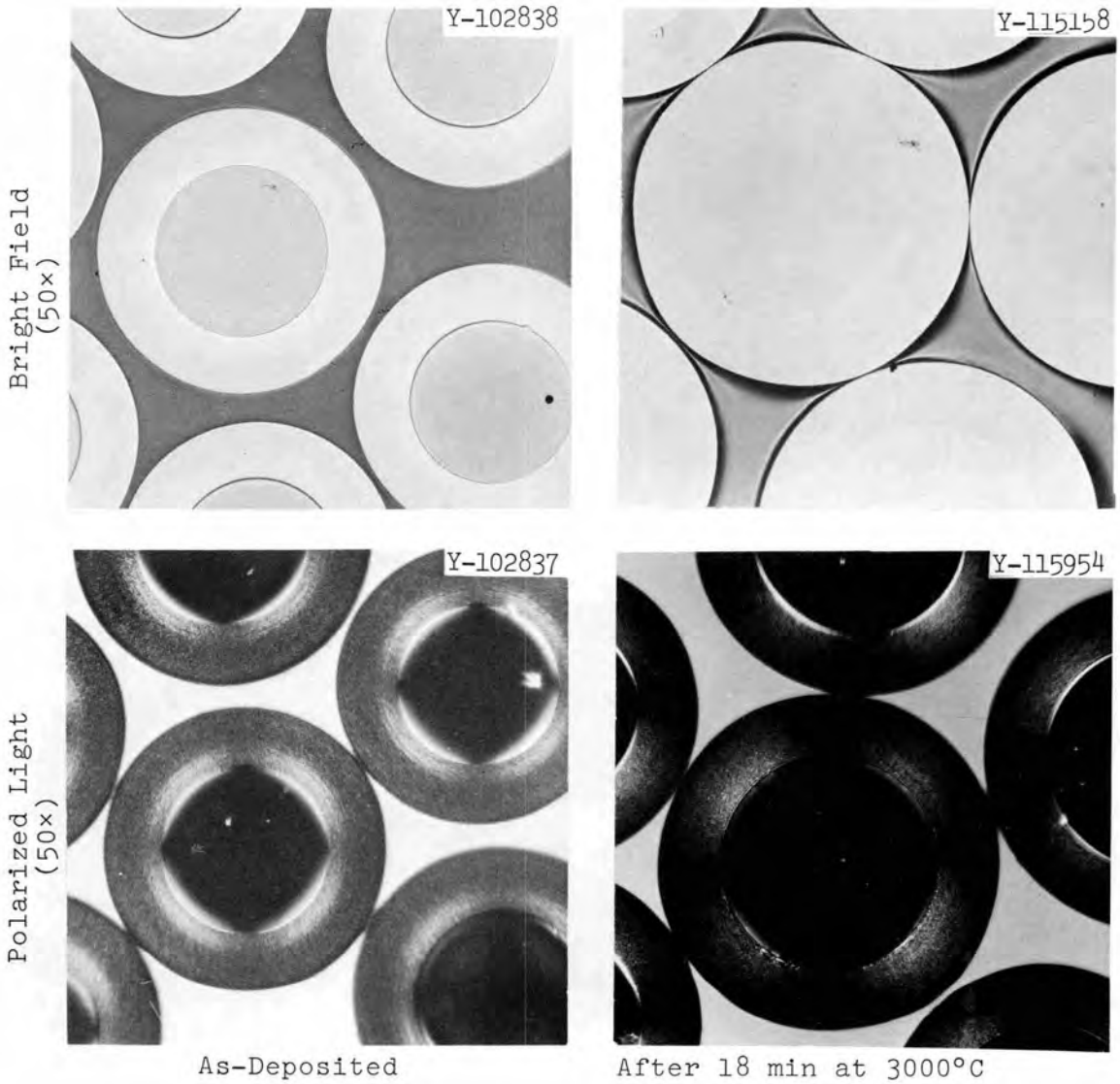

Fig. 4(f). Microstructure of Specimen C-4 As-Deposited and After Heat Treatment for 18 min at 3000°C.

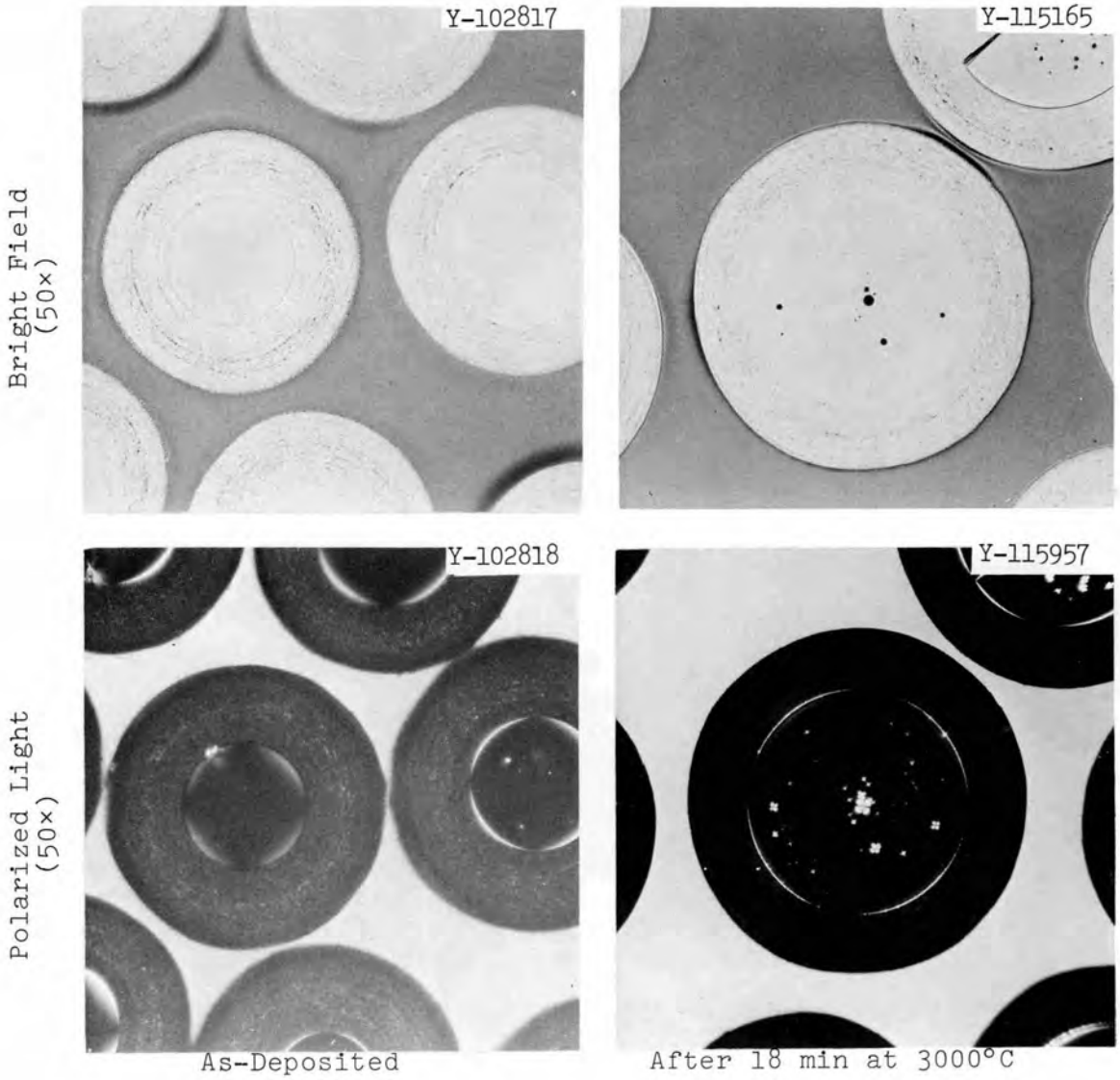

Fig. 4(g). Microstructure of Specimen C-8 As-Deposited and After Heat Treatment for 18 min at 3000°C.

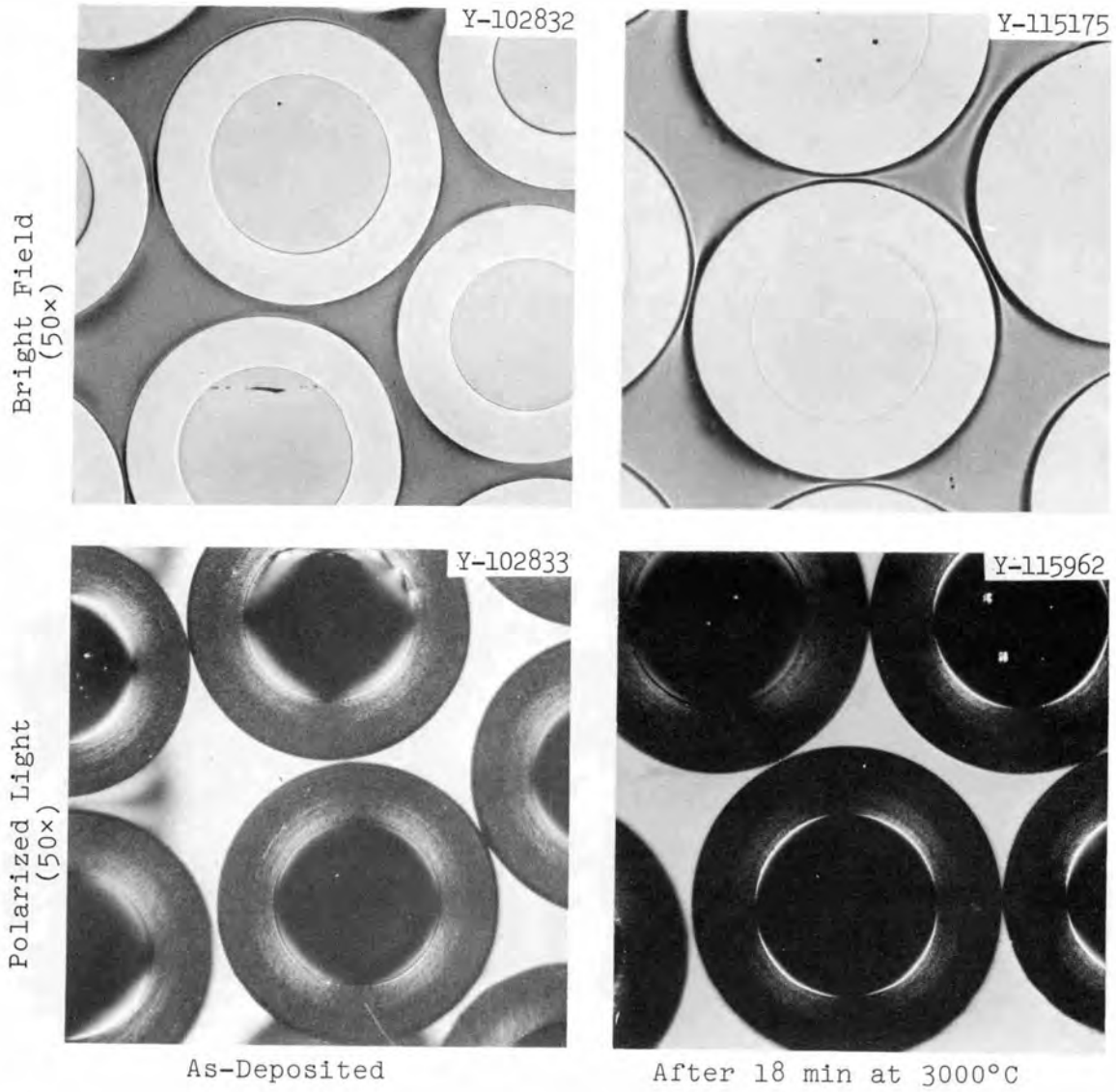

Fig. 4(h). Microstructure of Specimen C-5 As-Deposited and After Heat Treatment for 18 min at 3000°C.

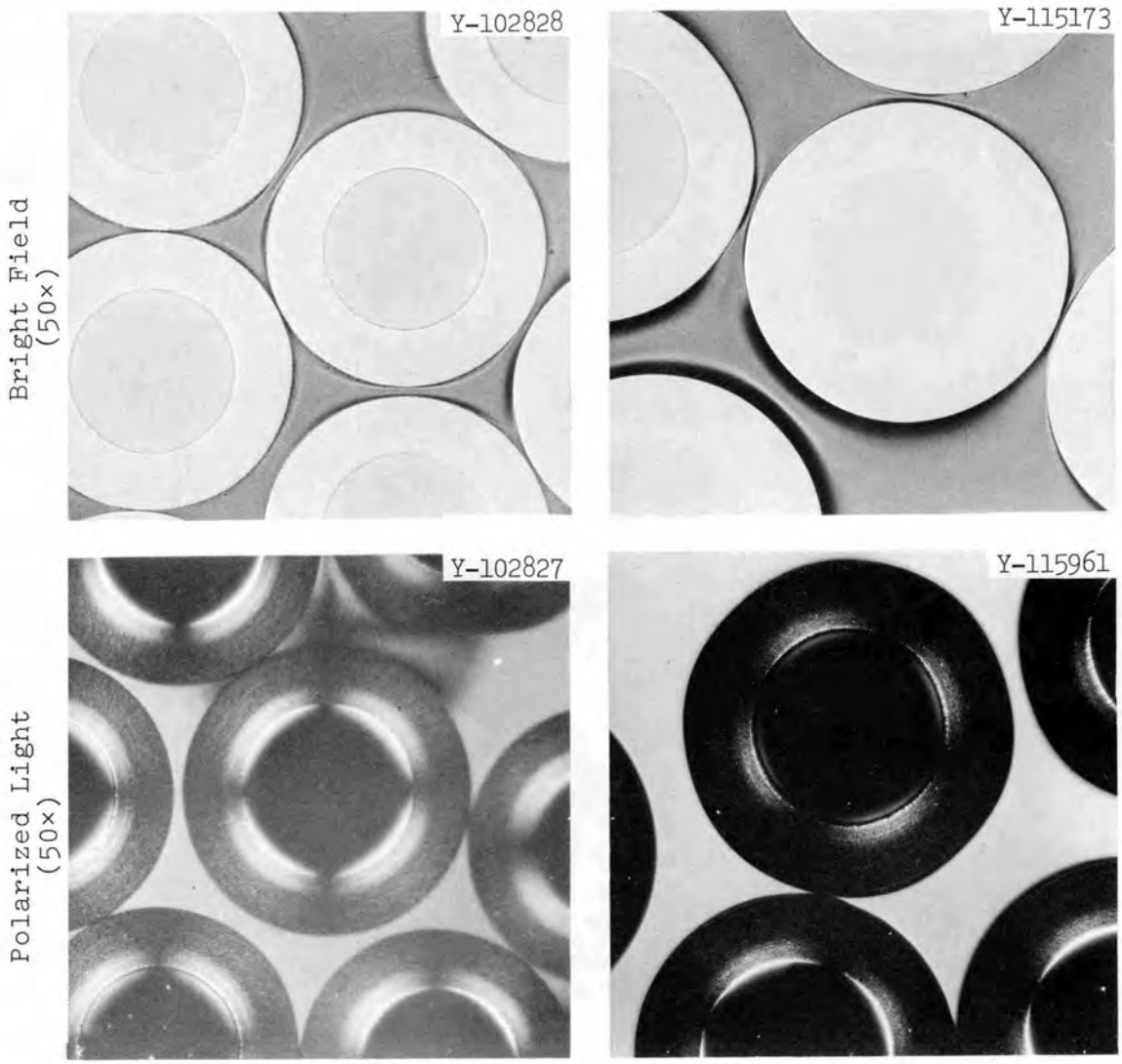

As-Deposited After 18 min at 3000°C

Fig. 4(i). Microstructure of Specimen C-6 As-Deposited and After Heat Treatment for 18 min at 3000°C.

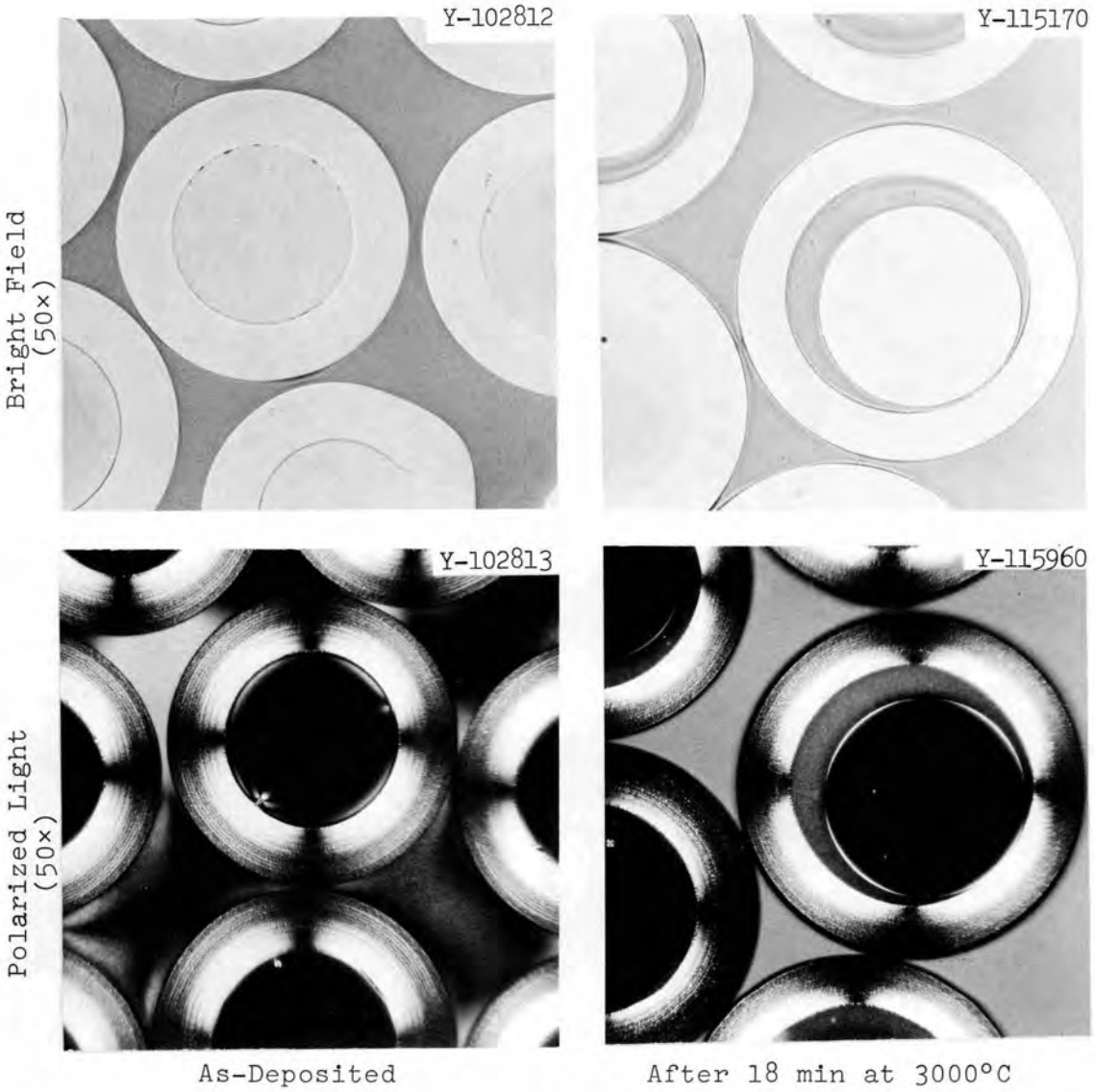

Fig. 4(j). Microstructure of Specimen C-9 As-Deposited and After Heat Treatment for 18 min at 3000°C.

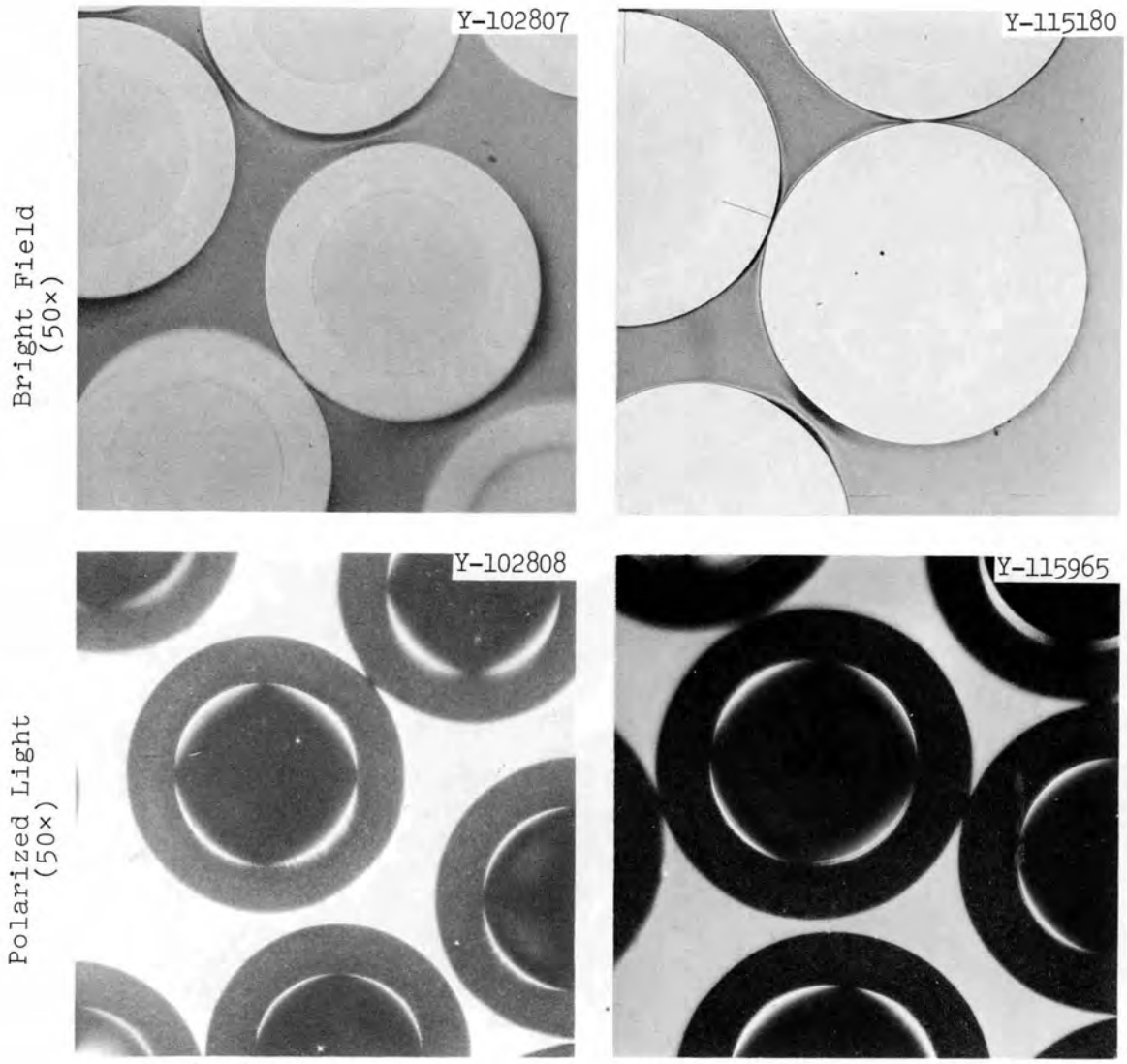

As-Deposited

After 18 min at 3000°C

Fig. 4(k). Microstructure of Specimen C-10 As-Deposited and After Heat Treatment for 18 min at 3000°C.

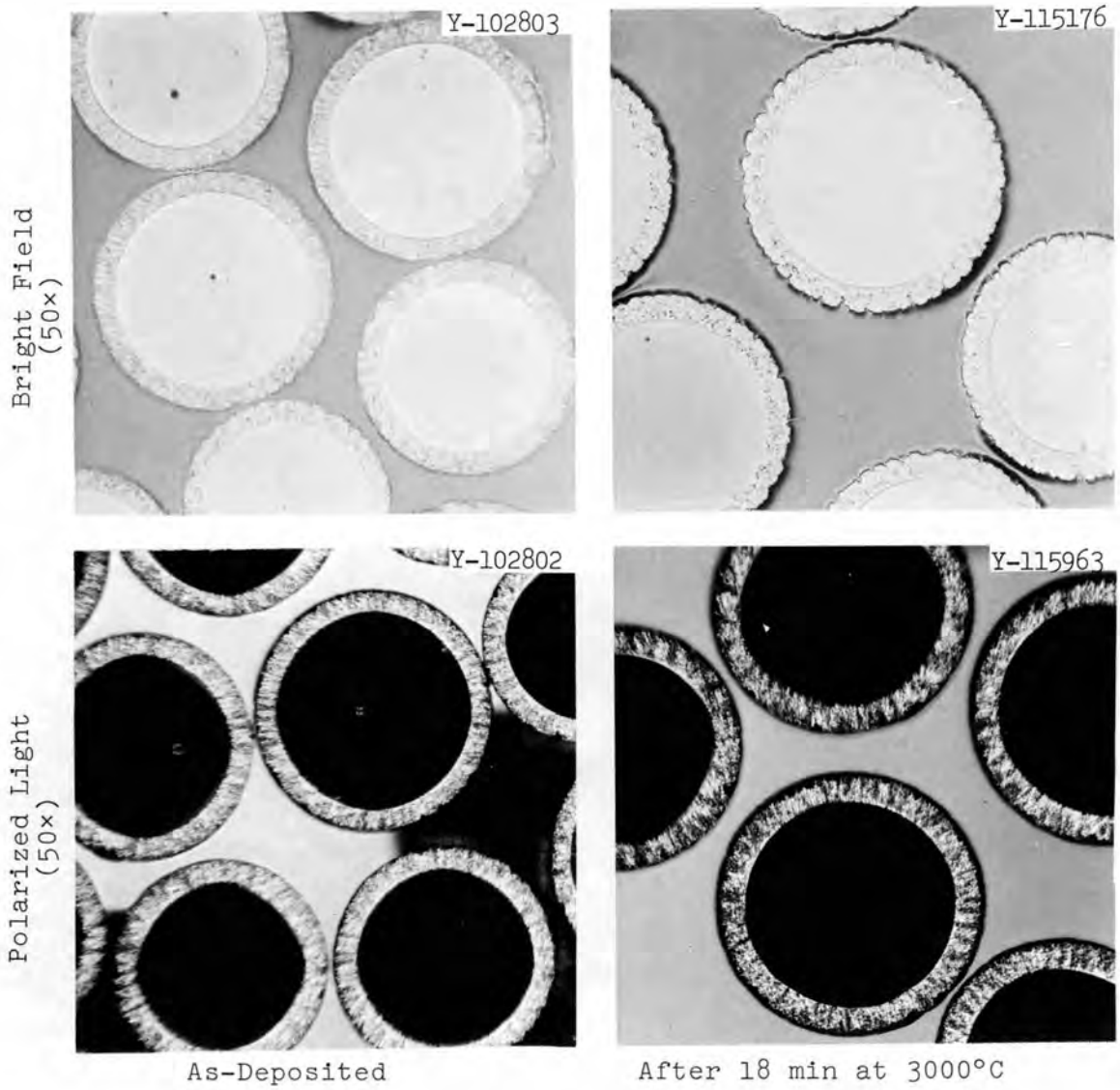

Fig. 4(1). Microstructure of Specimen C-11 As-Deposited and After Heat Treatment for 18 min at 3000°C.

not necessarily related to the microscopic anisotropy of small crystallite groups. The microscopic anisotropy referred to is evident in the optical activity of C-11, Fig. 4(l), and on a much finer scale in the 1150°C deposits C-12 and C-13, Fig. 4(a) and (b). The significance of this micro-anisotropy will be discussed later.

Other distinguishing features of the as-deposited microstructures include some apparent radial inhomogeneities in C-7, C-4, C-8, C-5, and C-6, best seen in the polarized light photographs, and a large amount of visible porosity in C-9, Fig. 4(j), shown clearly in the bright-field photograph. The radial inhomogeneities present in coatings deposited under nominally constant conditions may be accounted for in the following way. It has been well established by systematic fluidized-bed coating studies [4] that coating properties depend sensitively on a number of processing parameters. These include temperature, hydrocarbon species, concentration and flux, gas velocity or contact time, and bed surface area. Hydrocarbon concentration is easily controlled, and with due care, temperature can be well regulated. However, in depositing very thick coating layers such as those used in the present work, the bed surface area increases continuously, and the increasing particle mass requires increasing gas velocity to maintain adequate fluidization. Therefore, some changes in actual deposition conditions are unavoidable as the coating builds up. In some ranges of deposition conditions, these changes are relatively unimportant, but in

other ranges they result in some radial variation of coating properties. As will be shown later, these inhomogeneities are insignificant for magnetic susceptibility analysis, but can cause difficulty with density measurements.

The radial cracks in the C-12, C-13, C-1, and C-3 coatings which form during sectioning of the microspheres suggest the existence of large circumferential tensile stresses in the as-deposited coatings at room temperature. This in turn indicates that these coatings have higher thermal expansions than do the glassy carbon kernels if sizeable tensile stresses are to be developed on cooling from the deposition temperature.

Effect of Heat Treatment

The visible effect of heating for 18 min at 3000°C on the microstructure is significant in four of the twelve carbons, C-12, C-13, C-7, and C-8 [Fig. 4(a), (b), (c), and (g)]. The other specimens do not look very different as a result of this rather severe heat treatment. It should be noted that some of the microspheres are not ground down to the equatorial plane, resulting in apparent size differences before and after heat treatment. This discrepancy can be judged by the separation distance of the polished surfaces and from the polarized light photograph which allows viewing into the mount. There may also be small differences in actual magnification even though all magnifications are nominally the same. The most noticeable heat treatment effect on C-12,

C-13, C-7, and C-8 is the gap formed between the kernel and coating. Since the glassy carbon kernels had been stabilized by a similar heat treatment prior to coating, it can be assumed that they did not shrink during heating of the coatings. Also, gaps are not present inside the other coatings which were deposited onto kernels from the same lot. The gap then clearly resulted from circumferential growth of the coating during heat treatment. The presence of the gaps was verified by microradiography, shown in Fig. 5, to eliminate any question of their being metallographic artifacts. Differences in gap size shown by the two techniques may be attributed to the metallographic sections not being at the kernel midplane. The apparent correlatable property of these four specimens which caused them to expand circumferentially during heat treatment while the others did not, at least to a noticeable extent, is preferred orientation. The necessary preferred orientation was present in C-7 and C-8 as deposited, and a much smaller orientation was apparently induced in C-12 and C-13 during heat treatment. The greater anisotropy of the heat treated C-12 and C-13 coatings compared with their as-deposited counterparts can be seen readily in the polarized light photographs in Fig. 4(a) and (b). The circumferential delaminations formed in C-7 during heat treatment, visible in both the polished sections and the radiograph, is further evidence of radial inhomogeneity in that specimen.

Y-131511

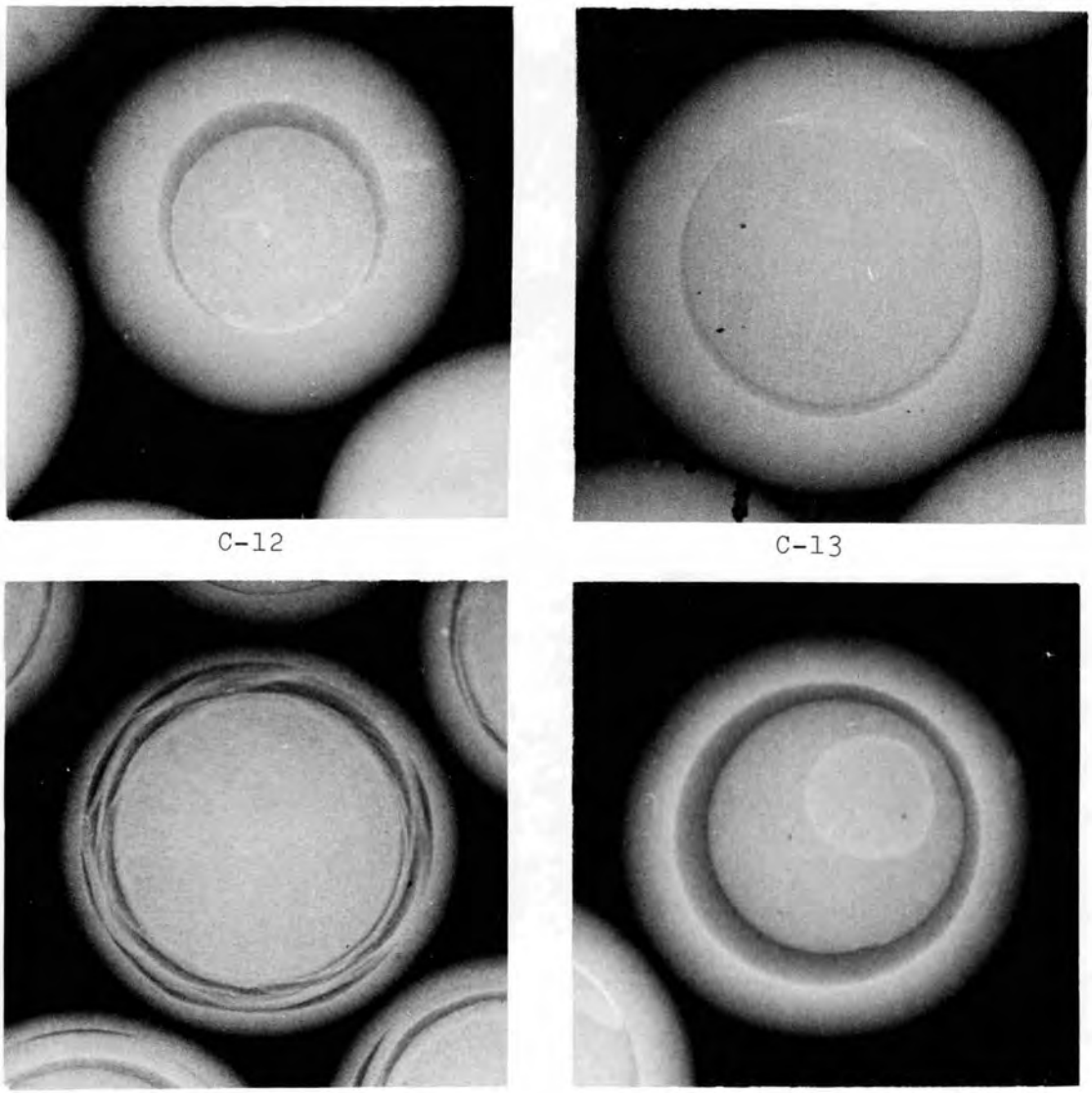

Fig. 5. Radiographs (75×) of Coated Microspheres After Heat Treatment for 18 min at 3000°C.

Effect of Heat Treatment on Properties

The thermally induced property changes of the twelve carbons studied are shown in Fig. 6(a) through (l) in the form of 18-min isochronal plots. Figure 6 contains corresponding plots of the density, crystallite size, interlayer spacing, and susceptibility data for easy comparison in the later discussion. The isochronal plots are a useful means of presenting a coherent picture of the change in different properties with heat treatment for each specimen. However, isothermal plots of density and susceptibility data were employed in all activation energy determinations, and representative isothermal plots are shown in Figs. 7 and 8(a) and (b). Complete tabulations of density and susceptibility data are given in Appendix V.

Density

The density change of each carbon as a function of heat-treatment temperature at constant time can be seen in the plots of Fig. 6. These data were taken from the 18-min points of the isothermal curves and were obtained from measurements on microsphere coatings removed from the kernels prior to heat treatment. Selected points, including the 3000°C end point, of each isochronal density plot were checked by measurements on coatings removed from the kernels after heat treatment. Within the measurement precision there was no difference in densification behavior due to the constraints

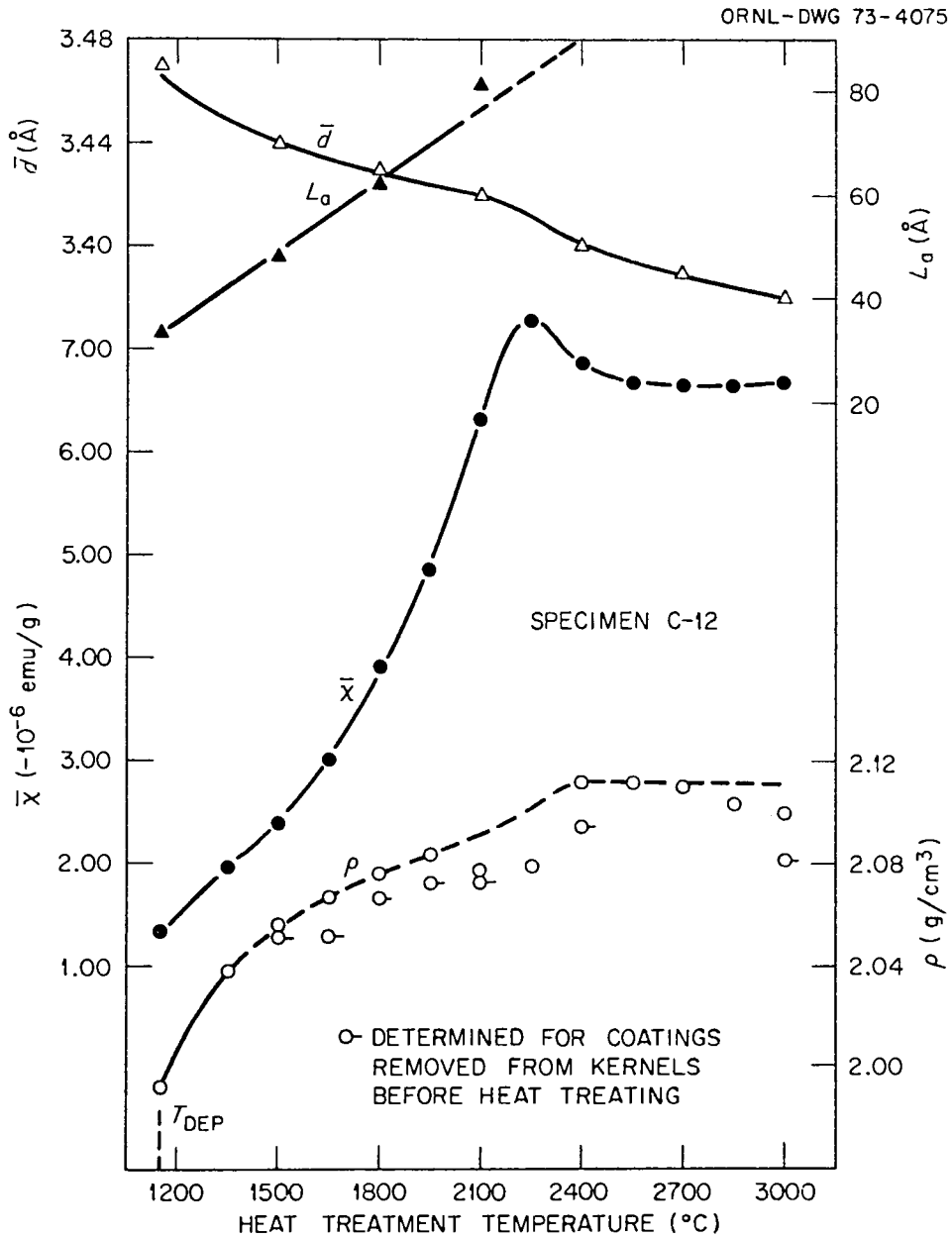

Fig. 6(a). Effect of Heat Treatment Temperature on Isochronal (18-min) Changes in: Density, ρ; Diamagnetic Susceptibility, $\bar{\chi}$; Crystallite Diameter, L_a; Interlayer Spacing, $\bar{d}$.

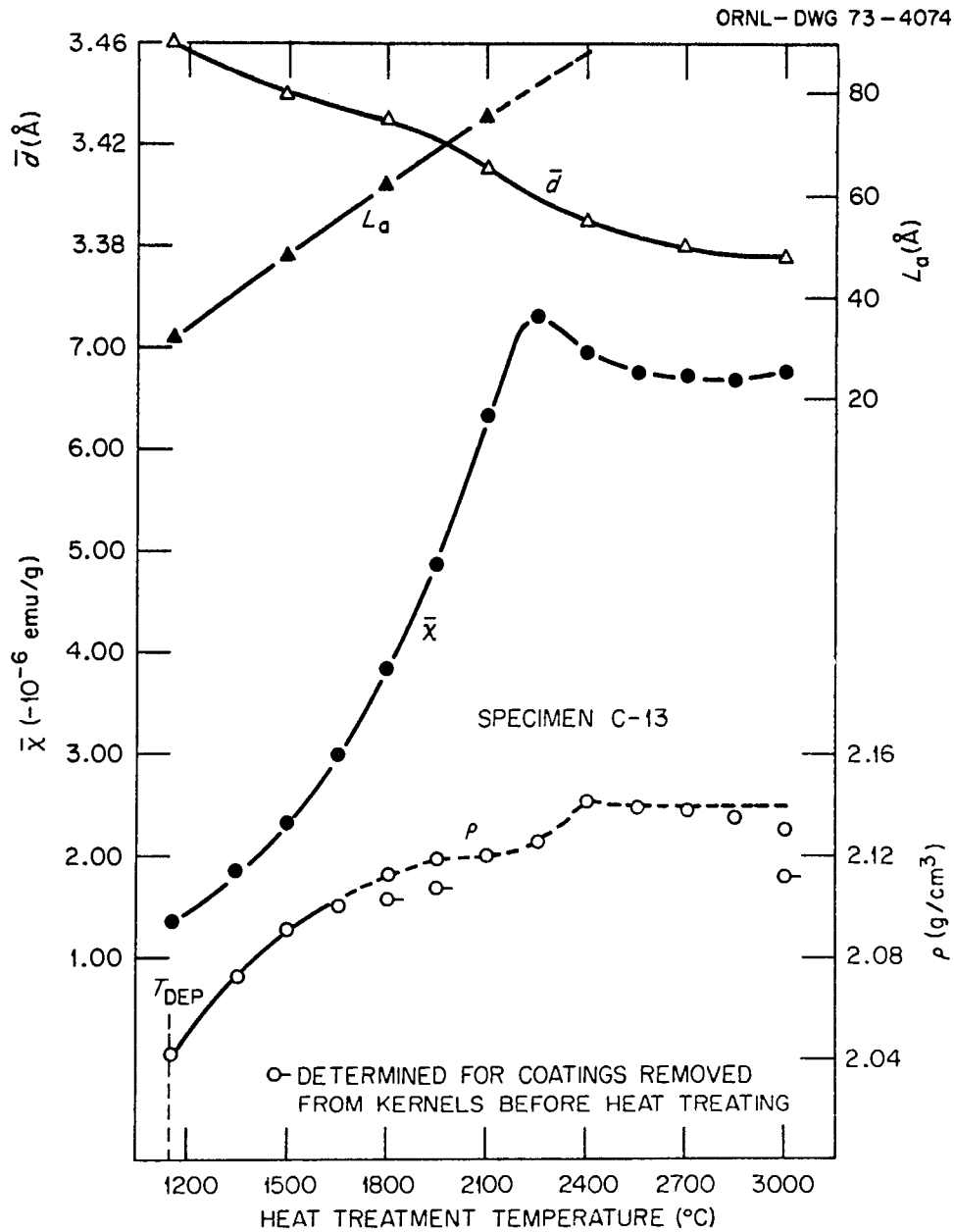

Fig. 6(b). Effect of Heat Treatment Temperature on Isochronal (18-min) Changes in: Density, ρ; Diamagnetic Susceptibility, $\bar{\chi}$; Crystallite Diameter, L_a; Interlayer Spacing, $\bar{d}$.

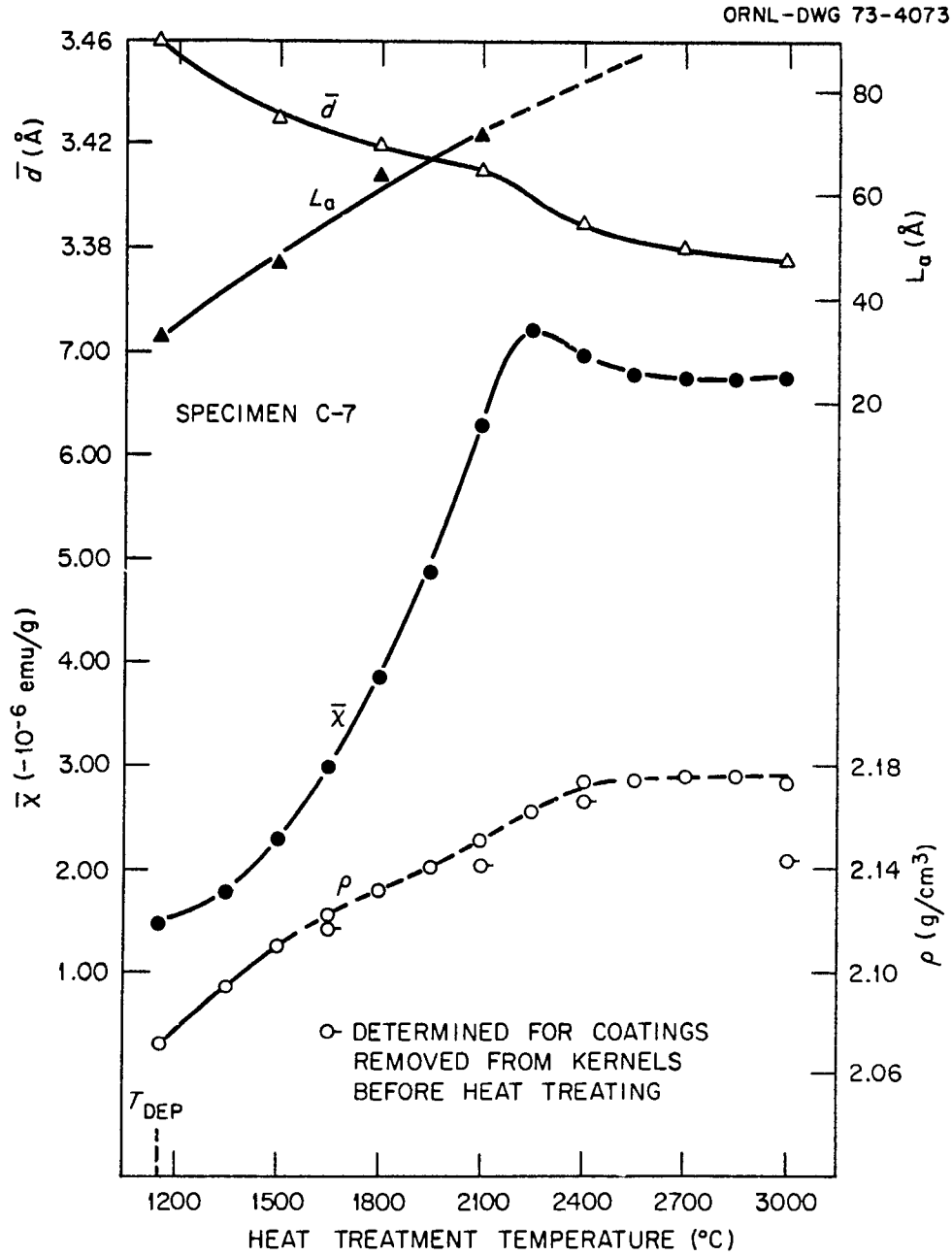

Fig. 6(c). Effect of Heat Treatment Temperature on Isochronal (18-min) Changes in: Density, ρ; Diamagnetic Susceptibility, $\bar{\chi}$; Crystallite Diameter, L_a; Interlayer Spacing, $\bar{d}$.

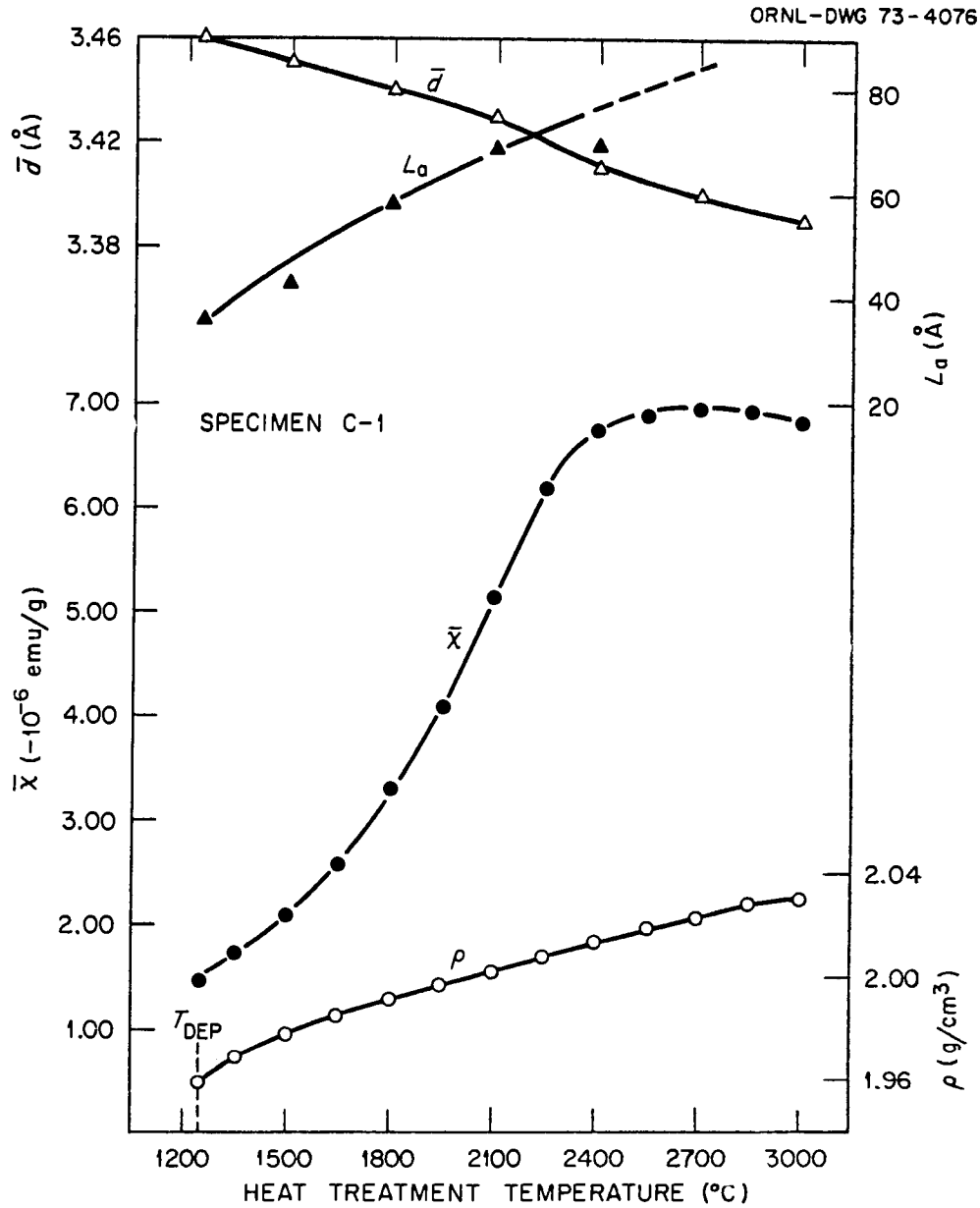

Fig. 6(d). Effect of Heat Treatment Temperature on Isochronal (18-min) Changes in: Density, ρ; Diamagnetic Susceptibility, $\bar{\chi}$; Crystallite Diameter, L_a; Interlayer Spacing, $\bar{d}$.

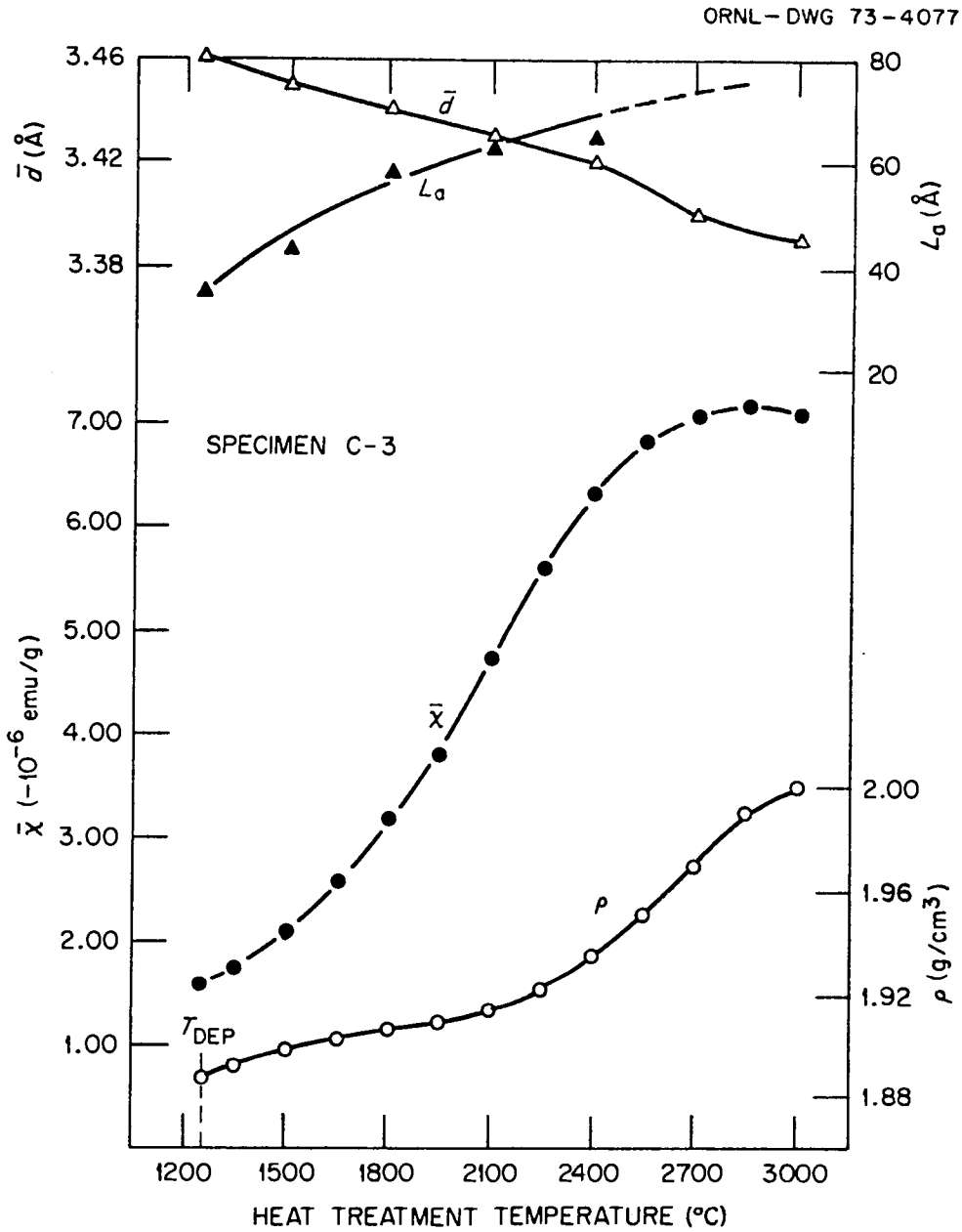

Fig. 6(e). Effect of Heat Treatment Temperature on Isochronal (18-min) Changes in: Density, ρ; Diamagnetic Susceptibility, $\bar{\chi}$; Crystallite Diameter, L_a; Interlayer Spacing, $\bar{d}$.

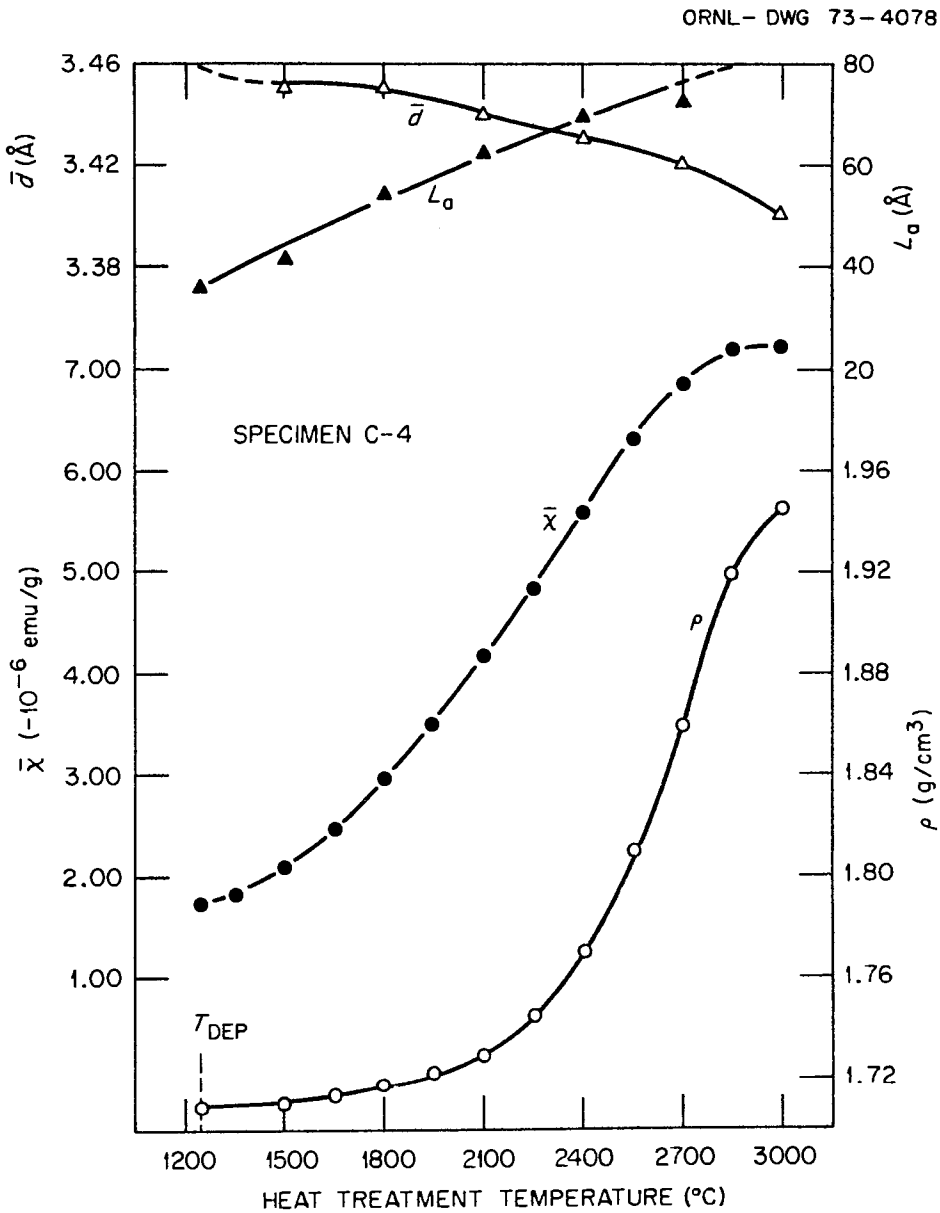

Fig. 6(f). Effect of Heat Treatment Temperature on Isochronal (18-min) Changes in: Density, ρ; Diamagnetic Susceptibility, $\bar{\chi}$; Crystallite Diameter, L_a; Interlayer Spacing, $\bar{d}$.

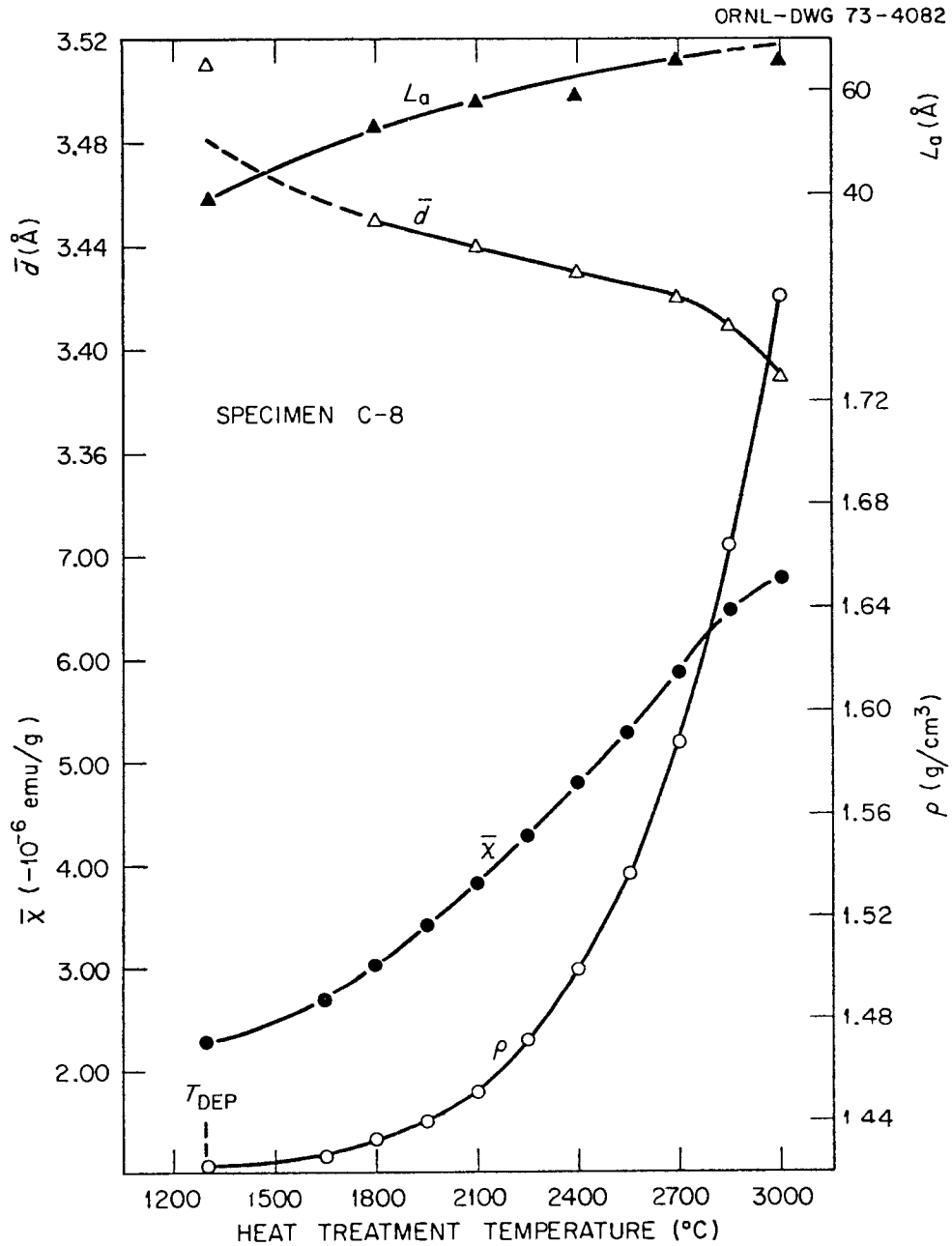

Fig. 6(g). Effect of Heat Treatment Temperature on Isochronal (18-min) Changes in: Density, ρ; Diamagnetic Susceptibility, $\bar{\chi}$; Crystallite Diameter, L_a; Interlayer Spacing, $\bar{d}$.

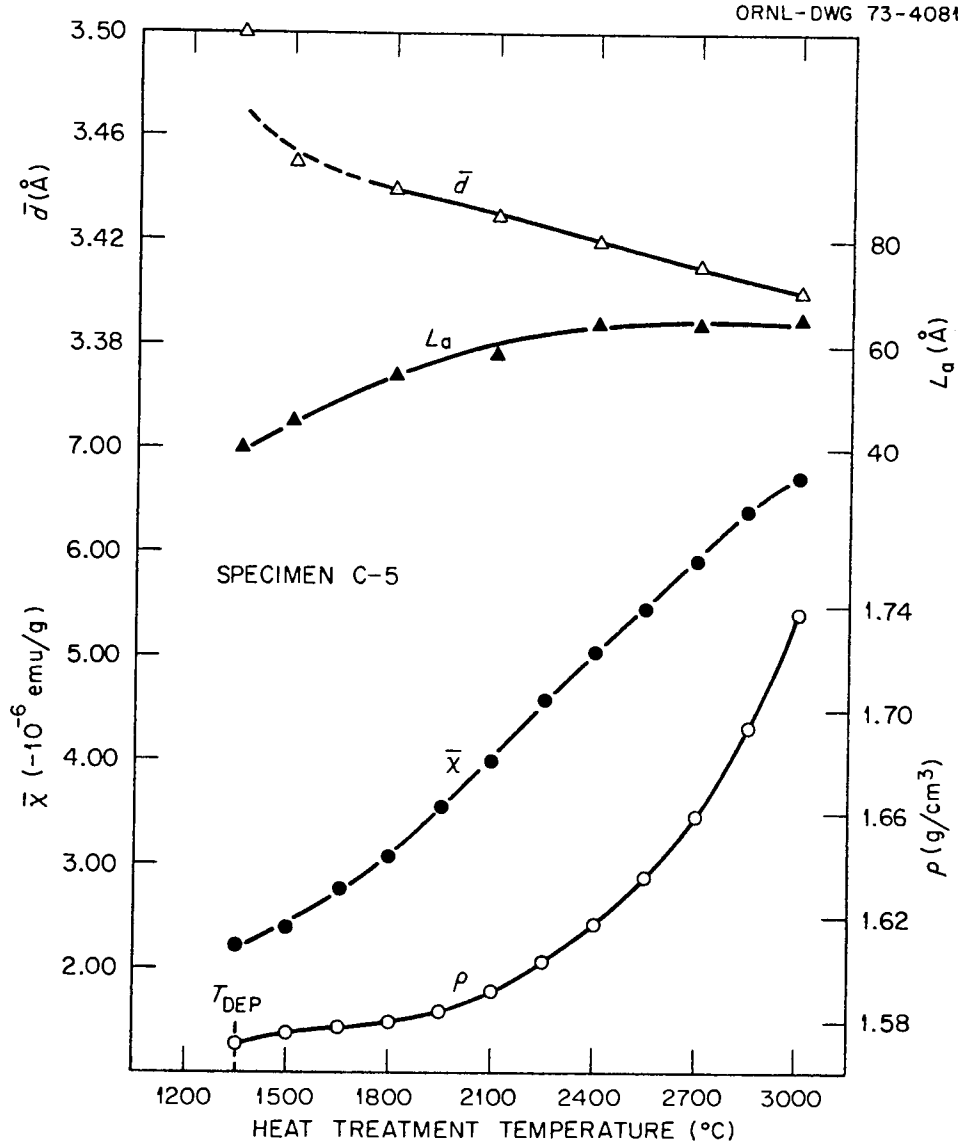

Fig. 6(h). Effect of Heat Treatment Temperature on Isochronal (18-min) Changes in: Density, ρ; Diamagnetic Susceptibility, $\bar{\chi}$; Crystallite Diameter, L_a; Interlayer Spacing, $\bar{d}$.

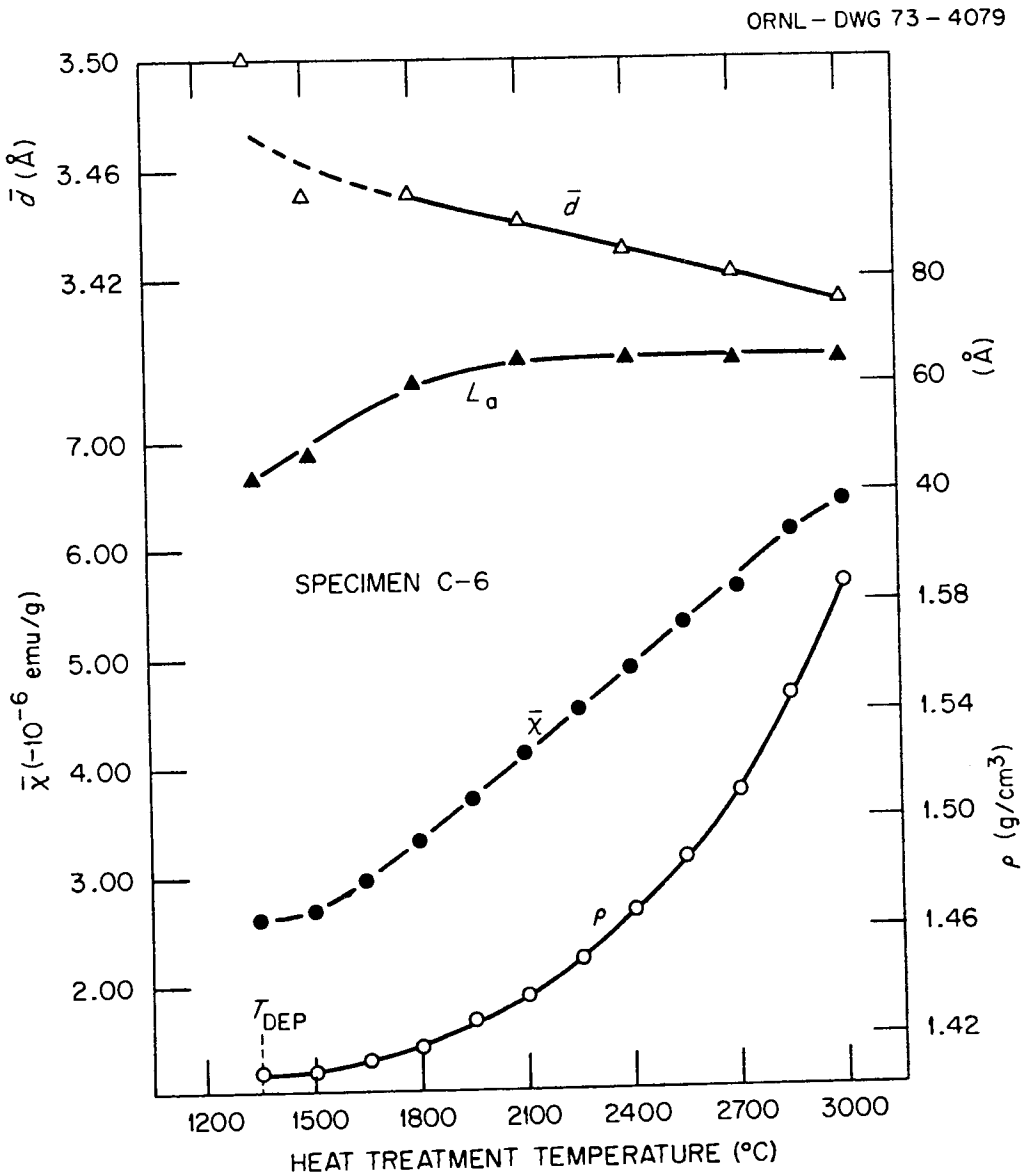

Fig. 6(i). Effect of Heat Treatment Temperature on Isochronal (18-min) Changes in: Density, ρ; Diamagnetic Susceptibility, $\bar{\chi}$; Crystallite Diameter, L_a; Interlayer Spacing, $\bar{d}$.

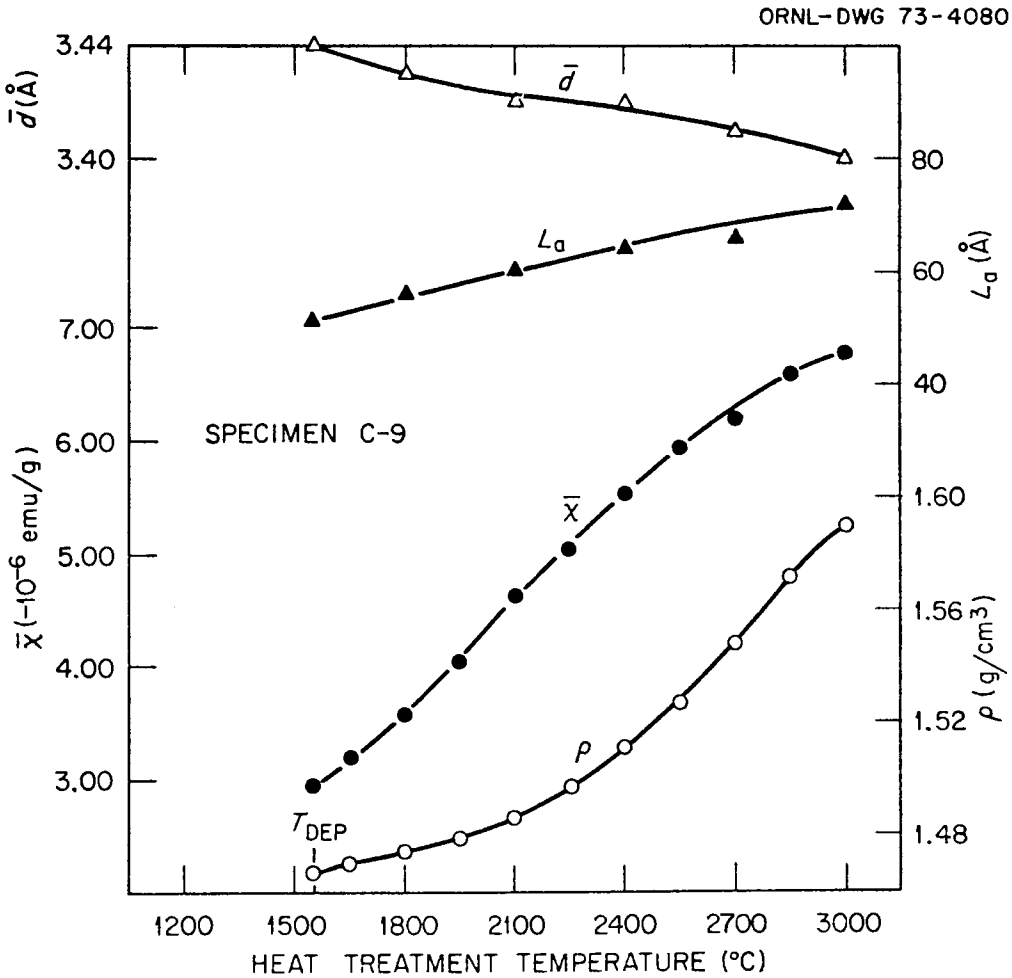

Fig. 6(j). Effect of Heat Treatment Temperature on Isochronal (18-min) Changes in: Density, ρ; Diamagnetic Susceptibility, $\bar{\chi}$; Crystallite Diameter, L_a; Interlayer Spacing, $\bar{d}$.

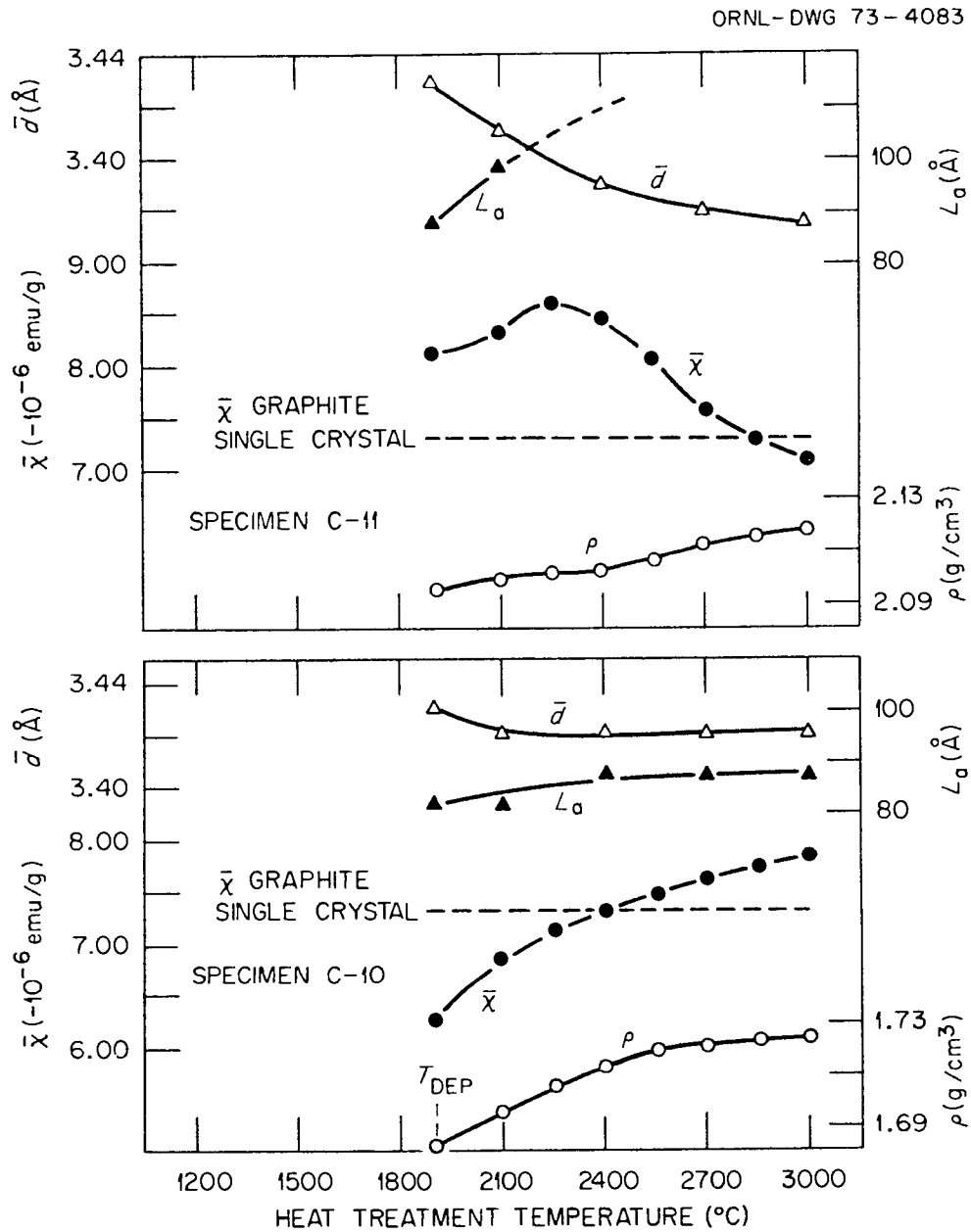

Fig. 6(k,l). Effect of Heat Treatment Temperature on Isochronal (18-min) Changes in: Density, ρ; Diamagnetic Susceptibility, $\bar{\chi}$; Crystallite Diameter, L_a; Interlayer Spacing, $\bar{d}$.

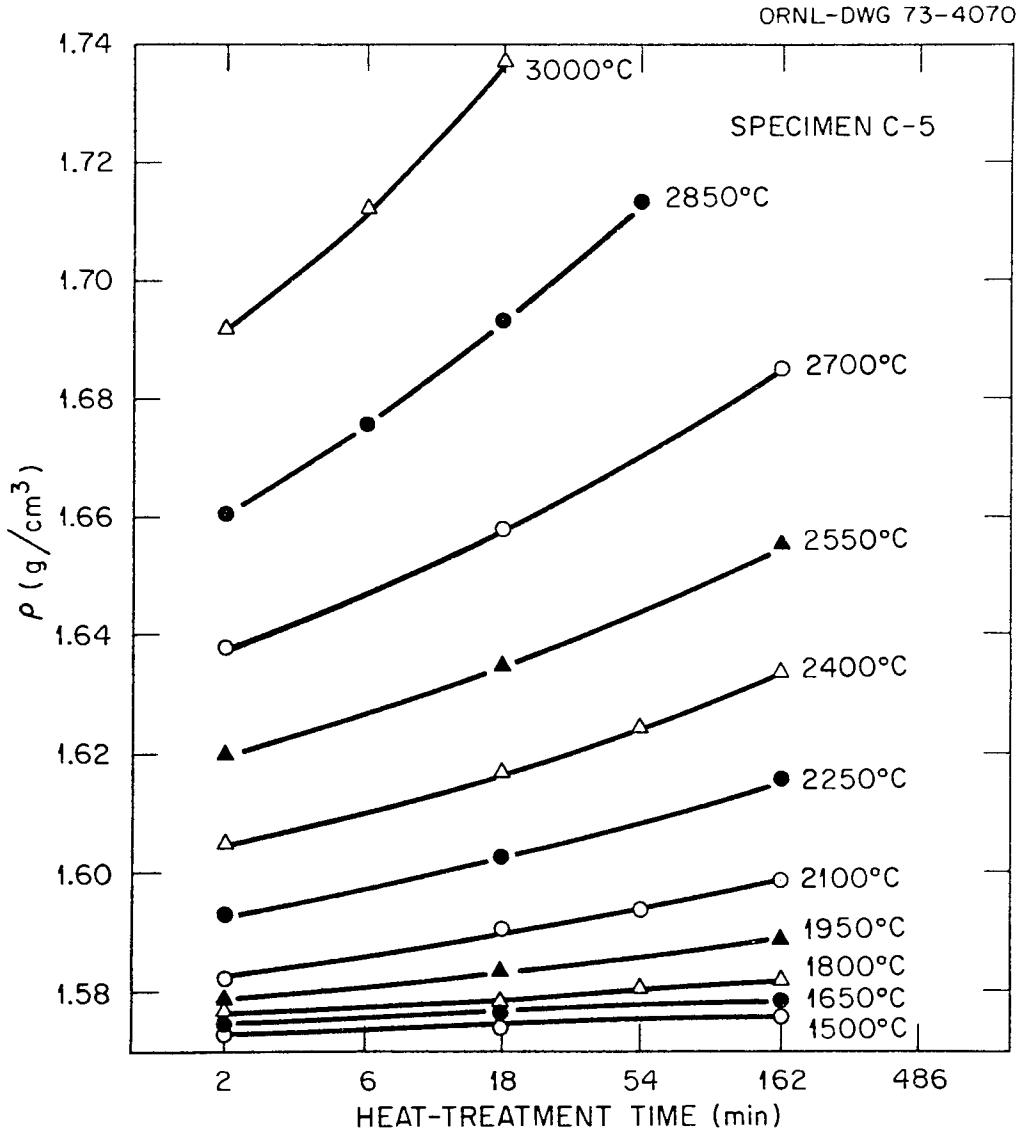

Fig. 7. Effect of Time on Isothermal Densification.

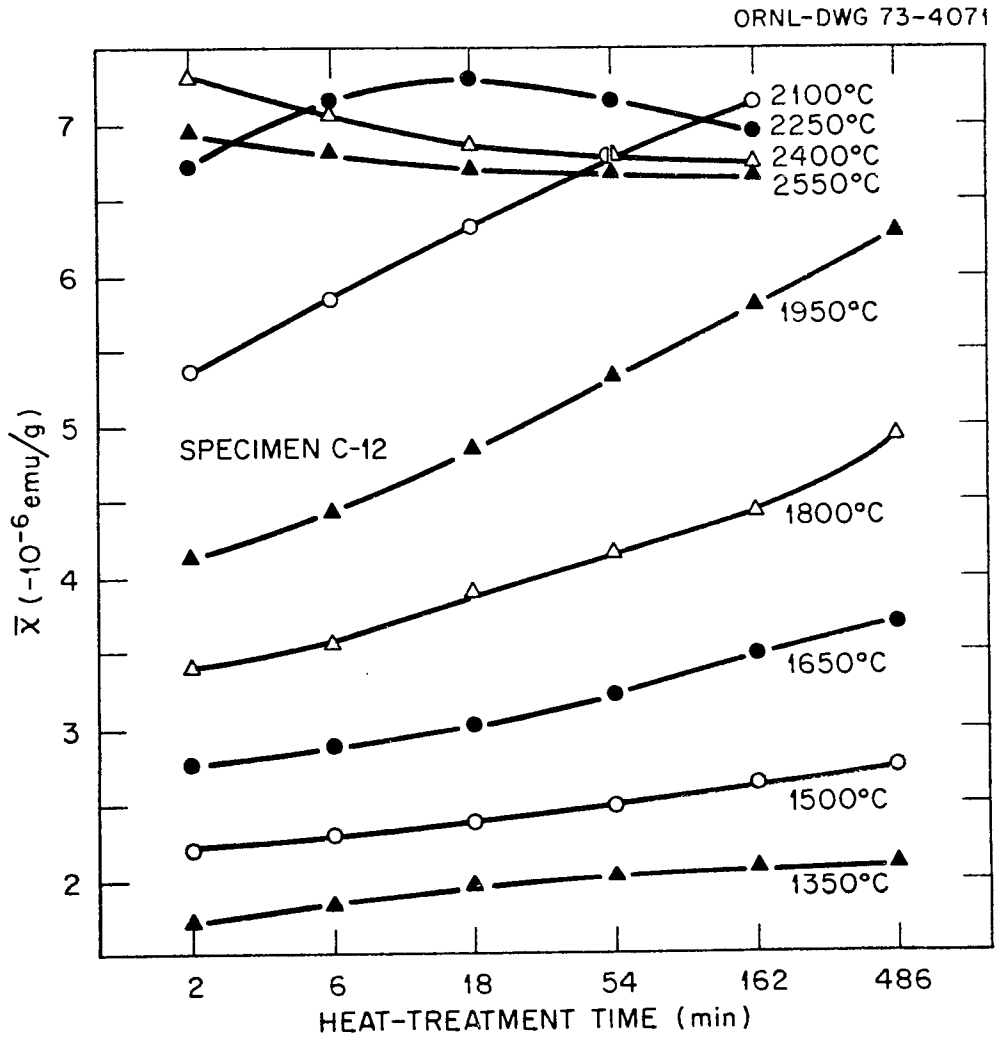

Fig. 8(a). Effect of Time on Isothermal Change in Mean Diamagnetic Susceptibility ($\bar{\chi}$).

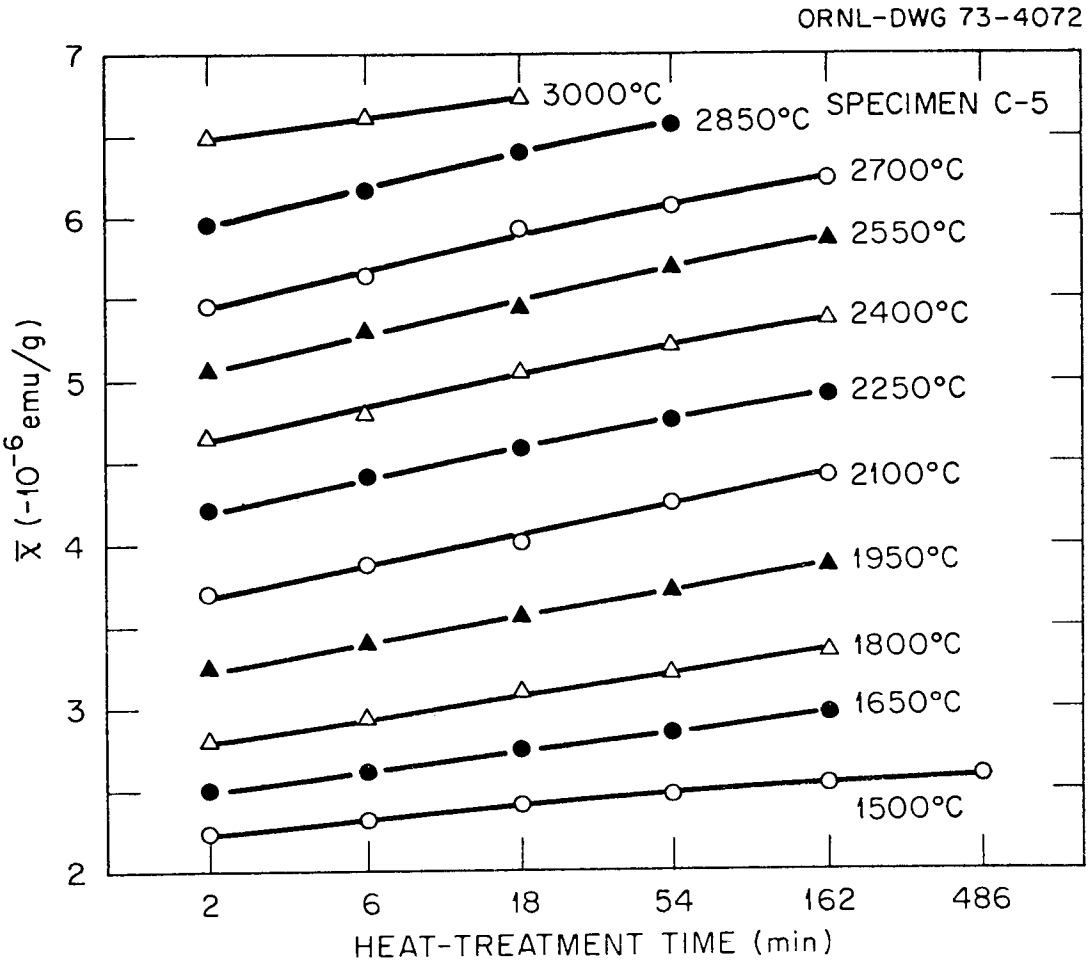

Fig. 8(b). Effect of Time on Isothermal Change in Mean Diamagnetic Susceptibility ($\bar{\chi}$).

of the rigid kernels or spherical geometry for any specimens except possibly the three 1150°C deposits, C-7, C-13, and C-12. The source of the densification data scatter for these specimens is not certain, but may be due to coating delaminations which would result in carbon pieces of various densities if radial density inhomogeneities were present. The variable presence of internal voids is also suggested by the heat-treated microstructure of C-7 shown in Fig. 4(c).

The isochronal densification curves from Fig. 6 are grouped on a common scale in Fig. 9 to show the great variation in behavior among the different materials. The 1150°C deposits, C-12, C-13, and C-7, show very rapid density increases at temperatures just above the deposition temperature even though their as-deposited densities are high. This initial rapid densification was verified to be real by repeated measurements with minimal data scatter for the lower heat-treatment temperature. Specimen C-12, which showed the most rapid initial shrinkage, densifies nearly 2.3% in 18 min at 1350°C as shown in Fig. 6(a). Moreover, the first 1.7% of densification occurs in just 2 min at the same temperature. At higher temperatures the initial densification rate is, of course, much higher. The three 1250°C deposits, which are progressively lower in as-deposited density in the order C-1, C-3, C-4 as shown in Fig. 6(d), (e), and (f), show a sort of transition in densification temperature dependence between the high density deposits formed at low temperatures and the lower density materials formed at intermediate

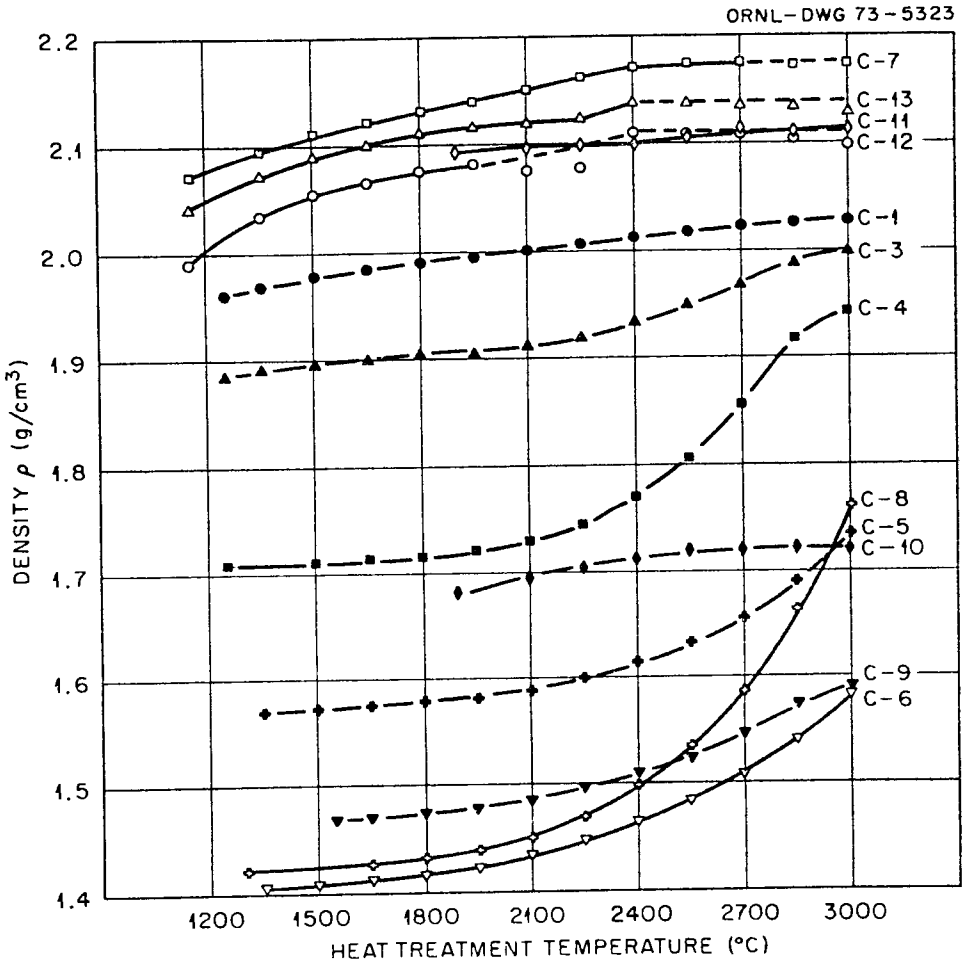

Fig. 9. Effect of Heat Treatment Temperature on Isochronal (18-min) Densification.

deposition temperatures. The specimen C-1, deposited at 1250°C from undiluted propylene, densifies fairly rapidly, though much less rapidly than the 1150°C deposits, up to 1650°C. It continues to densify at a decreased rate, and nearly linearly with increasing HTT, up to 2850°C and then to approach an equilibrium density after 18 min at 3000°C. The densification of the lower-initial-density C-3 material proceeds about half as rapidly as does C-1 with increasing HTT up to 2100°C and then accelerates up to about 2850°C before slowing down, though not saturating, at 3000°C. The lowest-propylene-flux, lowest-density, 1250°C deposit C-4 densifies very slowly at low HTT, but then contracts increasingly rapidly with temperature up to 2850°C. Further increase in density accrues more slowly near 3000°C and it appears that a saturation value in the range 1.95 to 1.98 g/cm^3 may be approached at higher HTT, or alternatively in much longer time at 3000°C.

The three low-density carbons deposited at 1300 to 1350°C from low concentrations of methane, C-8, C-5, and C-6, show in common rather slow densification at temperatures less than 400°C above the deposition temperature, followed by increasingly rapid volume contraction at higher temperatures. Within the limit of the experiments, 18 min at 3000°C, none of these materials showed any indication of approaching a saturation density. The low-density C-9 deposited from a high concentration of propylene at 1550°C exhibited similar densification behavior except that the rate is decreasing at

3000°C with the density attaining a maximum value in the experiment of only 1.59 g/cm^3. This suggests a rather low saturation density for this material.

The isochronal density curves for C-10 and C-11, deposited from methane at 1900°C, contrast in Fig. 9 with the curves for the lower-temperature deposits. Specimen C-10 densifies slowly up to 2550°C, then seems to approach a low saturation density near 1.73 g/cm^3. Specimen C-11 which has a much higher as-deposited density, in fact the highest of the twelve carbons studied, densifies very slowly over the entire HTT range and achieves a final value in the experiment of only 2.12 g/cm^3, slightly lower than the final values attained by C-7 and C-13.

Density changes vary widely on a percentage basis among the twelve carbons. Amounts and percentages of densification after 18 min at 1800°C and after 18 min at 3000°C are listed in Table III for comparison. It can be seen that density increases due to heat treating for 18 min at 3000°C range from just over 1% for the initially high-density C-11 to nearly 24% for the low-density C-8. It may be noted, however, that densification is not simply related to initial density. For example, C-10 which has a fairly low density as deposited, densifies only 2.56% within the limit of the experiment and does not show signs of potential further significant increase. Other points of comparison include C-4, which has about the same initial density as C-10, but densifies more than five times as much, and C-6 with approximately the same as-deposited

Table III. Densification of Carbons Due to Heat Treatment for 18 min at 1800°C and 18 min at 3000°C

Specimen	Density, g/cm³			Densification			
	As-Deposited	18 min at 1800°C	18 min at 3000°C	18 min at 1800°C		18 min at 3000°C	
				g/cm³	%	g/cm³	%
C-12	1.992	2.076	2.100[a]	0.084	4.22	0.108[a]	5.42[a]
C-13	2.041	2.113	2.130[a]	0.072	3.53	0.089[a]	4.36[a]
C-7	2.072	2.132	2.173	0.060	2.90	0.101[a]	4.87[a]
C-1	1.960	1.994	2.030	0.034	1.74	0.070	3.57
C-3	1.886	1.906	2.001	0.020	1.06	0.115	6.10
C-4	1.708	1.717	1.944	0.009	0.53	0.236	13.82
C-8	1.422	1.433	1.761	0.011	0.77	0.339	23.84
C-5	1.571	1.579	1.737	0.008	0.51	0.166	10.57
C-6	1.406	1.416	1.585	0.010	0.71	0.179	12.73
C-9	1.467	1.474	1.590	0.007	0.48	0.123	8.38
C-10	1.681	b	1.724			0.043	2.56
C-11	2.094	b	2.118			0.024	1.15

[a]Value slightly uncertain due to data scatter.

[b]Not measured.

density as C-8, but which densifies only about half as much. Of course, nothing can be said about the densification curves of C-6 or C-8 at times or temperatures beyond 18 min at 3000°C, except that they will have to show saturation at some point. A further point on the large density increase of C-8 is that it occurs at an extremely high rate at 3000°C; the first 17% increase requires only 2 min. Large densification occurring in much shorter times, inferred from temperature-compensated time scaling, will be discussed later in conjunction with the determination of activation energies.

As noted above the amount of densification effected by the most extreme treatment employed, 18 min at 3000°C, is not a function of as-deposited density when all twelve specimens are considered. However, densification at an arbitrarily selected midtreatment condition (e.g., 18 min at 1800°C) is shown in Table III to be generally greater with higher initial density for specimens formed below this temperature. This relationship has been observed previously by Stevens [141] for the limited type of low-temperature, isotropic, fluidized-bed pyrocarbons. If all the low- and intermediate-temperature carbons studied here, including highly anisotropic deposits, are compared, densification is seen not to be a monotonic function of initial density. However, if densifications occurring in 18 min at 1800°C, conditions known to remove nearly all residual hydrogen [141, 142], are compared on the basis of as-deposited hydrogen content, the relationship is shown in Fig. 10. Densification

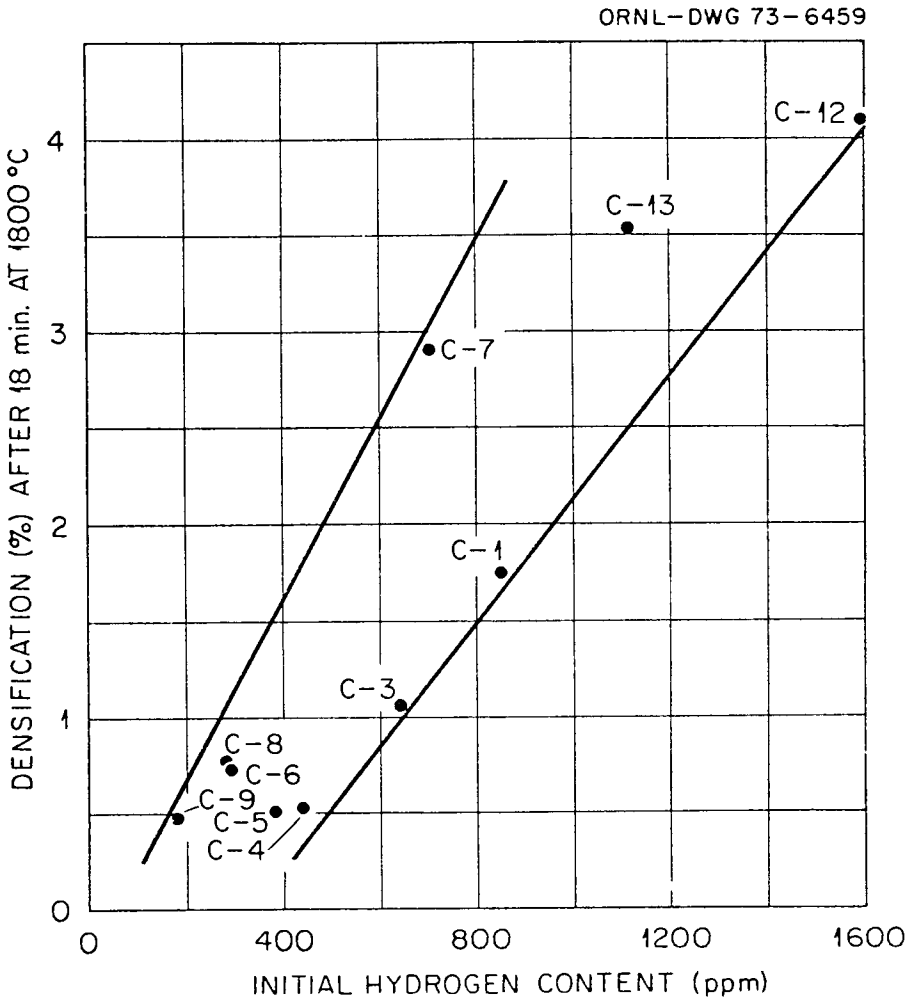

Fig. 10. Effect of Initial Hydrogen Content on Densification After 18 min at 1800°C.

at relatively low treatment temperatures thus appears to be strongly enhanced by residual hydrogen. It is known [143,144] that hydrogen content of vapor deposited carbon increases rapidly with decreasing deposition temperature for constant deposition time. Since forming times varied greatly for the carbons studied here, it seems likely that a significant part of the as-deposited hydrogen was removed with concomitant densification during the deposition process for the more slowly deposited specimens. This probably accounts for much of the width of the densification-hydrogen content band shown in Fig. 10.

While the isochronal plots graphically illustrate the effect of heat-treatment temperature on each carbon, isothermal curves are much more useful for kinetic analysis. A family of isothermal density versus log time curves was obtained for each carbon, and a representative set (for C-5) is shown in Fig. 7. This family of curves requires a large number of measurements for its construction and employs all the density data obtained for the specimen. Use of the isothermal curves for kinetic analysis will be discussed later. As indicated earlier, the 18-min points from the isothermal curve family were used in constructing the isochronal plots. Of course, isochronal plots could be made from any set of fixed time data points, or from any constant time cross section of the isothermal property surface. Any alternate isochronal representation of longer or shorter heat-treatment time would simply lead or lag the 18-min plot, respectively.

X-Ray Parameters

The x-ray diffraction parameters L_a and $\bar{d}$ were determined in this work to provide a measure of graphitization progress in each specimen and to assist structural interpretation of magnetic susceptibility results. The evolutionary patterns of L_a and $\bar{d}$ curves will be discussed separately and in conjunction with $\bar{\chi}$ curves, but the significance of the parameters themselves must be considered briefly. L_a is an important parameter because it is frequently correlated with various properties including magnetic susceptibility. In the past it has been common to consider L_a as an actual crystallite diameter. However, it is now well established that L_a measured by the usual techniques is, in general, somewhat smaller than the average layer diameter. This is the reason for terming L_a an "apparent" crystallite diameter. L_a is actually a measure of the size of a coherently diffracting region, and should be understood as an average size of planar, defect-free layer regions. Thus, large layers which are bent or have holes would give small L_a values. While L_a is not necessarily a true measure of layer size, it is still an extremely useful parameter. Changes in L_a of a given carbon resulting from heat treatment, or differences in L_a of similar carbons, give useful relative information, although care must be exercised in comparing L_a values for different types of carbons.

In this work only a limited number of x-ray measurements were made on each specimen, and all L_a results, obtained from microsphere coating sections removed from the kernels prior to heat treatment, are shown as isochronal plots in Fig. 6(a) through (l). No isothermal curves were generated. All specimens showed some L_a growth with heat treatment, with the 1150°C deposits exhibiting the largest and most rapid increases. The 1250°C deposits showed somewhat slower L_a growth, and the intermediate-temperature deposits still slower. The apparent crystallite diameters of C-5 and C-6 appear to saturate at an L_a value of about 65 Å at temperatures above 2100 to 2400°C. In the 1900°C deposit, C-10, L_a appears to increase very little, even from the as-deposited value, and saturates at about 87 Å above 2400°C. Some early L_a growth is indicated in C-11, but there is insufficient data to give a clear picture.

Since all L_a values were determined from broadening of the (10) line, only the very difficult to graphitize specimens could be measured after heat treatment at the higher temperature. Incipient modulation of the (10) in the more graphitizable deposits precluded further meaningful measurements from broadening of this line. This occurred in 18 min below 2400°C in C-12, C-13, C-7, C-1, and C-11, at about 2400°C in C-3, at approximately 2700°C in C-4, and near 3000°C in C-8. L_a values in the range 70 to 80 Å were attained by these specimens, except C-11 which reached about 100 Å, before (10) modulation occurred. The other carbons

showed no (10) modulation even after 18 min at 3000°C. The most graphitizable carbons of the group, C-12, C-13, C-7, and C-11, developed fairly narrow (hkl) lines at high temperature, suggesting L_a growth far beyond the 70 to 100 Å measured prior to (10) modulation. However, quantitative comparison of measurements from the different lines would have little merit.

The significance of $\bar{d}$ is a mean value of a distribution of interlayer spacings [14]. Carbons with identical $\bar{d}$ values may not necessarily have the same distribution of interlayer spacings, and again care must be taken in comparing different carbons on the basis of $\bar{d}$ values. For highly distorted carbons such as the lower temperature deposits used in this study, the initial decreases in $\bar{d}$ with heat treatment probably result from removal of layer defects. As $\bar{d}$ decreases below about 3.41 Å in these materials, it gives a useful qualitative picture of the development of layer ordering. However, the sometimes employed calculation of a "degree of graphitization" from $\bar{d}$ data is of questionable significance.

Determinations of $\bar{d}$ in this work were made from the position of the (004) line on the same x-ray patterns used for L_a measurements. All $\bar{d}$ results are shown as isochronal plots in Fig. 6(a) through (l). All deposits except C-10 showed large reductions in $\bar{d}$ with heat treatment. Specimen C-10, which also showed the least change in other parameters, dropped from an as-deposited $\bar{d}$ of 3.43 Å to only about 3.42 Å

at 2100°C and remained there through the 18-min, 3000°C heat treatment. The lowest $\bar{d}$ value attained by any of these carbons was 3.375 Å, still considerably above the graphite value of 3.354 Å. The 3.375 Å value was reached by two 1150°C deposits, C-13 and C-7, and by the 1900°C deposit, C-11. The $\bar{d}$ versus HTT curves were essentially straight lines for only two carbons, C-5 and C-6. Rapid reduction steps can be seen in the $\bar{d}$ curves of C-12, C-13, C-7, C-1, and C-11 between 2100 and 2400°C, the same temperature range in which modulation of the (10) line caused discontinuation of L_a measurements. Both of these factors, of course, are indicative of layer ordering. A corresponding rapid $\bar{d}$ reduction can be seen in C-3 above 2400°C, and C-4 above 2700°C, again corresponding in each case to the (10) modulation range.

The relationship between $\bar{d}$ and L_a for all twelve carbons is shown in Fig. 11. There is considerable scatter in this plot when all data are included but the interdependence of L_a and $\bar{d}$ does appear to vary with the type of carbon. As noted on the isochronal plots of Fig. 6 the L_a values for some of the nongraphitizing specimens stopped increasing at high temperatures but $\bar{d}$ never stopped decreasing except for one 1900°C deposit (C-10). Figure 11 shows L_a values ranging from about 70 to 110 Å for $\bar{d}$ spacings near 3.39 Å. These results indicate that for a given mean interlayer spacing more readily graphitizing carbons attain larger "apparent" crystallite diameters as measured by broadening of an x-ray diffraction profile.

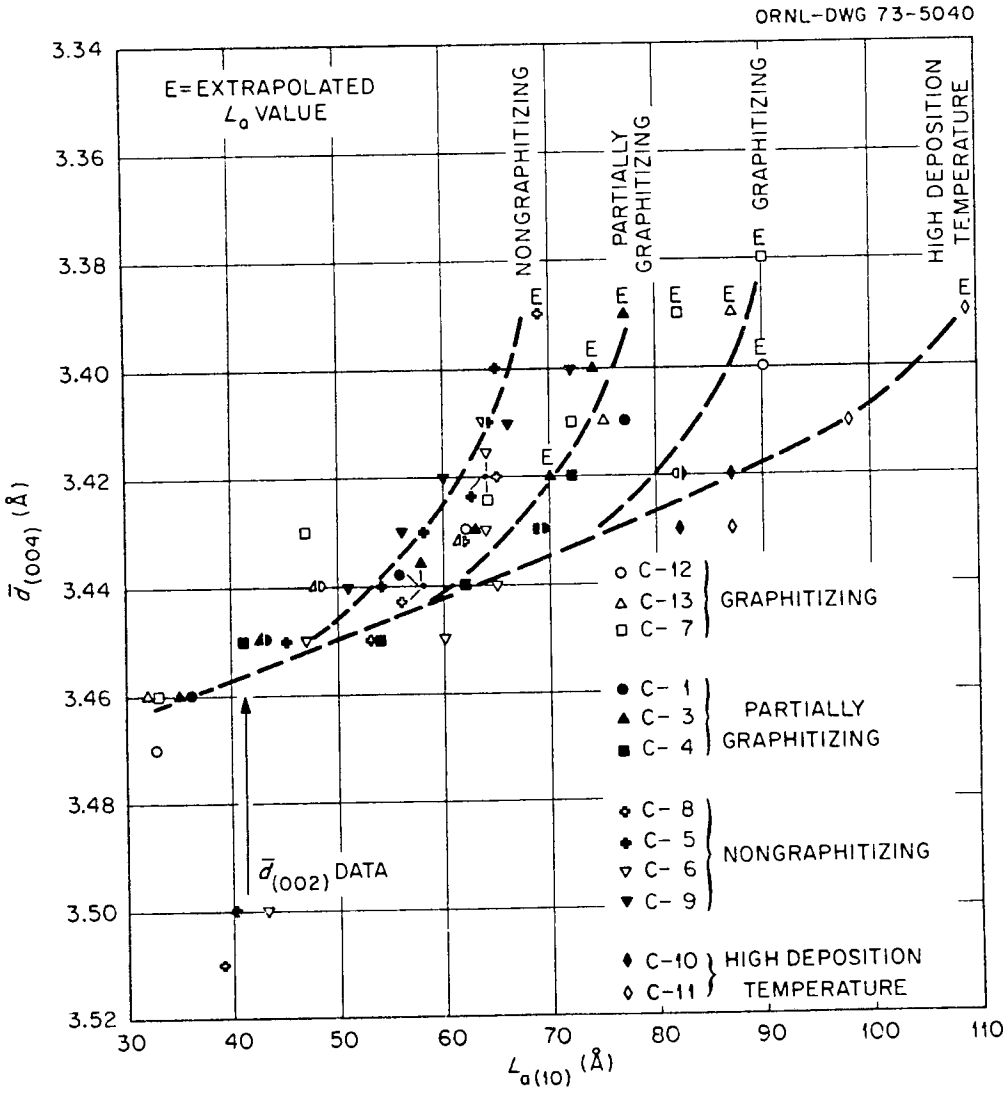

Fig. 11. Correlation of Crystallite Diameter (L_a) with Mean Interlayer Spacing ($\bar{d}$).

The observation of smaller L_a for given $\bar{d}$ for carbons which are very difficult to graphitize is at variance with conclusions drawn by some other workers. Takahashi, Kuroda, and Akamatu [63], using a "degree of graphitization" relationship, plotted $(1 - P_1)$ versus L_a data of several workers for both hard and soft carbons and found all the data to be fit rather well by a single curve. The curve was a hyperbola given by the equation $(1 - P_1) \times L_a = 110$, making $P_1 = 1 - 110/L_a$, where P_1 is considered to be a relative frequency of finding nearest neighbor layers ordered into the graphite structure. Maximum treatment temperatures employed by the different workers were not given.

Honda, Kobayashi, and Sugawara [145] studied two soft and four hard carbons by measuring x-ray diffraction parameters including $\bar{d}$ (002) and L_a (110) as functions of treatment temperature up to 3000°C. They interpreted their (002) profiles of the hard carbons as showing two- or three-phase graphitization, but their $\bar{d}$ (002) and L_a (110) data were all fit to a single plot. The curve was continuous though not a smooth hyperbola like that obtained by Takahashi *et al.* [63]. Of particular interest are L_a values as high as 300 Å determined by Honda *et al.* for cellulose and resin carbons which they call nongraphitizing. These large L_a (110) values presumably result from measurement of fairly well modulated (11) profiles but this point is not discussed by the authors. Occurrence of measurable (hkl) lines, of course, indicates considerable graphitization. There was no

apparent (10) modulation for the hardest carbons examined in the present work even after the highest HTT.

A relationship similar to that found by Honda *et al.* between $\bar{d}$ and L_a has been noted also by Maahs [146] for his own data and data of others. Maahs observed some discrepancies among the L_a-$\bar{d}$ relationships reported and noted that different methods of calculation used for L_a and use of different degree of graphitization parameters rather than direct $\bar{d}$ measurements can lead to significantly different results.

The small crystallite diameters (less than 70 Å) shown in Fig. 11 for $\bar{d}$ (004) values less than 3.41 Å were obtained only at temperatures above 2700°C for very difficult to graphitize carbons. No indication of multiphase development nor any sign of layer ordering was observed in the x-ray diffraction patterns of any of these specimens so the small L_a values derive from the very broad (10) profiles. It may be noted that if data for several of the hardest carbons, C-5, C-6, C-8, and C-9, but not C-10, treated at temperatures above 2700°C were omitted from Fig. 11, the remaining data could be reasonably well fit to a single curve.

Mean Diamagnetic Susceptibility

The changes in mean diamagnetic susceptibility, $\bar{\chi}$, as a function of heat-treatment temperature at constant time (18 min) for the twelve carbons are shown in Fig. 6(a) through (l), along with the corresponding density and x-ray parameter plots. Again the effects of heat treatment vary

widely among the materials but can be considered in groups. The isochronal $\bar{\chi}$ curves for the three 1150°C deposits, C-12, C-13, and C-7, are remarkably alike. They each show $\bar{\chi}$ increasing rapidly with increasing HTT up to 2100°C, exhibit a distinct maximum near the graphite single-crystal value of 7.33 at 2250°C, then decrease to about 6.7 at 2700°C, and remain nearly flat to 3000°C. It should be noted that the sharp $\bar{\chi}$ maxima occur in precisely the same temperature range as the rapid decreases in $\bar{d}$ and the appearance of (10) modulation. The three 1250°C deposits again seem to cover a transition range between the 1150°C materials and those formed at intermediate temperatures. The $\bar{\chi}$ curves of the 1250°C carbons increase less rapidly with HTT than those of the 1150°C deposits, and level off at progressively higher temperatures in the order C-1, C-3, C-4, the order of decreasing density, without showing sharp maxima. However, C-1 and C-3 do show very broad maxima at 2700 and 2850°C, respectively. In the 1250°C materials the notable x-ray parameter changes appear to coincide with the rounding off of the $\bar{\chi}$ curves just preceding the broad maxima. The four intermediate temperature materials, C-8, C-5, C-6, and C-9, all show $\bar{\chi}$ increasing monotonically with HTT at somewhat lower rates than occur initially in the lower temperature deposits. However, C-8 shows a marked rounding of the $\bar{\chi}$ curve just below 3000°C, again corresponding with the significant $\bar{d}$ and (10) profile changes. The two 1900°C carbons exhibited very different $\bar{\chi}$ changes with heat treatment. C-11

increased from its very high as-deposited value to a distinct maximum at 2250°C and then decreased continuously through the 18-min, 3000°C heat treatment. The $\bar{\chi}$ peak coincides with those of the 1150°C carbons and with a rapid decrease in $\bar{d}$ and incipient (10) splitting. The $\bar{\chi}$ curve of C-10 increases monotonically with HTT, but at a gradually decreasing rate through the final heat treatment. The isochronal $\bar{\chi}$ curves are replotted as a group in Fig. 12 to emphasize similarities and differences in $\bar{\chi}$ development of the different carbons.

A family of isothermal $\bar{\chi}$ curves was developed for each of the twelve carbons, again primarily for use in kinetic analysis. Representative isothermal $\bar{\chi}$ curve families for C-12 and C-5 are shown in Fig. 8(a) and (b), respectively. Each isothermal curve for C-5 increases monotonically in $\bar{\chi}$ with HTt and lies above its lower temperature counterparts. The same pattern is followed by C-12 only through the 2100°C heat treatment. At 2250°C $\bar{\chi}$ passes through a maximum in about 18 min, and at higher temperatures a monotonic decrease with time is evident.

The relationship between $\bar{\chi}$ and crystallite diameter is shown in Fig. 13. As reported by numerous investigators $\bar{\chi}$ generally increases with increasing L_a. However, the non-graphitizing carbons studied here show continued $\bar{\chi}$ increase after L_a reaches a plateau at about 65 Å. For the graphitizing carbons, only data up to the $\bar{\chi}$ maxima are included in Fig. 13 since the maxima represent the beginning of graphitization,

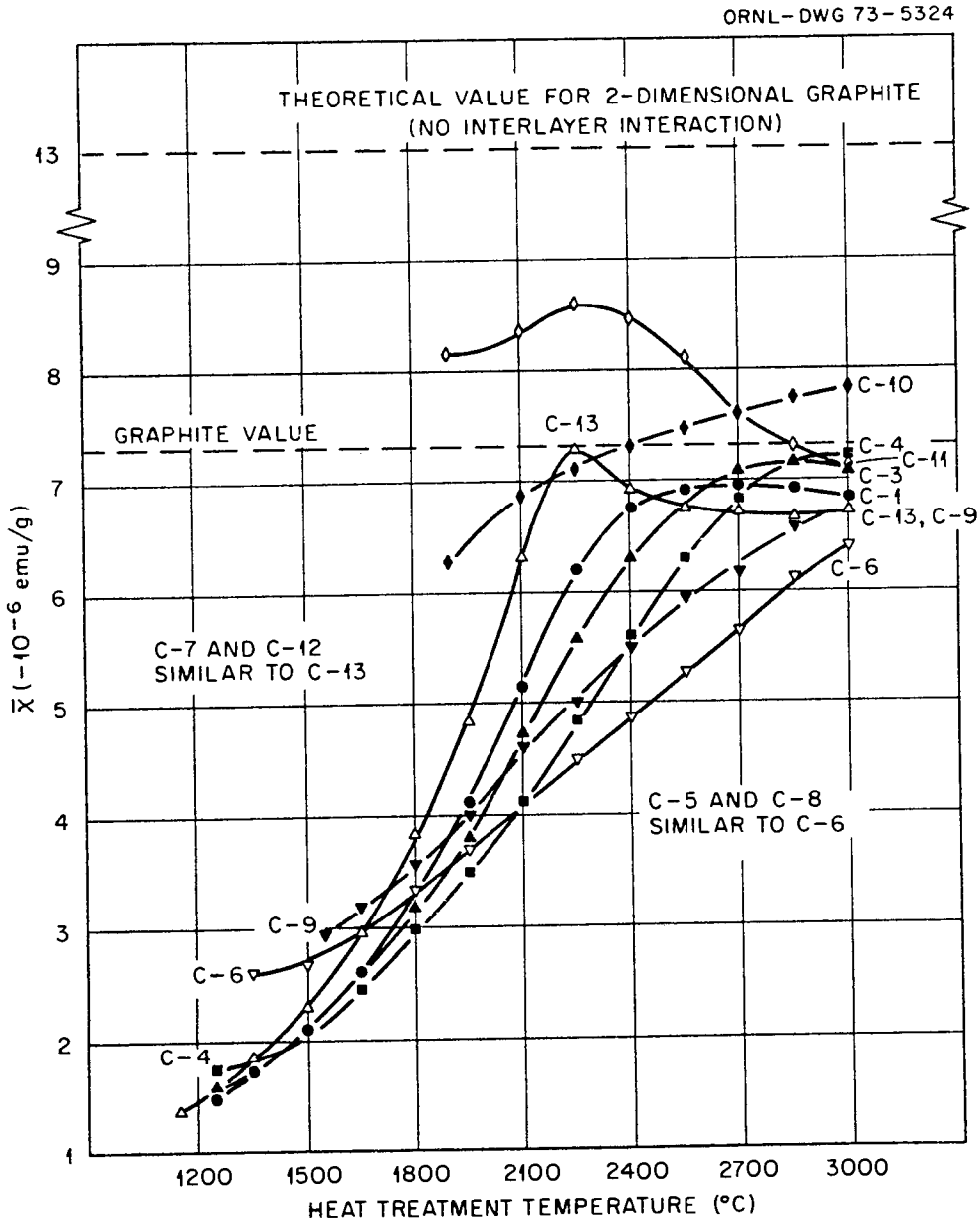

Fig. 12. Effect of Heat Treatment Temperature on Isochronal (18-min) Change in Mean Diamagnetic Susceptibility ($\bar{\chi}$).

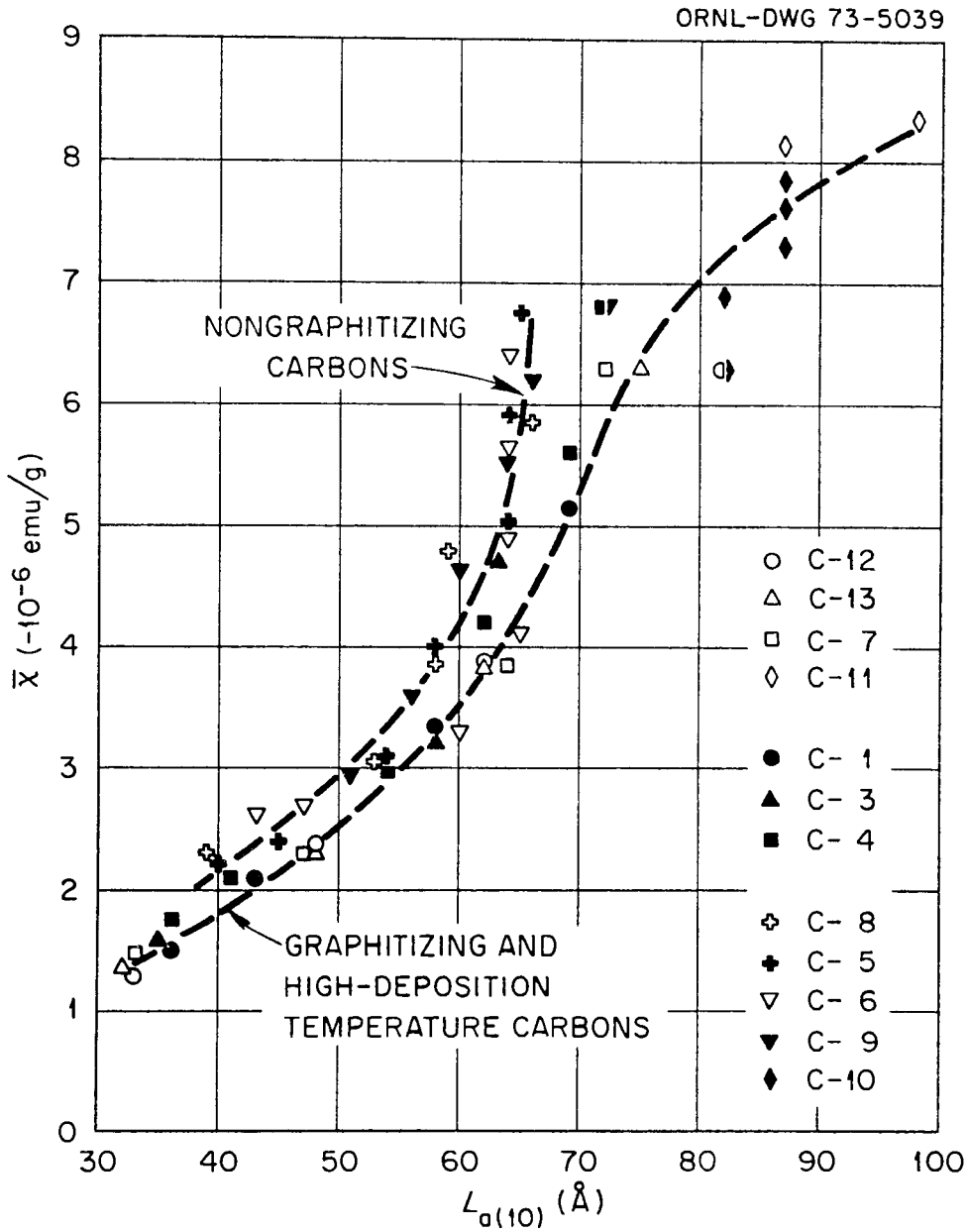

Fig. 13. Correlation of Crystallite Diameter (L_a) with Mean Diamagnetic Susceptibility ($\bar{\chi}$).

splitting of the (10) x-ray diffraction profile, and discontinuation of L_a measurements in this work. After graphitization begins, $\overline{X}$ decreases while L_a increases (evident from narrowing of all diffraction profiles even though not measured) so that an extension of the curve for graphitizing carbons on Fig. 13 would go through a maximum. The data shown, however, indicate that the nongraphitizing carbons attain a higher $\overline{X}$ value for given L_a than do the nongraphitizing carbons.

Fischbach has noted that glassy carbon attains a given magnetic susceptibility with a much lower L_a value than is the case for high-temperature pyrolytic carbon [89]. He attributes this to the different significance of the L_a measurements for these materials.

Activation Energy for Graphitization

The results described above show that properties of various pyrolytic carbons change as functions of both time and temperature of heat treatment. The changes with isothermal heat-treatment time and the rapidly increasing rates of change with increasing heat-treatment temperature are clear indications that graphitization is thermally activated.

To obtain an activation energy from rate data without a priori knowledge of the detailed processes involved, it is desirable to deal with only the rate temperature dependence. This is commonly achieved in graphitization studies by a

method of isothermal curve superposition. The basis for the curve superposition method of analysis is a temperature-compensated time relationship. For a single first-order process with constant activation energy the usual Arrhenius-type rate equation is

$$k = k_0 \exp(-\Delta H/RT) ,$$

where the preexponential or frequency factor k_0 is a constant independent of temperature, R is the gas constant, T is absolute temperature, and ΔH is the activation energy. The Boltzmann factor $\exp(-\Delta H/RT) = K(T)$, however, describes the rate temperature dependence irrespective of reaction order or mechanistic details. Therefore, treatment of ΔH as an effective activation energy does not require assumptions about reaction order or specific mechanisms.

The time-temperature relationship for a property change rate may be shown for the case of a single first-order process as follows. At temperatures T and time t, if property P increases,

$$P_{T_1,t_1} = P_0 + (P_\infty - P_0)[1 - \exp(-k_1 t_1)] ,$$

and

$$P_{T_2,t_2} = P_0 + (P_\infty - P_0)[1 - \exp(-k_2 t_2)] ,$$

where k_1 and k_2 are rate constants which are functions of temperature. Now if

$$P_{T_1,\ t_1} = P_{T_2,t_2} ,$$

$$\exp(-k_1t_1) = \exp\ (-k_2t_2) ,$$

$$\ln(k_1t_1) = \ln(k_2t_2) ,$$

$$\ln(k_2/k_1) = \ln\ t_1 - \ln\ t_2 .$$

The same relationship holds for a decreasing property where

$$P_{T_1,t_1} = P_\infty + (P_0 - P_\infty)\ \exp(-k_1t_1),\ \text{etc.}$$

Now since

$$k_1 = k_0\ \exp(-\Delta H/RT_1) = k_0\ K(T_1) ,$$

and

$$k_2 = k_0\ \exp(-\Delta H/RT_2) = k_0\ K(T_2) ,$$

$$\ln(k_2/k_1) = \ln[K(T_2)/K(T_1)] = \ln\ t_1 - \ln\ t_2 ,$$

and a temperature-compensated time relationship is established. From this relationship it can be seen that an isothermal property change curve at T differs from a corresponding curve at a reference temperature T_0 by the scale factor $\ln[K(T)/K(T_0)]$ on the time scale expressed as $\ln\ t_0 - \ln\ t$. The T curve can therefore be superimposed on the T_0 curve by translation parallel to the log t axis. The amount of translation is a direct measure of the rate temperature dependence of the process and thus provides a means of determining the effective activation energy for the range

$T - T_0$. As indicated earlier, the principal advantage of the superposition technique lies in avoiding specification of the preexponential factor, thereby rendering the method particularly appropriate for analyzing rate data comprising a distribution of unresolved processes. The method requires only that the distribution of processes (i.e., the distribution of preexponential factors) is not a function of temperature in the range $T - T_0$. This is a reasonable assumption if $T - T_0$ is small enough to allow overlap of the respective isothermal curves. Probably the best argument for the validity of the isothermal curve superposition method for analyzing graphitization is that good superposition is obtained for experimental data.

Representative master curves of a property versus temperature-compensated time (equivalent time at reference temperature) on a log scale have been plotted utilizing all the available isothermal data in each case. Master curves of $\overline{X}$ versus log HTt (1350°C equivalent minutes) are shown in Fig. 14(a) and (b) for C-12, C-1, C-5, C-9, C-10, and C-11. These plots suggest that processes which occur in a few minutes at 3000°C in these carbons would require geologic time (somewhat greater than the accepted age of the earth) at 1350°C. This, of course, is a consequence of the high activation energies involved. For example, a process requiring a ΔH of 240 kcal/mole would proceed about 10^{16} times faster at 3000°C than at 1350°C, and a 330 kcal/mole process would require on the order of 10^{22} times longer at 1350°C than at

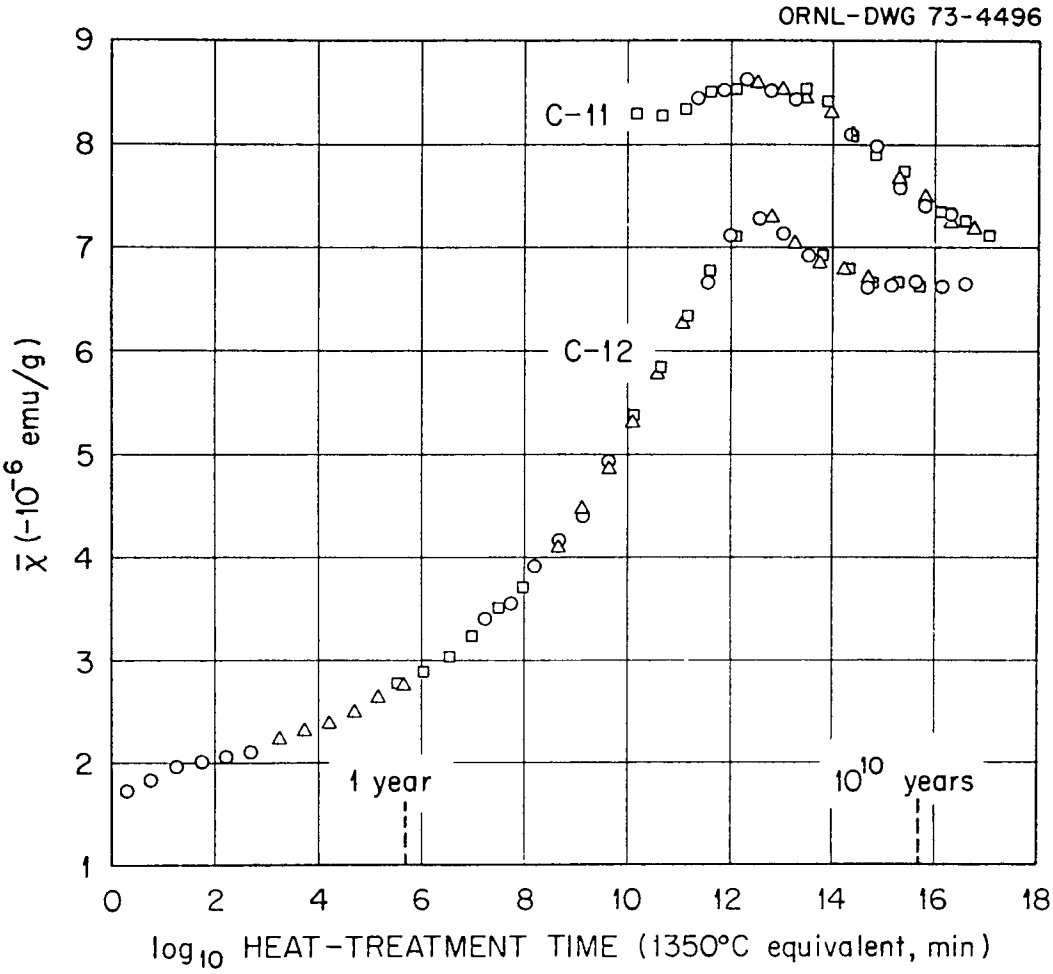

Fig. 14(a). Master Curves Formed by Superimposing Isothermal Diamagnetic Susceptibility ($\bar{\chi}$) Data.

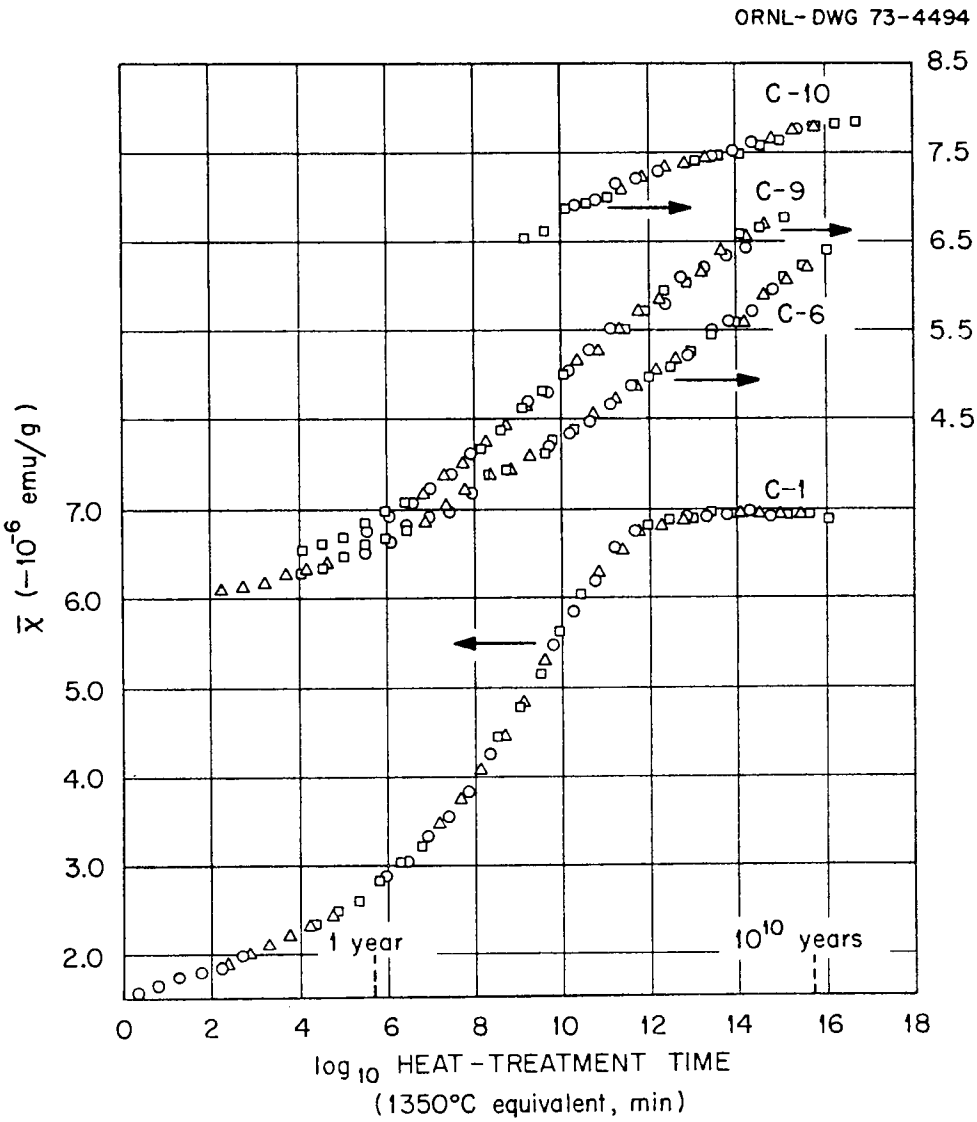

Fig. 14(b). Master Curves Formed by Superimposing Isothermal Diamagnetic Susceptibility ($\bar{\chi}$) Data.

3000°C. The similarity of the superimposed isothermal master curves to the corresponding isochronal curves in Figs. 6 and 12 should be noted. Of course, the isochronal and superimposed isothermal plots should give the same picture since they are constructed from the same data, but the important point is that they are plotted on different, albeit equivalent, scales. The continuity of the master curves should be considered as confirmation of the validity of the superposition method. Master plots of density versus log HTt (1650°C equivalent minutes) for C-5 and C-9 are shown in Fig. 15(a). Again the correspondence with the appropriate isochronal curves in Figs. 6 and 9 may be seen. The gaps in the master density plots are due to the fewer density data obtained, compared with $\overline{X}$ data, and not to reduced curve overlap. The temperature-compensated time scale may, of course, be established with respect to any reference temperature and the density of C-8 has been plotted on 3000°C and 1800°C equivalent time scales in Fig. 15(b). C-8 is the carbon which densified nearly 24% in 18 min and 17% in 2 min at 3000°C. It can be seen in Fig. 15(b) that at 3000°C the density of C-8 would reach about 1.535 g/cm^3, an increase of nearly 8%, in 1 sec and approximately 1.458 g/cm^3, an increase of more than 2.5%, in 1 msec.

Effective activation energies were obtained in this study by superposition of isothermal density and magnetic susceptibility curves. The density curves for C-5, Fig. 7, and the susceptibility plots for C-12 and C-5, Fig. 8(a) and

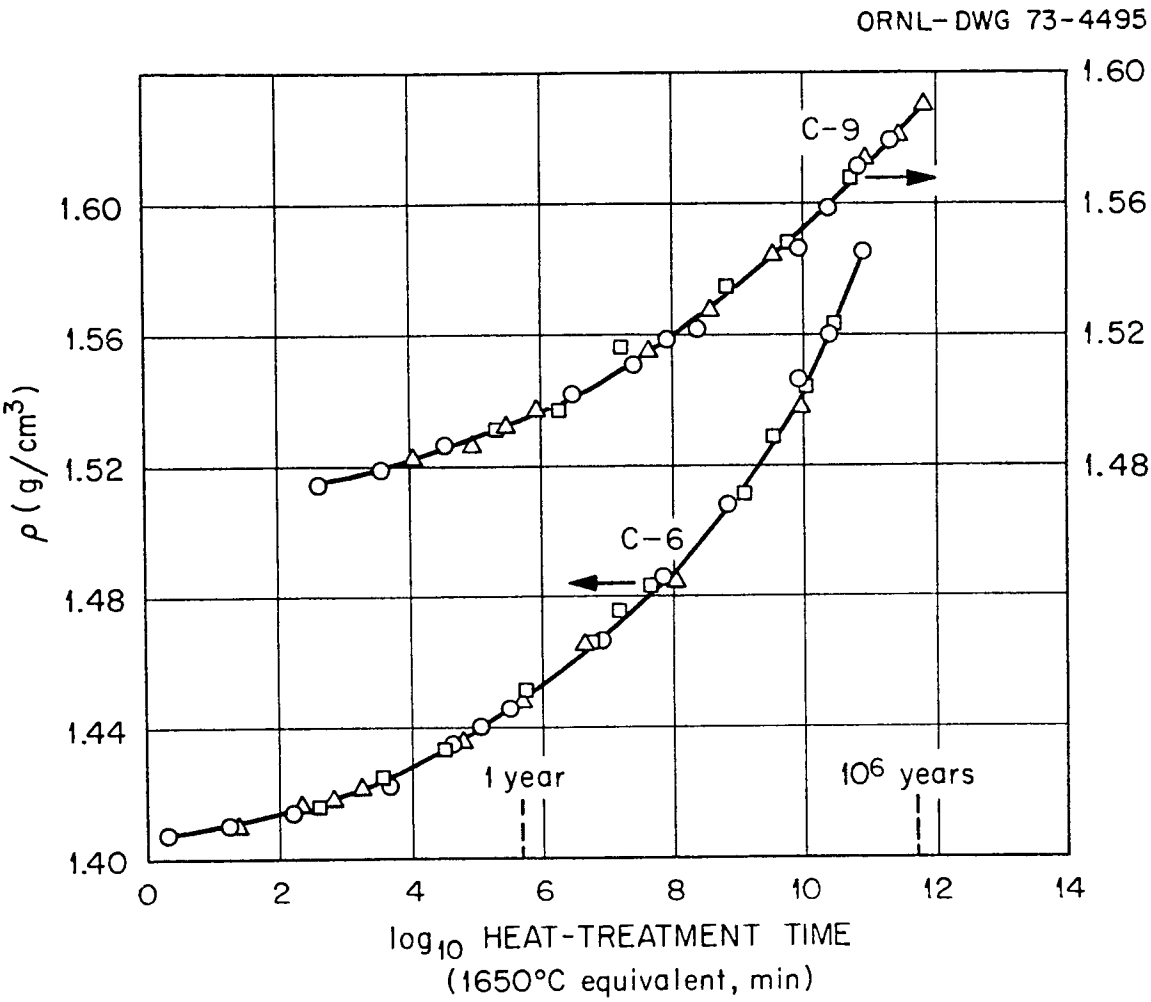

Fig. 15(a). Master Curves Formed by Superimposing Isothermal Density (ρ) Data.

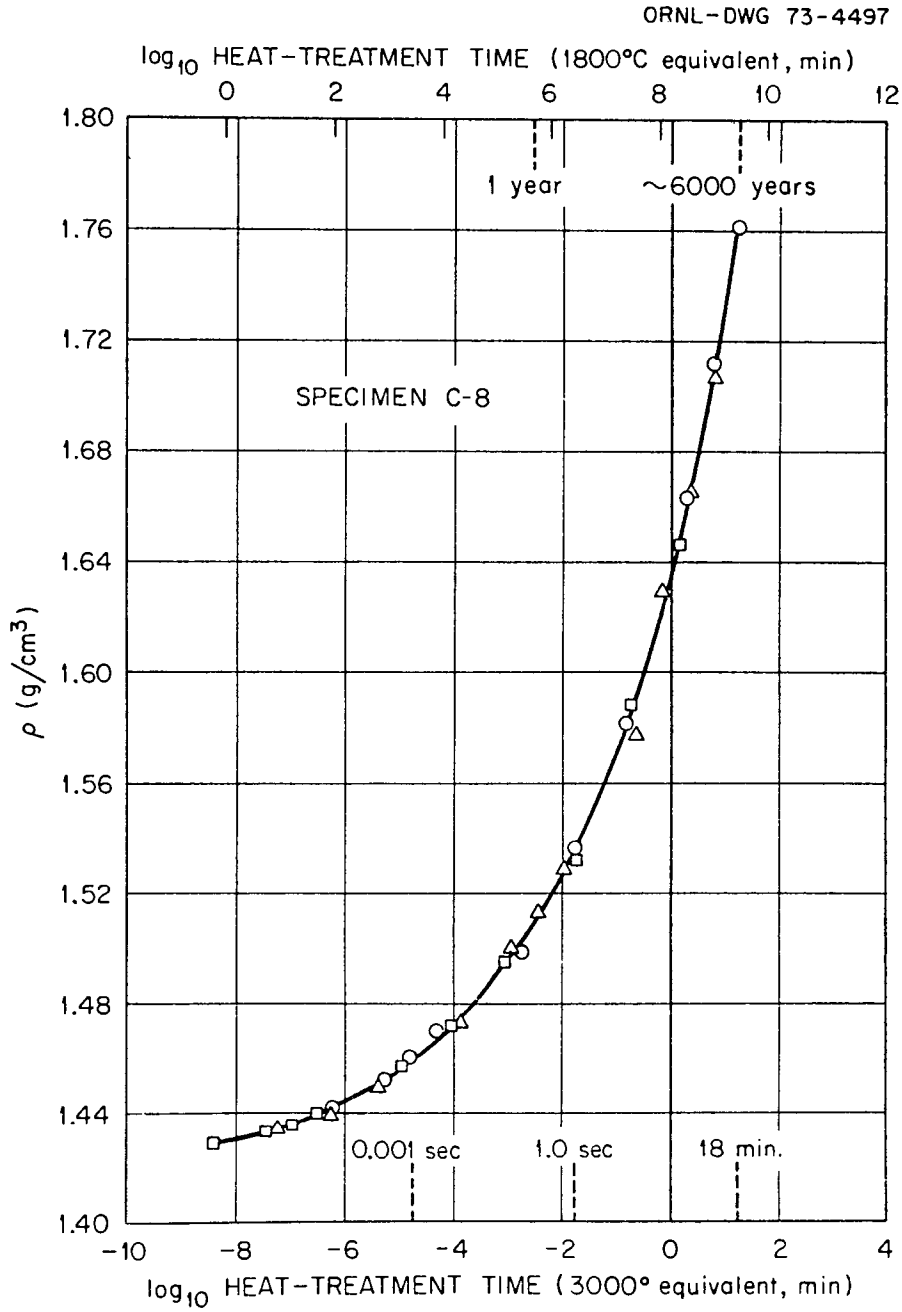

Fig. 15(b). Master Curves Formed by Superimposing Isothermal Density (ρ) Data.

(b), are representative of the curve families developed and analyzed for the twelve carbons. It can be seen by inspection of these figures that each isothermal curve can be positioned to overlap the next-lower-temperature curve of its family by translating it to the right parallel to the log time axis. The amount of translation required to effect this superposition, $\ln t_0 - \ln t$, gives a relative rate constant value, $\ln[K(T)/K(T_0)]$. An Arrhenius plot can then be constructed from the $\ln[K(T)/K(T_0)]$ values versus the reciprocal of absolute temperature.

The Arrhenius plots obtained for the twelve carbons from susceptibility and density data are shown in Figs. 16 and 17, respectively. The susceptibility data proved useful for activation energy analysis of all the carbons over a broad temperature range, starting with the lowest heat-treatment temperature employed in each case. Since the 1150 and 1250°C deposits all exhibited flattening of the $\bar{\chi}$ curves with further heat treatment at high temperature, cutoffs were imposed on their respective Arrhenius plots as shown. All other deposits, however, showed adequate $\bar{\chi}$ changes to allow analysis to the 3000°C heat-treatment limit. More limitations were encountered with the density data. In the two 1900°C deposits, the amount of densification was too small and there was too much data scatter to allow meaningful analyses. All the intermediate temperature, low-density deposits densified so little at the lower heat-treatment temperatures that the data were useful only after treatment well above the

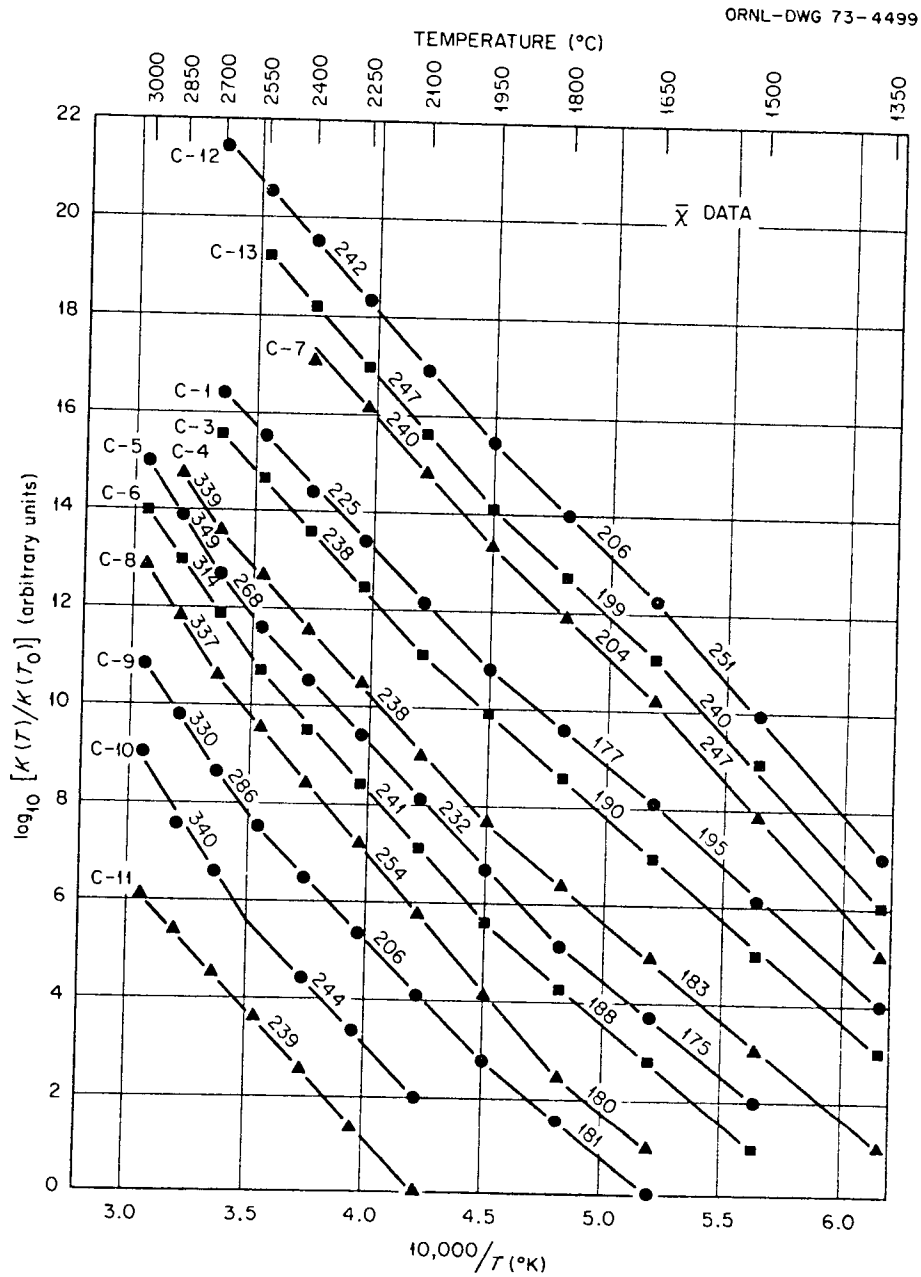

Fig. 16. Arrhenius Plots of Relative Rate Constants Showing Activation Energies (kcal/mole) for Change in Mean Diamagnetic Susceptibility ($\bar{\chi}$).

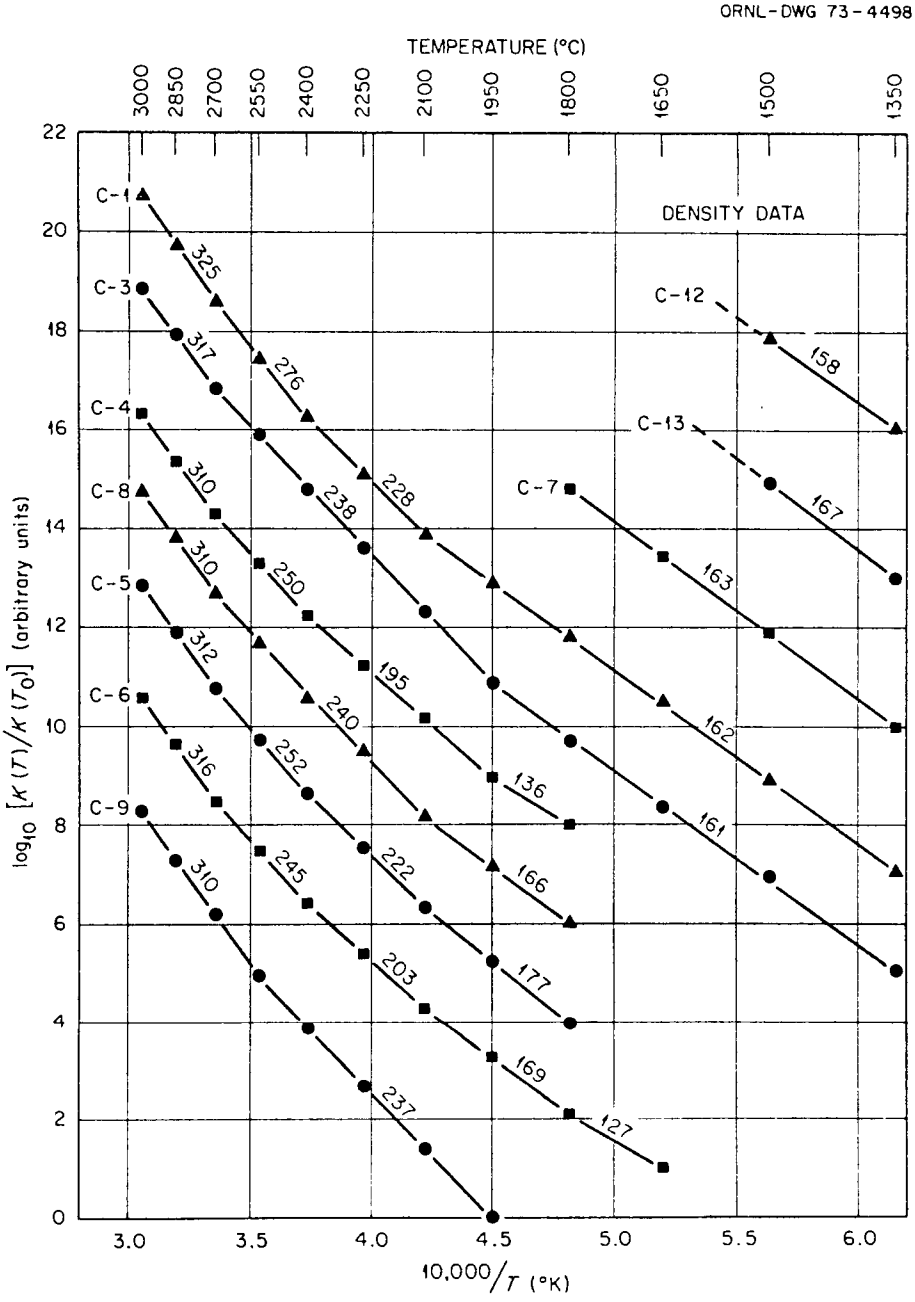

Fig. 17. Arrhenius Plots of Relative Rate Constants Showing Activation Energies (kcal/mole) for Densifications.

deposition temperatures. The problem of data scatter due to delamination of the 1150°C coatings discussed earlier seriously limited meaningful Arrhenius plots for these materials; only two points each were obtained for C-12 and C-13.

All the Arrhenius plots but one obtained from both $\overline{\chi}$ and density data indicate multiple-valued activation energies over the heat-treatment temperature range studied. Thus the data points are connected by straight-line segments, some very short, which emphasize the non-single-valuedness of ΔH. The numbers accompanying the plots in Figs. 16 and 17 are ΔH values in kcal/mole calculated for the proximate line segments as drawn. It may be noted that in many cases the plots could be segmented in different ways, but this would only average the ΔH values slightly differently in particular ranges, and would not affect the conclusions. The multiple-valued activation energy obtained from both density and $\overline{\chi}$ data for each carbon and the groupings of ΔH values for different HTT ranges are shown graphically in Fig. 18.

The effective activation energies determined from $\overline{\chi}$ data fall generally into three ranges, with several exceptions, with regard to heat-treatment temperature. Most of the specimens showed ΔH values of 180 ± 10 kcal/mole in the HTT range below 1950°C, 240 ± 15 between 1950 and 2700°C, and 330 ± 20 above 2700°C. The values of 180 and 240 are in good agreement with most of the literature values reported for the respective temperature ranges. However, ΔH values above

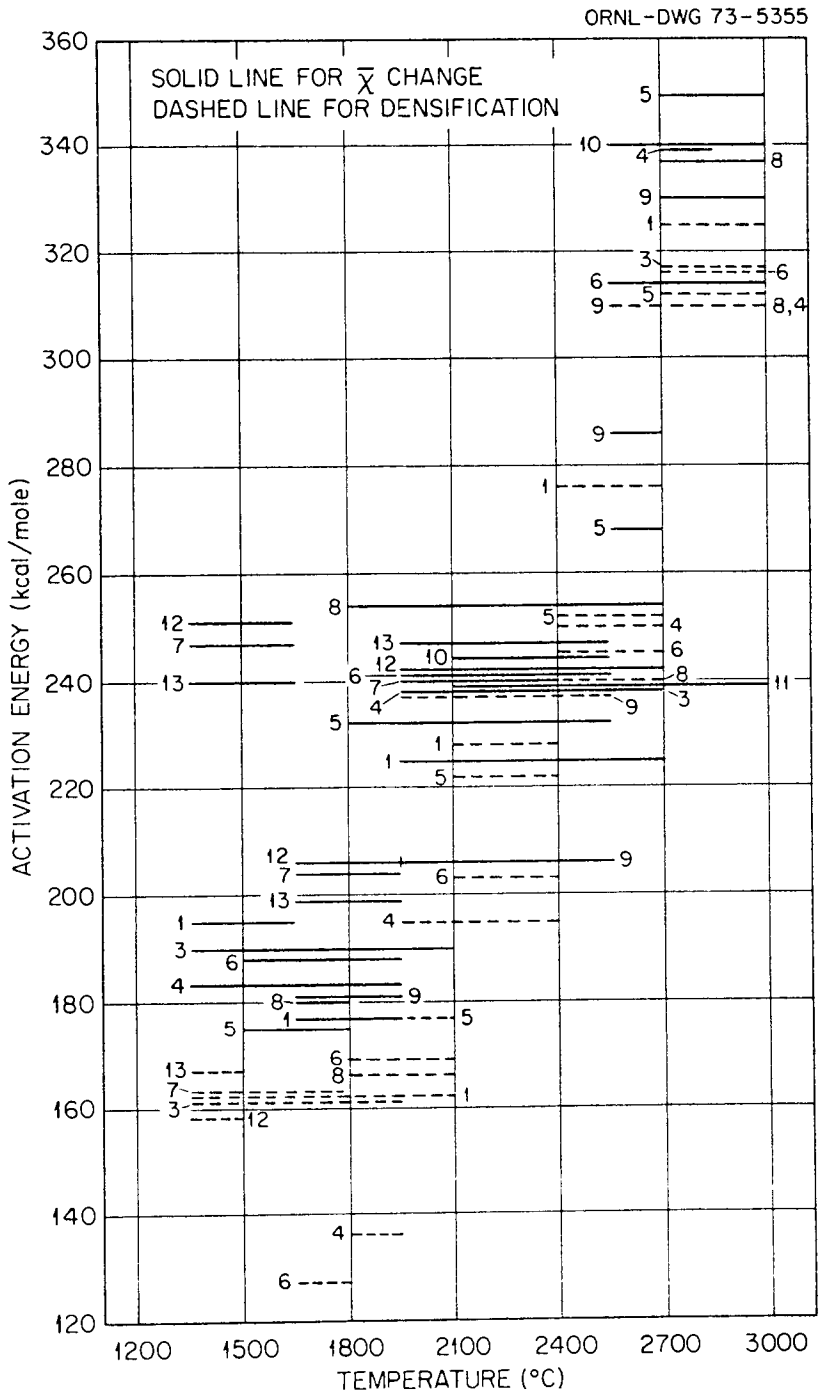

Fig. 18. Effect of Temperature on Activation Energies for Densification and Diamagnetic Susceptibility ($\overline{\chi}$) Change for Twelve Carbons.

300 kcal/mole have been reported by only one investigator [147] based on creep in glassy carbon.

The major exceptions to the general pattern here were the three 1150°C deposits which showed much higher activation energies at low temperatures. It may be noted that the data for these materials could be fitted, with some scatter, in each case by a single straight line corresponding to a ΔH of about 235 kcal/mole. However, this is probably fortuitous. The surprising features of these plots are the very high initial ΔH values in the range 240 to 250 kcal/mole below 1650°C, the decrease in ΔH above 1650°C, and the nearly identical values obtained for the three specimens. Since these initial ΔH values are much higher than most values reported in the literature for this temperature range, the experimental procedures were inspected for systematic errors in either heat treatment of $\overline{X}$ measurements. However, in all cases the three 1150°C deposits and the three 1250°C specimens were processed experimentally as a group. Thus, systematic experimental errors leading to erroneously high activation energies, if in any, should have shown up in all six specimens. Since this did not happen, the appearance of the high activation energy in three specimens gives credence to its reality. A slight indication of the pattern shown in the plots for the 1150°C specimens may be seen in that of C-1, the highest-propylene-flux, 1250°C deposit. C-1 shows a slightly higher ΔH value below 1650°C than above, though much lower in both ranges than the 1150°C specimens. However, if

the C-1 data are averaged from 1350 to 1950°C, ΔH falls in the range of 180 ± 10 kcal/mole, essentially the same as the higher temperature deposits.

An exception to the ΔH range of 240 ± 15 kcal/mole obtained from the $\overline{X}$ data in the 1950 to 2700°C HTT range occurred in C-9 which showed a ΔH of 206 kcal/mole between 1950 and 2550°C. The only other exceptions are transition values, which are variable depending on how the plot is segmented, between the basic ΔH ranges.

Effective activation energies determined from the density data show many similarities, and several marked differences to the pattern obtained from the $\overline{X}$ data. Density ΔH values increased with increasing treatment temperature in all cases where values were obtained over an extended range. At temperatures above 2700°C, energies in the range 310 to 325 kcal/mole were found, in excellent agreement with the $\overline{X}$ results. In the HTT range 1950 to 2700°C where the $\overline{X}$ data yielded largely single-valued energies of 240 ± 15 kcal/mole, the density results can be averaged to give similar results. However, several of the density plots show changes of slope within this range, with values of 195 to 230 kcal/mole below 2400°C and 245 kcal/mole or higher above 2400°C. An exception is C-9 which showed a higher average ΔH, 237 kcal, between 1950 and 2550°C, the same range where it gave the low value of 206 in the $\overline{X}$ plot.

For the lower heat-treatment temperatures all specimens showed lower ΔH values in the density plots than were

obtained from the $\overline{X}$ data. Below 1950°C all density ΔH values fell in a range of 167 ± 10 kcal/mole except much lower values for the first steps shown for C-4 and C-6. These values of 136 and 127 kcal/mole, respectively, are probably not significant because the densification occurring in these ranges is too small to allow accurate analysis. Activation energies obtained from density data of the 1150°C deposits for the initial heat treatments, before coating fragmentation caused undue data scatter, are in excellent agreement with low-temperature ΔH values obtained from density plots of other specimens. However, they are at great variance with the results from the $\overline{X}$ data of the same specimens. For all three 1150°C deposits, initial ΔH values determined from density measurements are about 75 to 90 kcal/mole lower than values obtained from $\overline{X}$ data. The density values are in good agreement with activation energies reported in the literature for this HTT range. Only one investigator [148] has reported a much higher ΔH(265 kcal/mole) for the HTT range below 2100°C, also determined from susceptibility data.

CHAPTER V

DISCUSSION

Kinetic studies in recent years have established that graphitization is a thermally activated process, but the detailed mechanisms by which it proceeds are not well understood. Mechanisms have been proposed by inference from kinetic data, but clear evidence for specific processes is difficult to establish. The literature pertaining to graphitization contains activation energies ranging from 75 to 350 kcal/mole. This diversity stems, apart from experimental uncertainties, from the use of different types of carbon starting materials, the employment of various heat-treating temperature ranges, and treatment of the data by different analytical methods.

In the present study carbons of widely different initial microstructures were examined over a very broad range of heat-treatment temperatures so that respective effects of these variables on kinetic behavior could be observed. The results obtained show that for the different carbons, rates of change of properties vary greatly under given heat-treatment conditions. In most cases the effective activation energies determined for the different carbons in the same HTT range were in good agreement with each other, but notable exceptions were found. The results also show clearly that the activation energy for graphitization of individual carbons is single-valued only in special cases and not as a general rule if a

broad enough range of treatment temperatures is studied. However, the term graphitization is applied broadly in this work to property changes induced by heating in the entire temperature range from 1350 to 3000°C. Some authors denote the HTT range below 2000°C as a pregraphitization range, and the large as-deposited hydrogen contents suggest that the initial heat treatments of the 1150°C deposits could also appropriately be considered to involve the final stages of carbonization.

The effects of heat treatment on the diamagnetism of the twelve carbons studied will now be examined. As noted earlier, the diamagnetic susceptibilities of the as-deposited carbons ranged from values just above those of large aromatic molecules for the 1150°C deposits to well above the graphite single-crystal value for C-11. It is of particular interest that these four specimens, which represented the upper and lower extremes of the as-deposited susceptibilities, were the only carbons studied which showed distinct $\overline{\chi}$ maxima with heat treatment. The common factor, as discussed earlier, was the greater tendency of these high-density specimens to graphitize. The susceptibility maxima result from the well known dual dependence of the diamagnetism of carbon on crystallite size and layer stacking order.

The diamagnetism increases rapidly with increasing size and perfection of the small graphite-like layers. This is shown in the early concomitant increase in apparent crystallite diameter and susceptibility for all specimens studied.

As long as significant interlayer interactions are not involved, $\bar{\chi}$ increases toward a limiting value of about 13 (in units of -10^{-6} emu/g) as shown by McClure's [78] two-dimensional band structure model. The graphite $\bar{\chi}$ value of 7.3 is not significant in terms of the two-dimensional structure. Thus, the large as-deposited $\bar{\chi}$ value in C-11 can be accounted for on the basis of the large L_a and the lack of layer stacking order as evidenced in the large $\bar{d}$ value. Similarly the $\bar{\chi}$ increase of C-10 through the graphite value with heat treatment is seen to be related to L_a growth without accompanying decrease in $\bar{d}$.

In the four most graphitizable specimens, C-12, C-13, C-7, and C-11, the $\bar{\chi}$ increase due to layer growth and improvement is checked after a few minutes at 2250°C (or equivalent, i.e., temperature-compensated time, heat treatment). While further L_a measurements were not made on these specimens due to modulation of the (10) line, L_a growth probably continued at a fairly rapid rate with further heat treatment. The subsequent decrease in $\bar{\chi}$ is due to the overriding effects of the interlayer interactions resulting from the development of layer ordering. The ordering is evidenced by the rapid decrease in $\bar{d}$ accompanying the $\bar{\chi}$ maxima, and the appearance of (hkl) diffraction maxima just beyond the $\bar{\chi}$ maxima. The continued decrease in $\bar{\chi}$ of C-11 with further heat treatment indicates that the layer interaction contribution to the diamagnetism increases more rapidly than the layer growth contribution. The flattening of the $\bar{\chi}$ curves for the 1150°C

deposits at high temperatures suggests that the two effects almost exactly cancel each other, not that nothing is happening. The reason for the nearly exact cancellation is not clear and may be a coincidence. However, a strikingly similar behavior in susceptibility development has been observed for a coke-pitch composite [149,150].

The 1250°C deposits show decreasing graphitizabilities in the order C-1, C-3, and C-4, the order of decreasing propylene flux or concentration employed in their deposition and the order of decreasing hydrogen content. The rates of increase in $\overline{\chi}$ decrease in the same order, and are lower than observed for the 1150°C deposits. This corresponds with slightly lower rates of L_a growth than found in the 1150°C carbons, and with postponed development of layer stacking order and maximizing of the $\overline{\chi}$ curves. In each case a rapid decrease in $\overline{d}$, indicating the development of stacking order, is seen to coincide with approach to a maximum in $\overline{\chi}$. The intermediate temperature deposits are all very resistant to graphitization. Susceptibilities increase slowly with heat treatment as do the apparent crystallite diameters, while $\overline{d}$ decreases slowly through the final heat treatment. An exception to this behavior may be seen for C-8, the specimen which had a high macroscopic preferred orientation as deposited. During the final heat treatments, C-8 exhibited a very rapid decrease in $\overline{d}$ and a concomitant rounding over of the $\overline{\chi}$ curve. Very faint (hkl) diffraction maxima were observed for the sample heated for 18 min at 3000°C. These

changes suggest that C-8 may graphitize to a considerable extent at higher temperature or longer time at 3000°C. The effects of more extreme heat treatment on this material would indeed be of interest.

As noted earlier, the macroscopic anisotropy characteristic in C-8 should not be confused with the microscopic anisotropy characteristic of the high-density deposits. The deposition conditions employed in producing C-8 evidently favored formation of species having greater planarity than those involved in forming the other deposits. This effect has been considered in studies of the pyrolysis process [4, 151–156]. These planar species formed in the gas phase tend to deposit parallel to the substrate surface, thereby building up a body of some preferred orientation. However, the low density of this deposit shows that packing of the planar species is very inefficient, and suggests that extensive microporosity must be included in the structure. Such microporosity has been observed directly by transmission electron microscopy in similar materials by Steigler *et al.* [157]. Since the structure is thus known to comprise small planar units very poorly packed together, it is apparent that on the average a large angular mismatch exists between crystallites, and that extensive structural rearrangement will be necessary for significant densification. The situation is probably similar in the other low-density deposits except that the building units are less planar and the packing orientation is more nearly random.

Effects on graphitizability of the type of anisotropy extant in C-8 will now be considered. Compare the property changes induced by heat treatment in C-8 and C-6, Fig. 6(g) and (i), preferred orientation being the only large apparent difference in these two specimens as deposited. The initial densities are nearly the same, and densification rates differ little up to about 2250°C. Other property change rates also are very similar in this range. Evidently the higher preferred orientation per se in C-8 is of little importance to the processes involved. However, above 2250°C the densification rate of C-8 increases much more rapidly than that of C-6, and at the experimental limit, 18 min at 3000°C, C-8 shows a rapid decrease in mean interlayer spacing and the beginning of three-dimensional order development. The latter effects do not occur in C-6. The photomicrographs in Fig. 4, however, show extensive microstructural change in C-8 as a result of the 3000°C, 18-min heat treatment. The coating had densified about 24%, so it may be inferred from the micrograph that a large shrinkage perpendicular and expansion parallel to the deposition surface occurred. Similar behavior has been observed in massive pyrolytic carbons and described as a "dewrinkling" process [158–160]. Fischbach [11] has termed the effect "spontaneous plastic deformation produced by self-generated stresses," the stresses being attributed to the different thermal expansions in the "a" and "c" directions. The requirement for initiating the spontaneous deformation is the presence of some preferred orientation.

One result is to further increase preferred orientation and to effect better crystallite alignment. Thus, the enhanced graphitization rate observed in C-8 at high temperatures appears to be a direct result of plastic deformation, which in turn is a result of the as-deposited preferred orientation.

It should be noted that the enhanced graphitization rate in C-8 near 3000°C is not reflected in the activation energy. The ΔH values obtained from both density and $\overline{\chi}$ data at high temperatures for C-8 are in good agreement with those of the other difficult-to-graphitize specimens. It must be concluded, therefore, that the enhanced rate is accounted for by a larger preexponential factor as discussed by Murty, Biederman, and Heintz [102,103]. This reflects a change in the distribution of processes due to the plastic deformation, and is consistent with the concept of a single-valued activation energy if restricted to a particular type of carbon and a limited temperature range. The only other specimens showing significant anisotropic spontaneous deformation in this work were the three 1150°C deposits. The necessary initial macroscopic preferred orientation was apparently induced in C-12 and C-13 during early, rapid densification while the coatings were constrained by the rigid glassy carbon kernels. This would be equivalent to hot stretching, a common method of increasing preferred orientation. The anisotropic deformation shown by these specimens may have been less important to subsequent graphitization than was the case for C-8, but local spontaneous

deformation, reflected in the rapid densification, probably played an important role.

The variation in rates of graphitization for different carbons has been observed by numerous investigators, and the question of how to treat the different rates in the kinetic analysis arises. In any expression of reaction rate, the rate constant is the product of a Boltzmann probability factor, which contains the temperature dependence in exponential form, and a temperature-independent preexponential or frequency factor. Differences in rate constants then may be attributed either to a distribution of preexponential factors or to a distribution of activation energies or to both. Direct calculation of the preexponential factor, which would require knowledge of particular specified mechanisms including geometrical factors and entropy terms, cannot be made at the present level of understanding of the graphitization process. Therefore, the assumption is often made that graphitization occurs by single-atom transport processes which obey first-order kinetic laws, and a preexponential near the Debye frequency is used. With the preexponential factor thus fixed, differences in graphitization rate are related to different activation energies. On the other hand, if the temperature dependence of the graphitization rate can be determined without specification of a preexponential factor, the activation energy obtained is not biased by assumptions about details of the mechanism(s) involved. This is the strength of analysis based on a temperature-compensated time parameter.

Even in this case, however, the activation energy should be considered as a measure of the rate temperature dependence of the kinetic parameter employed, and as not necessarily due to a single process. Hence, the experimental ΔH values obtained in this work are referred to as effective activation energies.

There is a diversity of opinion in the literature as to whether graphitization entails a spectrum of activation energies or is characterized by a single-valued activation energy. Franklin's [12] concept of graphitization occurring by rearrangement of whole layers or groups of layers was rationalized as requiring a continuously increasing activation energy with increasing crystallite size and development. Fair and Collins [90], in one of the first attempts at detailed kinetic analysis of graphitization, also concluded from their results that the activation energy increases as the transformation from carbon to graphite progresses. More recently, however, strong arguments for a single-valued activation energy in the range 230 to 270 kcal/mole for graphitizing carbons have been produced by Fischbach [89,92-94] for the HTT range 2000 to 3000°C, and by Murty, Biederman, and Heintz [102,103] for the range 2300 to 2700°C, though the interpretation by Murty *et al.* of their data in terms of a single-valued ΔH has been questioned [161]. A limitation on the Murty *et al.* analysis is the very narrow range of treatment temperatures employed.

Fischbach and Murty *et al.* did observe differences in graphitization rates in different carbons, but they presented

very strong arguments in favor of attributing this to differences in the preexponential factor. Murty *et al.* noted a correlation between x-ray preferred orientation and preexponential factor for three cokes, the preexponential being larger for a coke of greater anisotropy. It seems reasonable that the preexponential factor should reflect the structural configurations of the starting materials as noted by Murty *et al.*, but the macroscopic anisotropy factor per se may not be a uniquely important parameter for all carbons. Microscopic anisotropy as observed optically has been noted by Kipling and Shooter [162] to be a measure of graphitizability for low-temperature carbons. This microscopic anisotropy, which must be a measure of the extent of localized crystallite alignment, may be of more fundamental significance in determining the rate and extent of graphitization. While macro- and micro-anisotropies may well be related in many carbons, the relationship is not universal. Fischbach [11] has observed that a distribution of preexponential factors should result from variation of the amount of diffusion required to produce a detectable change in any property. This could result either from differences in the nature and extent of the structural defects being removed or from differences in the concentration or distribution of defect sinks.

Results of the present work show that the activation energy for graphitization does vary with temperature over the treatment range 1350 to 3000°C. Moreover, there is no reason to suppose that ΔH should be single valued over this

temperature range, and most of the values obtained below 2700°C are in good agreement with those in the literature. The preponderance of evidence in the literature argues for activation energies in the range 150 to 190 kcal/mole in the temperature range below 2000°C, and 200 to 280 kcal/mole above 2000°C. Values above 300 kcal/mole have not been reported previously except in a study of creep in glassy carbon [147]. While most graphitization studies have been limited to temperatures below 2700 to 2800°C, probably due to furnace limitations, Fischbach [87,92–94] has accumulated a considerable amount of data for cokes and high-temperature pyrolytic carbons treated at 3000°C. These data have allowed extension to 3000°C of his straight-line Arrhenius plots for ΔH values of approximately 260 kcal/mole. In contrast, the present results from both density and $\overline{X}$ data show increases in the slopes of all Arrhenius plots for non-graphitizing carbons at temperatures above 2700°C. However, the single Arrhenius plot obtained for a graphitizing carbon (C-11) through 3000°C was single valued near 239 kcal/mole. It should be noted that Arrhenius plots were not obtained above 2700°C for the other graphitizing carbons studied (C-12, C-13, and C-7) because the kinetic parameters employed, density and $\overline{X}$, did not change significantly in this range. This does not mean that no microstructural changes were occurring in these carbons, but only that changes were not manifested in density and $\overline{X}$ measurements.

The observed activation energies may be conveniently discussed in terms of three HTT ranges, 1350 to 1950°C, 1950 to 2700°C, and 2700 to 3000°C. Values determined for treatment temperatures below 1950°C will be considered first. All analyzable density data for this range yielded effective ΔH values of 167 ± 10 kcal, except the initial steps shown on the C-4 and C-6 plots. These low values near 130 kcal may be attributed to the very small amount of densification involved which may not be representative of the amount of microstructural change occurring. It seems possible in structures of this type, which contain large amounts of microporosity and an extensive system of cross-link bonds, that a considerable amount of internal change could occur before being manifested in densification. This is consistent with sizable $\overline{X}$ increases observed in the lower density deposits prior to significant densification. It might, therefore, be expected that incipient densification for the low-density carbons would not produce a true picture of the rates of the processes involved. The value of 167 ± 10 kcal is in excellent agreement with results obtained by Stevens [115,141] for similar materials. From an analysis of isochronal dimensional change data based on the assumption of a fixed preexponential factor, Stevens obtained distributions of activation energies which peaked near 155 kcal for high-density deposits (i.e., for materials which showed significant dimensional change at low temperatures).

Activation energies determined from magnetic susceptibility data at temperatures below 1950°C fell in the range 185 ± 10 kcal for all carbons studied except the 1150°C deposits C-12, C-13, and C-7. The 1900°C deposits were, of course, not analyzed in this temperature range. This value also is in good agreement with literature values, and the low side of the range just overlaps the high side of the ΔH range obtained from density data on the same materials. The Arrhenius plots for the three 1150°C deposits, however, showed much higher initial ΔH values, in the range 240 to 251 kcal, for the treatment temperature range 1350 to 1650°C. As mentioned in the section on results, all work done in obtaining these values was carefully checked for systematic errors, but the large temperature dependence for $\overline{X}$ increase was clearly present. The difference between these results and the ΔH values obtained by Stevens [115,141] from dimensional change data for low-temperature, fluidized-bed deposits was first attributed [163] to the difference in method of analysis. However, subsequent ΔH determinations from density data of these 1150°C deposits gave values in excellent agreement with those of Stevens, and lower by an average of about 85 kcal/mole than the energies determined for the same materials by the same method of analysis (superposition) using $\overline{X}$ data [164]. Thus, at least two important questions are raised. What is the source of the much higher effective activation energy for $\overline{X}$ increase as compared with densification in the same carbons? And how is it possible

that a process requiring a ΔH of 240 to 250 kcal/mole can proceed at a measurable rate at temperatures below 1650°C?

Since the high initial activation energy for $\overline{X}$ development is encountered only in the three 1150°C deposits, microstructural differences between these and the other carbons studied must be considered. The most obvious differences are the higher densities, optical anisotropies, and hydrogen contents of the 1150°C deposits. Neither the structural compactness evidenced by higher density nor the better localized inter- and intracrystallite alignment manifested as higher optical anisotropy seem likely to account for the high ΔH anomaly. In particular, it is difficult to see why these features should lead to differences in the effective activation energies for densification and $\overline{X}$ increase. The higher hydrogen contents, on the other hand, suggest the possibility of a ΔH contribution due to hydrogen evolution.

Since only total hydrogen contents were determined in this work by heating at 2000°C, kinetic information on hydrogen release was not obtained. However, Stevens [141] has found the total evolution from a specimen containing more than 600 ppm of hydrogen to increase gradually with treatment temperature up to about 1800°C after which further evolution was not evident. He determined the activation energy for hydrogen evolution to be about 124 kcal/mole, and concluded that hydrogen evolution may be a precursor to the processes which cause dimensional change, but is not rate limiting.

The question thus becomes whether hydrogen evolution could influence the rate (i.e., contribute to the effective ΔH) of the increase in diamagnetism but not the rate of densification.

First the amount of hydrogen and its position in the carbon structure must be considered. The low-temperature deposits studied were shown to contain in the range 700 to 1600 ppm or about 1 to 2 at. % hydrogen. This hydrogen is probably not unformly distributed on an atomic scale, but rather concentrated at layer boundaries. Grisdale *et al.* have described the layers in vapor deposited carbons as giant molecules with peripheral valences satisfied by hydrogen or hydrocarbon fragments [151]. With the 30 to 35 Å crystallite diameters measured on the 1150°C deposits, the 1 to 2 at. % hydrogen contained could thus provide a near saturation of bonds at the periphery of every layer. As mentioned earlier, the $\overline{X}$ values measured on the as-deposited 1150°C carbons were, in fact, close to values for large aromatic molecules. This is consistent with the above concept of these structures as comprising in effect high molecular weight hydrocarbons.

Next consider the effect of initial heat treatment on the "hydrocarbon" microstructure. As the carbon-hydrogen bonds are broken the most likely means, from an energy-level standpoint, of satisfying the resulting free valences is formation of graphite-layer-type trigonal bonds. This probably involves carbon transport by diffusion within and between layers and particularly along layer edges or crystallite boundaries. Major effects on the microstructure would include healing of

intralayer defects as well as crystallite growth across low-angle boundaries, both of which would increase density and diamagnetic susceptibility.

The remaining difficulty is to explain the difference in effective activation energies observed for densification and for $\overline{X}$ increase. Since the energy barrier for hydrogen removal is appreciably lower than the 160 to 180 kcal/mole needed for carbon transport to effect densification, the hydrogen evolution would not be expected to be rate limiting in any case. However, as noted above, the large effective ΔH difference for increases in density and $\overline{X}$ were observed only in carbons of very high hydrogen content and only in the HTT range where the hydrogen is being evolved. Therefore, since the difference was about 85 kcal/mole, similar to known values of C-H bond strengths [165], the evidence for the rate of $\overline{X}$ increase being limited by consecutive C-H bond rupture and a carbon transport mechanism is considerable. This, of course, only rationalizes the high ΔH obtained at low temperature. The detailed mechanisms are not clear from the available data.

The conclusion that activation energies of 240 to 250 kcal obtain as the sum of values for consecutive processes in these materials in the HTT range 1350 to 1650°C also privides a basis for explaining the high rate of increase in diamagnetism. The difficulty in justifying such a high ΔH for a process which occurs rapidly at these temperatures has been noted by Price and Bokros [166] if the usual assumption is made for a

preexponential near a bond vibration frequency. However, if the change effected in a measured parameter requires consecutive reactions, the overall rate expression is the product of the rate expressions for the individual reactions; the activation energies are additive and the preexponential factors are multiplicative. Thus, from the usual assumption of a preexponential in the range 10^{13} to 10^{16} sec^{-1} for individual single-atom processes the appropriate factor for the total process in question may lie in the range 10^{26} to 10^{32} sec^{-1}. The claim made is not, of course, that a suitable preexponential factor has been determined, but only that an effective activation energy of 245 kcal/mole can be rationalized in this manner for a process which proceeds at a measurable rate of 1350°C.

The superposition method of analysis used in this work does not provide a means for determining preexponential factors. Since all rate constants employed are relative, extrapolation of the Arrhenius plots to infinite temperature produces only factors in arbitrary units. However, the determination of the effective activation energy for $\overline{X}$ development discussed above clearly emphasizes the importance of avoiding the usual a priori preexponential factor assumption. While similar conclusions may be reached with or without preexponential assumptions in some cases (e.g., Stevens' analysis of dimensional change data [115,141] and the present superposition analysis of densification data), the different analytical methods would clearly lead to different

conclusions about the processes involved in the increase in diamagnetism.

Attention may now be turned to activation energies obtained at intermediate heat-treatment temperatures. For the treatment range 1950 to 2700°C, the Arrhenius plot determined from either density or $\overline{X}$ data for every specimen analyzed shows an effective ΔH of 235 ± 25 kcal/mole, when averaged over that entire range. Energy barriers of this magnitude have been identified by several workers [92,93,102, 167–170] with diffusion by a vacancy mechanism, and will not be discussed further here. However, the results obtained in this work do not support very well the contention that the activation energy in this temperature range is the same for all carbons or is necessarily single valued for particular carbons. Again there may be differences between graphitizing and nongraphitizing carbons. It should be noted that ΔH values obtained in this work at temperatures above 1950°C for the most graphitizable of the materials studied, C-12, C-13, C-7, and C-11, showed a range of only 239 to 247 kcal/mole. This is consistent with the concept of a single mechanism being responsible for graphitization in graphitizing carbons. However, the possibility of multiple mechanisms, particularly in difficult-to-graphitize carbons, should be examined further.

As discussed earlier, the nongraphitizing carbons studied all showed effective activation energies of 330 ± 20 kcal/mole for changes in both denisty and $\overline{X}$ in the 2700 to 3000°C temperature range. The significance of such high ΔH values

must now be examined. Consider first the possibility of its being an artifact due to experimental error. Since the high activation energy was obtained in every case but one for which analyzable data were available, random measurement errors may be excluded, and precise duplication of systematic errors in density and magnetic susceptibility measurements is highly improbable. The most probable error then is heat-treatment temperature. However, if the measurement of the absolute temperature value is even approximately correct, the apparent activation energy is a function of relative temperatures. Extrapolation of an Arrhenius plot of 240 kcal from the 2700°C data point to the value obtained at 3000°C on a 330 kcal plot would project the "true" 3000°C temperature to about 3125°C. Thus, if the difference in actual temperatures of "2700°C" and "3000°C" experiments were 425°C rather than 300°C, the 240 kcal ΔH obtained below 2700°C could be extended to 3000°C. Since the same furnace and pyrometer were used throughout, and careful inspection of the viewing window after each heat treatment gave no evidence of window fogging during any run, a relative temperature error of 125°C is considered by the author as highly unlikely. The evidence, therefore, is strong for the high ΔH above 2700°C in the materials studied.

If an activation energy of 330 ± 20 kcal/mole for graphitization at high temperature is considered real, the questions of its origin and why it has not been observed in cokes and high-temperature pyrolytic carbons arise. The

exceptional (in this study) behavior of the Arrhenius plot determined from $\overline{X}$ data of specimen C-11 may provide the link between the much higher ΔH values obtained above 2700°C for most specimens in this study compared with values obtained for graphitizing carbons in the same temperature range by Fischbach. The plots of mean interlayer spacing as a function of heat treatment for the twelve carbons studied show that none could be classified as easily graphitizable, but that C-11, along with the three 1150°C deposits, was much more graphitizable than the others. Unfortunately, activation energies could not be determined from either density or $\overline{X}$ data for the 1150°C deposits above 2700°C, and the C-11 density data were inadequate for analysis. Further, the $\overline{X}$ data for C-11 in the 2550 to 3000°C range are less complete and precise than desirable for positive proof of the extension through this range of the single-valued ΔH near 240 kcal. Nevertheless, the author's best efforts at analyzing the available data indicate that the high ΔH which appears at temperatures near 3000°C in the Arrhenius plots for all the very difficult-to-graphitize specimens studied does not occur in the more graphitizable C-11. This result then is consistent with results reported for the graphitizing petroleum cokes and pyrolytics.

The apparent difference in energy barrier for continued structural development at very high temperatures must be related to some microstructural feature which is fundamentally different for graphitizing and nongraphitizing carbons. This

difference cannot be attributed to macroscopic (as measured by x-ray diffraction) preferred orientation which covered a broad range in both graphitizing and nongraphitizing carbons studied. The most obvious difference is density, with those carbons having an initial density greater than 1.98 g/cm^3 being fairly graphitizable, those having densities between 1.7 and 1.96 graphitizing slightly after extreme heat treatment, and those of density lower than 1.7 showing no tendency to graphitize unless plastically deformed (e.g., the self-induced deformation of C-8 discussed earlier). The question of importance then relates to the microstructural significance of density.

The occurrence of microporosity with voids on the order of a few tens of angstroms in low-density carbons has been noted by numerous investigators. These voids have been observed by small angle x-ray scattering [12,24–27,171] and by direct transmission electron microscopy [157,172]. The amount of micropore volume and the void size are apparently related to details of the carbonization process as evidenced by the variety of densities obtained for different deposition conditions in this work. Franklin has attributed the microporosity in nongraphitizing carbons to formation, in the early stages of carbonization, of a system of cross-link (tetrahedral or sigma) bonds between neighboring layers or layer stacks [12]. The cross-linking is maintained on heating and serves to interlock the structure and hinder crystallite realignment and coalescence necessary for graphitization.

Dense carbons, on the other hand, lack the extensive system of rigid cross-links and are able to graphitize with less drastic structural modification.

This difference in microporosity (density) and probable concomitant cross-linking thus appears to determine ultimate thermal graphitizability as well as to influence the rate at which changes occur at particular temperatures.

Consider then the effects of heat treatment on low- (1150°C) and intermediate-temperature deposits. Resulting property changes have been shown to occur much more rapidly in the low-temperature deposits for any given treatment. As discussed earlier, this is probably a function of the more compact structure formed as a result of the slower and less complete dehydrogenation during the deposition as well as a direct result of increased mobility during heat treatment due to residual hydrogen. In any event both low- and intermediate-temperature (i.e., high- and low-density) deposits may be assumed to contain some cross-link bonds. The differences in annealability have been observed previously [110] for similar fluidized-bed carbons and attributed to a variety of cross-link bond strengths [4]. This concept could lead to the conclusion that the high activation energies observed at high temperatures in the difficult-to-graphitize deposits are due to breaking the stronger cross-links which did not yield at lower temperatures. However, a single cross-link bond strength of 330 kcal is untenable.

A more likely explanation of the observed annealability difference lies in the amount of cross-linking. The low-density, intermediate-temperature deposits are likely to contain such an extensive system of cross-link bonding that significant changes in measurable properties may not be effected at low heat-treatment temperatures because the rate of cross-link rupture is too low. This is supported by rapid $\overline{X}$ increases preceding significant densification. It is also possible that the driving force for graphitization is less in the low-density structures which lack the macroscopic crystallite alignment of the higher density carbons.

Since the observed ΔH value of 330 ± 20 kcal is too large to be associated with any known single-point-defect mechanism, and since it was observed only in carbons of initial low density containing extensive microporosity and probable cross-links, the inference drawn is the following. During treatment in the 1950 to 2700°C range, structural modifications occur in the low-density carbons by defect mechanisms which can operate well below the level of 300 kcal. This may involve vacancy and/or interstitial diffusion as well as layer boundary rearrangement which result in densification and crystallite growth limited to varying degrees in the different structures. Processes requiring energies greater than 300 kcal are simply not operative to a measurable degree in this temperature range. However, at temperatures above 2700°C the structure is still highly cross-linked and atoms which can be unlocked only by multiple simultaneous

rupture of tetrahedral bonds can migrate by the various defect mechanisms. The multiple bond ruptures plus diffusion apparently require an activation energy in the range 300 to 350 kcal/mole and can occur at a rate rapid enough to be manifested in measurable property change rates only at temperatures above about 2700°C. The high ΔH is not observed in graphitizing carbons in this temperature range because the structure does not contain the extensive system of cross-links, and structural improvement continues as at lower temperatures, probably by vacancy diffusion. Since most graphitization kinetic studies have been confined to easily graphitizing carbons and to temperatures below 2700 to 2850°C, the effects discussed have not received attention. Obviously further work at temperatures above 2500°C, including both graphitizing and nongraphitizing carbons, is needed to clarify the situation.

CHAPTER VI

SUMMARY AND CONCLUSIONS

Graphitization behavior of pyrolytic carbons deposited in fluidized beds has been shown to be a strong function of initial microstructure as determined by deposition conditions. The most important deposition parameter with regard to affecting graphitizability was found to be temperature, with hydrocarbon flux or concentration increasing in importance with higher temperatures. For the carbons studied, as-deposited density and hydrogen content appeared to be of primary importance in determining subsequent graphitizability, though anisotropy on either a macro- or micro-scale was also shown to play an important role. Density, of course, is a measure of local crystallite alignment and thus might be expected to reflect the extent of structural rearrangement necessary for evolution of the graphite structure. Results of this study suggest that a carbon is thermally graphitizable to an appreciable extent only if the initial density is greater than about 1.95 g/cm^3. The role of anisotropy appears to lie in generating internal stresses which induce plastic deformation, which in turn favors further structural evolution.

For the carbons studied, diamagnetic susceptibility was found to be a very useful kinetic parameter, particularly when used in conjunction with density and x-ray diffraction measurements. The great structure sensitivity of the diamagnetism is of particular usefulness for monitoring development

in the highly distorted structures characteristic of the lower temperature deposits. In these carbons x-ray diffraction parameters cannot be measured with high precision until some structural improvement is effected by heat treatment. While susceptibility does stop changing significantly as a function of heat treatment for some graphitizing carbons at the highest temperatures, a useful monotonic increase obtains in all the nongraphitizing carbons studied through treatment at 3000°C. This feature distinguishes nongraphitizing from graphitizing carbons which exhibit $\overline{\chi}$ maxima, coinciding with pronounced decreases in $\overline{d}$, as a signal of incipient layer stacking order. Density was of slightly less general usefulness as a kinetic parameter, but provided valuable supplementary information for most of the carbons studied. For the group of pyrocarbons deposited at 1150°C, the difference in kinetic behavior determined from density data to that obtained from susceptibility results proved to be of special significance.

Effective activation energies for graphitization in the temperature range 1350 to 3000°C were determined by superposition analysis of isothermal density and $\overline{\chi}$ curves. Conclusions drawn from these analyses are the following:

1. At temperatures below 1950°C, the activation energy for structural development in carbons which do not contain large amounts of hydrogen is 175 ± 20 kcal/mole.
2. In carbons which contain large quantities of hydrogen as deposited, the hydrogen is evolved during initial heat

treatments. The hydrogen evolution is not rate limiting for densification, and the effective activation energy determined from density data reflects only processes other than hydrogen evolution. The resulting ΔH is therefore similar to that of carbons which contain little hydrogen. However, initial increases in diamagnetism, which probably involve a transition from a molecular to a solid-state band structure, are sensitively related to both hydrogen evolution and other structural rearrangements. Therefore, the kinetic behavior determined from $\overline{\chi}$ data reflects both processes, and the effective ΔH of about 245 kcal/mole is probably the sum of a C-H bond strength and the energy barrier for the other processes involved.

3. In the temperature range 1950 to 2700°C, the activation energy for development of graphitzing carbons is near 240 kcal/mole and may be single valued.
4. In the 1950 to 2700°C range, the effective ΔH for development of the difficult-to-graphitize carbons studied lies in the range 200 to 280 kcal/mole. The value is not the same for all carbons and is not necessarily single valued for individual specimens over this range.
5. In the one moderately graphitizable carbon analyzed at high temperatures, the single-valued ΔH near 240 kcal observed in the 2100 to 2700°C range appears to extend through 3000°C.

6. For all the difficult-to-graphitize carbons studied, structural development as monitored by density and $\overline{X}$ measurements progresses with an effective ΔH of 330 ± 20 kcal/mole in the temperature range 2700 to 3000°C.

In summary, the graphitization kinetic "signature" of different carbons was found to allow ranking of graphitizabilities based on initial densities and profiles of $\overline{X}$ and $\overline{d}$ change. The variety of initial microstructures and the broad HTT range studied combined to provide experimental information on an unusually broad range of "graphitizing" behaviors. In most cases, activation energies determined were in good agreement with results in the literature. However, the surprisingly high ΔH values observed for the hardest and softest carbons studied were obtained, respectively, in the HTT ranges 1350 to 1650°C and 2700 to 3000°C, above and below the HTT ranges commonly employed. The point to be emphasized is that care must be taken in generalizing conclusions about graphitization details based on any one type of carbon or on results from a narrow HTT range. These above areas and analysis of nongraphitizing or graphitization-resistant carbons at temperatures above 3000°C should be studied further. In particular, the differences in kinetic behavior of graphitizing and nongraphitizing carbons should receive increased attention.

REFERENCES

REFERENCES

1. Hull A. W., Phys. Rev. 10, 661 (1917).
2. Bernal J. D., Proc. Roy. Soc. (London) A106, 749 (1924).
3. Ergun S., Nature Physical Science 241, 65 (1973).
4. Bokros J. C., in Chemistry and Physics of Carbon (P. L. Walker, Jr., ed.) 5, 1–118 (1969).
5. Goeddel W. V., Nucl. Appl. 3, 599 (1967)
6. Dahlberg R. C., Turner R. F, and Goeddel W. V., Nucl. Eng. (December 1969).
7. Bokros J. C., LaGrange L. D., and Schoen F. J., in Engineering in Medicine-Bioceramics (C. W. Hall and S. F. Hulbert, eds.), to be published.
8. Bokros J. C. and Akins R. J., Status Rept. Gulf-EL-A10810 (August 1971).
9. Maire J. and Méring J., in Chemistry and Physics of Carbon (P. L. Walker, Jr., ed.) 7, 125–190 (1970).
10. Pacault A., in Chemistry and Physics of Carbon (P. L. Walker, Jr., ed.) 7, 107–154 (1971).
11. Fischbach D. B., in Chemistry and Physics of Carbon (P. L. Walker, Jr., ed.) 7, 1–105 (1971).
12. Franklin R. E., Proc. Roy. Soc. (London) A209, 196 (1951).
13. Ergun S., in Chemistry and Physics of Carbon (P. L. Walker, Jr., ed.) 3, 211–288 (1968).
14. Ruland W., in Chemistry and Physics of Carbon (P. L. Walker, Jr., ed.) 3, 1–84 (1968).

15. Fitzer E. and Weisenburger S., in Rev. Int. Hautes Temp. et Refract., to be published (1973).

16. Fitzer E. and Weisenburger S., Preprint Carbon '72, Baden-Baden 130 (June 1972).

17. Fitzer E. and Weisenburger S., Eleventh Conf. on Carbon, Abst., 22 (June 1973).

18. Bragg W. H. and Bragg W. L., Proc. Roy. Soc. (London) A89, 277 (1913).

19. Warren B. E., Phys. Rev. 59, 693 (1941).

20. Warren B. E., J. Chem. Phys. 2, 551 (1934).

21. Biscoe J. and Warren B. E., J. Appl. Phys. 13, 364 (1942).

22. Franklin R. E., Acta Cryst. 3, 107 (1950).

23. D. W. Stevens, Gulf General Atomic Rept. No. GA-9728 (September 1969).

24. Rothwell W. S., J. Appl. Phys. 39, 1840 (1968).

25. Fitzer E., Schaefer W., and Yamada S., Carbon 7, 643 (1969).

26. Perret R. and Ruland W., J. Appl. Cryst. 1, 308 (1968).

27. Perret R. and Ruland W., J. Appl. Cryst. 5, 183 (1972).

28. Franklin R. E., Acta Cryst. 4, 253 (1951).

29. Bacon G. E., Acta Cryst. 4, 558 (1951).

30. Houska C. R. and Warren B. E., J. Appl. Phys. 25, 1503 (1954).

31. Warren B. E. and Averbach B. L., J. Appl. Phys. 21, 595 (1950).

32. Warren B. E. and Averbach B. L., J. Appl. Phys. 23, 497 (1952).

33. Warren B. E., Proc. Sec. Conf. on Carbon, Buffalo, 1955, University of Buffalo Press, p. 49 (1956).

34. Guentert O. J., J. Chem. Phys. 37, 884 (1962).

35. Bowman J., Proc. Sec. Conf. on Carbon, Buffalo, 1955, University of Buffalo Press, p. 59 (1956).

36. Bacon G. E., Acta Cryst. 3, 137 (1950).

37. Bacon G. E., Acta Cryst. 7, 359 (1954).

38. Sawyer W. E., U.S. Patent 229, 355 (1880).

39. Brown A.R.G., Hall A. R., and Watt W., Nature 172, 1145 (1953).

40. Brown A.R.G. *et al.*, Brit. J. Appl. Phys. 7, 73 (1956).

41. Brown A.R.G. and Watt W., Ind. Carbon and Graphite, Soc. of Chem. Ind., 86 (1958).

42. Brown A.R.G., Clark D., and Estabrook J., J. Uncommon Metals 1, 94 (1959).

43. Guentert O. J., J. Chem. Phys. 37, 884 (1962).

44. Guentert O. J. and Cvikevich S., Proc. Fifth Conf. on Carbon, Penn. State Univ., 1961, Pergamon Press, 473 (1962).

45. Méring J. and Maire J., J. Chim. Phys. 57, 803 (1960).

46. Ruland W., Acta Cryst. 18, 992 (1965).

47. Ruland W., Carbon 2, 365 (1965).

48. Ruland W., Acta Cryst. 22, 615 (1967).

49. Ruland W., Eighth Conf. on Carbon, Buffalo, Paper No. S159 (June 1967).

50. Perret R. and Ruland W., J. Appl. Cryst. 1, 257 (1968).

51. Krishman K. S., Nature (London) 133, 174 (1934).

52. Ganguli N., Phil. Mag. 21, 355 (1936).

53. Krishnan K. S. and Ganguli N., Nature (London) 139, 155 (1937).

54. Ganguli N. and Krishnan K. S., Proc. Roy. Soc. (London) A177, 168 (1941).

55. Poquet E. *et al.*, J. Chim. Phys. 57, 866 (1960).

56. Soule D. E. and Nezbeda C. W., WADD Tech. Rep. 61-72, Vol. XXXIX (1963).

57. Landau L., Z. Physik. 64, 629 (1930).

58. Peierls R. E., Z. Physik. 80, 763 (1933).

59. Peierls R. W., Quantum Theory of Solids, Oxford University Press, London (1955).

60. Cornuault P. *et al.*, Proc. Third Conf. on Carbon, Buffalo, 1957, Pergamon Press, 627 (1959).

61. Eatherly W. P. and McClelland J. D., Phys. Rev. 89, 661 (1953).

62. Miura M., Sci. Repts., Tohoku Univ. 23, 242 (1934).

63. Takahashi H., Kuroda H., and Akamatu H., Carbon 2, 432 (1965).

64. Pinnick H. T., Phys. Rev. 94, 319 (1954).

65. London F., J. Phys. et Radium 8, 397 (1937).

66. Brooks H., J. Chem. Phys. 8, 939 (1940).

67. Lonsdale K., Proc. Roy. Soc. (London) 159, 149 (1937).

68. Mrozowski S., Phys. Rev. 85, 609 (1952).

69. Mrozowski S., Phys. Rev. 86, 1056 (1952).

70. Dorfman Y. S., Diamagnetism and the Chemical Bond, American Elsevier Publishing Co., Inc., New York (1961).

71. Kiive P. and Mrozowski S., Proc. Third Conf. on Carbon, Buffalo, 1957, Pergamon Press, 165 (1959).

72. Pinnick H. T. and Kiive P., Phys. Rev. 102, 58 (1956).

73. Honda H., Proc. Third Conf. on Carbon, Buffalo, 1957, Pergamon Press, 159 (1959).

74. Adamson A. F. and Blayden H. E., Proc. Third Conf. on Carbon, Buffalo, 1957, Pergamon Press, 147 (1959).

75. Pacault A. and Marchand A., Proc. Third Conf. on Carbon, Buffalo, 1957, Pergamon Press, 37 (1959).

76. Marchand A. and Lumbroso N., Proc. Fourth Conf. on Carbon, Buffalo, 1959, Pergamon Press, 189 (1960).

77. McClure J. W., J. Chim. Phys. 57, 859 (1960).

78. McClure J. W., Phys. Rev. 104, 666 (1956).

79. Wallace P. R., Phys. Rev. 71, 622 (1947).

80. Haering R. R. and Wallace P. R., J. Phys. Chem. Solids 3, 253 (1957).

81. McClure J. W., Phys. Rev. 119, 606 (1960).

82. Fischbach D. B., Phys. Rev. 123, 1613 (1961).

83. Fischbach D. B., Proc. Fifth Conf. on Carbon, Penn. State Univ., 1962, Pergamon Press, Vol. 2, 27 (1963).

84. Fischbach D. B., Jet Propulsion Laboratory Tech. Rept. 32-1208 (December 1967).

85. Wagoner G. and Eckstein B. H., WADD-TR-61-72, Vol. XX (1963).

86. Chang J. Y., USAEC Report ORNL-3764 (March 1965).

87. Fischbach D. B., Jet Propulsion Laboratory Tech. Rept. 32-532 (1966).

88. Poquet E., J. Chim. Phys. 60, 566 (1963).

89. Fischbach D. B., Carbon 5, 565 (1967).

90. Fair F. V. and Collins F. M., Proc. Fifth Conf. on Carbon, Penn. State Univ., 1962, Pergamon Press, Vol. 1, 503 (1963).

91. Mizushima S., Proc. Fifth Conf. on Carbon, Penn. State Univ., 1962, Pergamon Press, Vol. 2, 439 (1963).

92. Fischbach D. B., Nature 200, 1281 (1963); JPL-TR-32-570.

93. Fischbach D. B., Appl. Phys. Letters 3, 168 (1963).

94. Fischbach D. B., Symp. on Carbon, Tokyo, Paper Nos. III-23, -23 (July 1964).

95. Pacault A., Marchand A., and Gasparoux H., Symp. on Carbon, Tokyo, Paper No. III-16 (July 1964).

96. Pacault A., Marchand A., Gasparoux H., and Flandrois S., Seventh Conf. on Carbon, Cleveland, Paper No. 125 (June 1965).

97. Pacault A., Marchand A. Gasparoux H., and Flandrois S., Compt. Rend. 260C, 4999 (1965).

98. Pacault A., Nobel Symp. 5: Fast Reactions and Primary Processes in Chemical Kinetics, Interscience, New York (1968).

99. Marchand A. and Amiell J., Carbon 8, 707 (1970).

100. Noda T., Carbon 6, 125 (1968).

101. Noda T., J. Chim. Phys. (Special Issue April) 151 (1969).

102. Murty H. N., Biederman D. L., and Heintz E. A., Carbon 7, 667 (1969).

103. Murty H. N., Biederman D. L., and Heintz E. A., Carbon 7, 683 (1969).

104. Fischbach D. B., J. Chim. Phys. (Special Issue) 121 (1969).

105. Kitchener J. A., Ion Exchange Resins, Wiley, New York (1967).

106. Bokros J. C., Nature 202, 1004 (1964).

107. Bokros J. C., Carbon 3, 167 (1965).

108. Bacon G. E., J. Appl. Chem. 6, 477 (1956).

109. Price R. J., Bokros J. C., Koyama K., and Chin J., Carbon 4, 263 (1966).

110. Bokros J. C. and Price R. J., Carbon 3, 503 (1966).

111. Wood W. D., Deem H. W., and Goldthwaite W. H., USAEC Rept. BMI-1739 (August 1965).

112. Bokros J. C., Price R. J., and Koyama K., Carbon 4, 293 (1966).

113. Bokros J. C. and Price R. J., Carbon 4, 441 (1966).

114. Bokros J. C., Dunlap R. W., and Schwartz A. S., Carbon 7, 143 (1969).

115. Stevens D. W., Tenth Conf. on Carbon, Lehigh Univ., Paper No. SS-74 (1971).

116. Stevens D. W., Carbon, to be published.

117. Beatty R. L., USAEC Rept. ORNL-TM-1649 (January 1967).

118. Beatty R. L., Carlsen F. L., Jr., and Cook J. L., Nucl. Appl. 1, 560 (1965).

119. Beatty R. L., Scott J. L., and Kiplinger D. V., USAEC Rept. ORNL-4531 (April 1970).

120. Soule D. E., Nezbeda C. W., and Czandrea A. W., Rev. Sci. Inst. 35, 1504 (1964).

121. Selwood P. W., Magneto-Chemistry, 2nd Ed., Interscience, New York, 11ff (1956).

122. Scott C. B., Thesis, University of Washington (1971).

123. Davy N., Phil. Mag. 33, 575 (1942).

124. Donoghue J. J., Phys. Rev. 81, 663 (1951).

125. Bates L. F., Modern Magnetism, Cambridge University Press (1961).

126. Oster G. and Yamamoto M., Chem. Rev. 63, 257 (1963).

127. Canada D. C. and Laing W. R., Anal. Chem. 39, 691 (1967).

128. Engle G. B., Norris W. H., and Bailey L., Carbon 8, 393 (1970).

129. Jones J. M., J. Sci. Instr. 38, 367 (1961).

130. Klug H. P. and Alexander L. E., X-Ray Diffraction Procedures, Wiley, New York (1954).

131. Tassone G., Carbon 8, 387 (1970).

132. Ergun S. and Schehl R. R., Tenth Conf. on Carbon, Lehigh Univ., Paper No. SS-77 (1971).

133. DuBose C.K.H. and Gray R. J., USAEC Rept. ORNL-TM-521 (June 1963).

134. McClung R. W., USAEC Rept. ORNL-3511 (October 1961).

135. Koizlik K., Schulze H. A., Gruebmeier H. B., and Scheidler G. P., KFA Rept. Jül-589-RW (April 1969).

136. Koizlik K., KFA Rept. Jül-868-RW (June 1972).

137. Koss P. and Wallish K., Carbon '72 Conf., Preprints, Baden-Baden, 256 (June 1972).

138. Stevens D. W., Eleventh Conf. on Carbon, Abst., 165 (June 1973).

139. Stevens D. W., Eleventh Conf. on Carbon, Abst., 167 (June 1973).

140. Koizlik K. and Koss P., Eleventh Conf. on Carbon, Abst., 169 (June 1973).

141. Stevens D. W., Gulf General Atomic Rept. GA-10448 (June 1971), to be published in Carbon.

142. Lefevre R.L.R., Praizey J. P., Price M.S.T., and Thomas J. P., Carbon '72 Conf., Preprints, Baden-Baden, 139 (June 1972).

143. Oxley J. H. *et al.*, Jour. A.I.Ch.E. 7, 498 (1961).

144. Blackman L. C., Saunders G., and Ubbelohde A. R., Proc. Roy. Soc. (London) A264, 19 (1961).

145. Honda H., Kobayashi K., and Sugawara S., Carbon 6, 517 (1968).

146. Maahs H. G., Carbon 7, 509 (1969).

147. Fischbach D. B., Carbon 9, 193 (1971).

148. Flandrois S., Thesis, University of Bordeaux (1967).

149. Gasparoux H., Thesis, University of Bordeaux (1965).

150. Pacault A. and Gasparoux H., Compt. Rend. 264C, 1160 (1967).

151. Grisdale R. O., Pfister A. C., and Roosbroeck van W., Bell System Tech. J. 30, 271 (1951).

152. Grisdale R. O., J. Appl. Phys. 24, 1082 (1953).

153. Johnson G.R.L. and Anderson R. C., Proc. Fifth Conf. on Carbon, Penn. State Univ., 1961, Pergamon Press, Vol. 1, 395 (1962).

154. Hirai T. and Yajima S., J. Mat. Sci. 2, 18 (1967).

155. Bokros J. C., Carbon 3, 201 (1965).

156. Palmer H. B. and Cullis, C. F., in Chemistry and Physics of Carbon (P. L. Walker, Jr., ed.), Vol. 2, 265–325, Dekker (1966).

157. Steigler J. O., DuBose C.K.H., and Cook J. L., Seventh Conf. on Carbon, Cleveland, 1965; Abst. in Carbon 3, 339 (1965).

158. Stover E. R., General Electric Research Laboratories Rept. TR-62-RL-2991M, Schenectady, New York (May 1962).

159. Carlsen F. L., Jr., USAEC Rept. ORNL-TM-1080 (June 1965).

160. Kotlensky W. V. and Martens H. E., Jet Propulsion Laboratory Rept. 32-71 (March 1961).

161. Pacault A., Flandrois S., and Marchand A., Carbon 9, 87 (1971).

162. Kipling J. J. and Shooter P. V., Carbon 4, 1 (1966).

163. Beatty R. L. and Fischbach D. B., Carbon '72 Conf., Preprints, Baden-Baden, 127 (June 1972).

164. Beatty R. L. and Fischbach D. B., Eleventh Conf. on Carbon, Abst., 30 (June 1973).

165. Cottrell T. L., The Strength of Chemical Bonds, Butterworths Science Publishers, London (1958).

166. Price R. J. and Bokros J. C., Carbon 9, 205 (1971).

167. Kanter M. A., Phys. Rev. 107, 655 (1957).

168. Coulson C. A. *et al.*, Proc. Roy. Soc. (London) A274, 461 (1963).

169. Hennig G. R., J. Appl. Phys. 36, 1482 (1965).

170. Henson R. H. and Reynolds W. N., Carbon 3, 277 (1965).

171. Koizlik K., Krautwasser P., and Nickel H., Eleventh Conf. on Carbon, Abst., 247 (June 1973).

172. Kaae J. L., Gulden T. D., and Laing S., Carbon 10, 701 (1972).

APPENDIX I

Force Constant (dH_z^2/dx) Determined from Magnetic Susceptibility Standards

Standard	M (g)	χ (10^{-6} emu/g)	Average ΔW (g)	dH_z^2/dx (G^2/cm)
Pd (wire)	0.1016	+5.23[a]	$+6.09 \times 10^{-3}$	2.25×10^7
Sugar (granulated cane)	0.2077	−0.553[b]	-1.32×10^{-3}	2.25×10^7
Water (distilled)	0.2781	−0.720[c]	-2.30×10^{-3}	2.25×10^7

[a]Hoare F. E. and Walling J. C., Proc. Phys. Soc. B64, 337 (1951).

[b]Woernley D. W., J. Biol. Chem. 207, 717 (1954).

[c]Piccard and Devaud, Arch. Sci. Phys. Nat. 2, 455 (1920).

APPENDIX II

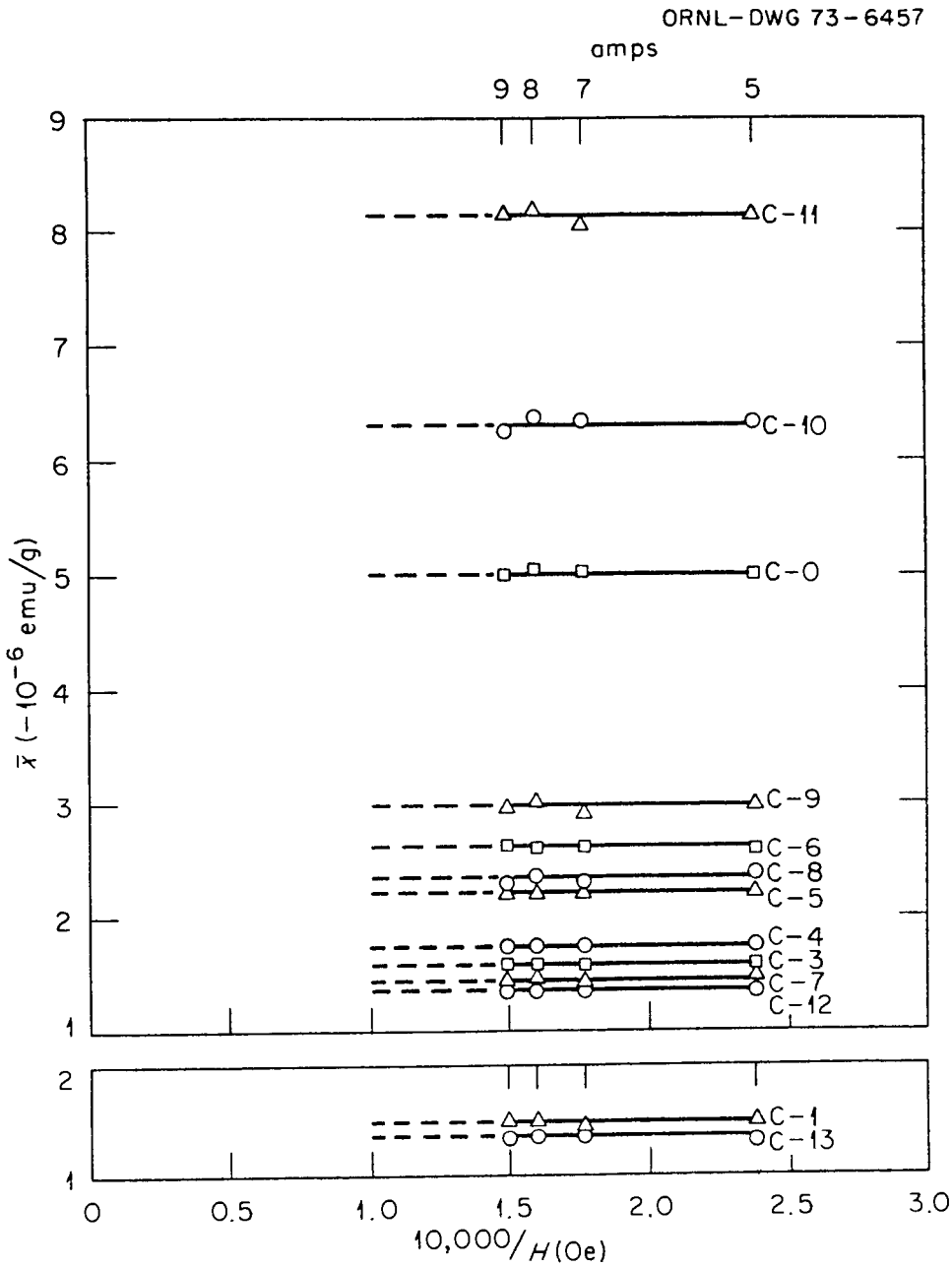

Fig. II-1. Honda-Owen Plots for Experimental Carbons.

APPENDIX III

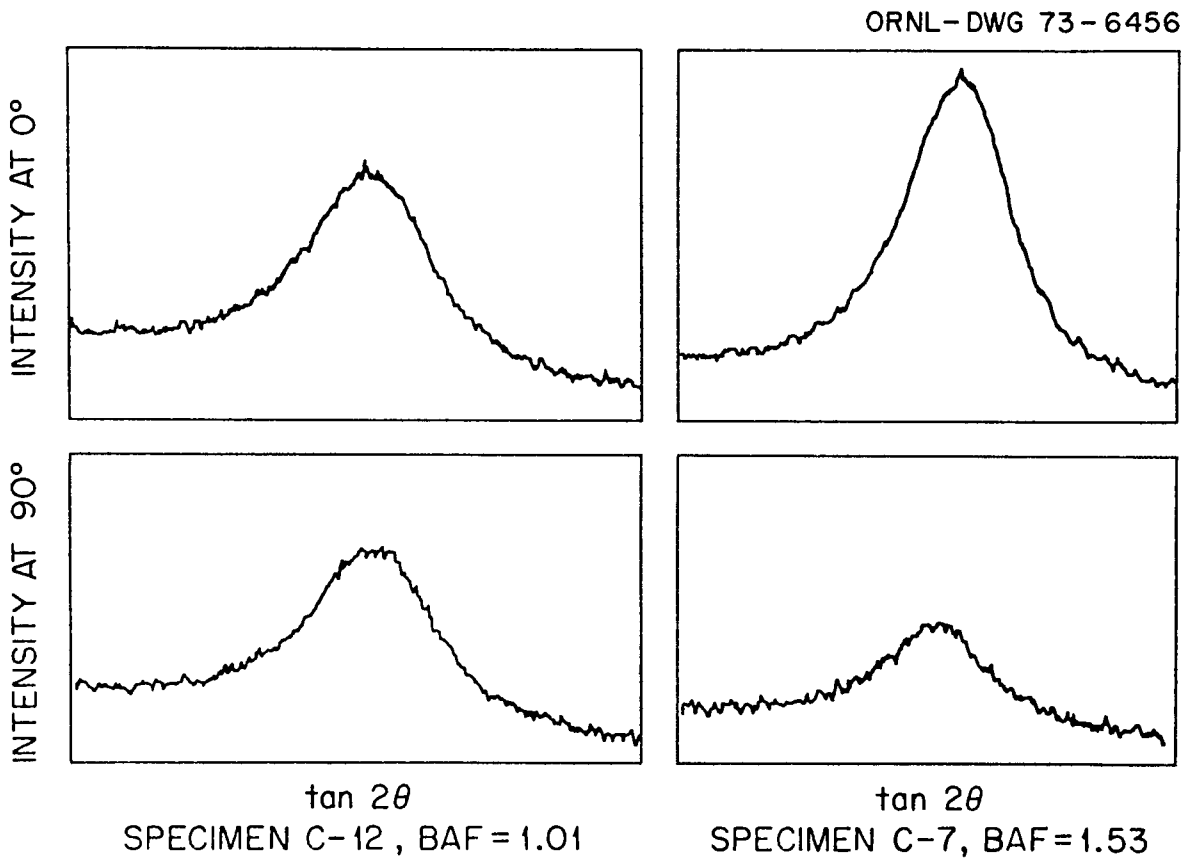

Fig. III-1. Microdensitometer Tracings of BAF Films at 0 and 90° for an Isotropic Carbon and Anisotropic Carbon.

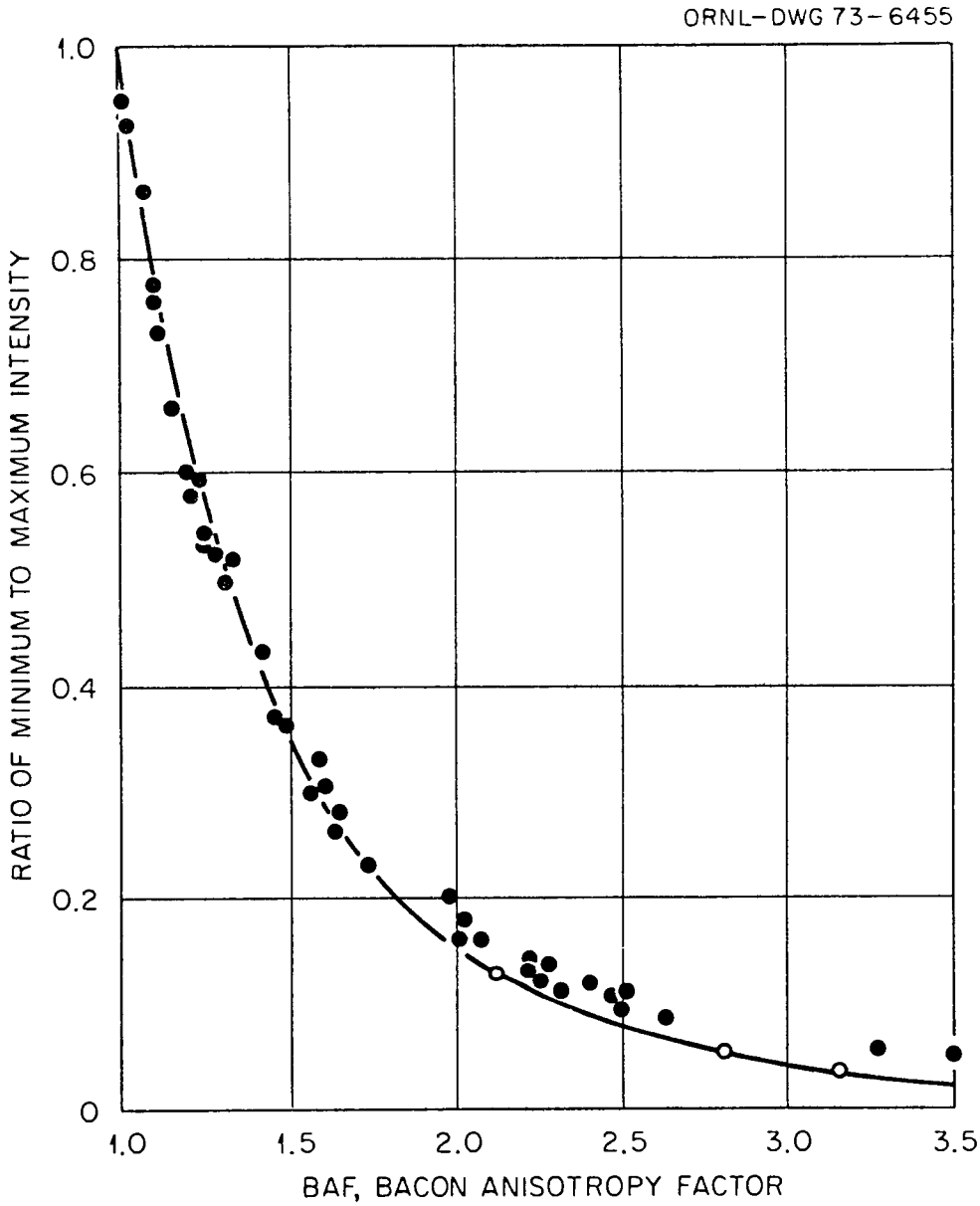

Fig. III-2. Curve for BAF Determination from Ratio of Minimum to Maximum Intensity (Reproduced from Ref. 132).

Specimen	BAF		
	Outer[a]	Inner[b]	Average
C-12	1.03	1.02[R]	1.01
C-13	1.04	1.00	1.02
C-7	1.47	1.57	1.53
C-1	1.03	1.04	1.03
C-3	1.08	1.03	1.06
C-4	1.10	1.19	1.14
C-8	1.63	1.60	1.62
C-5	1.14	1.09	1.12
C-6	1.18	1.14	1.16
C-9	1.04	1.03	1.04
C-10	1.03[R]	1.01	1.00
C-11	1.28	1.19	1.24

[a]X-rayed with outer surface to beam.

[b]X-rayed with inner (substrate) side to beam.

[R]Ratio inverted from usual with I(90°) > I(0°).

APPENDIX IV

Density Standards for Gradient Column

Density, g/cm^3	
Specified	Recalibrated
1.3011	a
1.4051	1.4059
1.4984	1.4991
1.5955	1.5969
1.7019	1.7037
1.7955	1.7907
1.8014	1.7995
1.8983	1.8979
1.9902	1.9826
2.1012	2.1017
2.2015	2.1980
2.3063	a

[a]Not measured.

APPENDIX V

Tabulation of Density, Magnetic Susceptibility ($\overline{X}$), and X-Ray Diffraction ($\overline{d}$ and L_a) Data

Density Data

HTT (°C):	1350	1500	1650	1800	1950	2100	2250	2400	2550	2700	2850	3000
HTt (min)	Density, g/cm^3											
						C-12						
2	2.026	2.041	2.042	2.039	2.074	2.054	2.058	2.108	2.108	2.105	2.101	2.101
6						2.071					2.102	2.105
18	2.035	2.051	2.050	2.060	2.072	2.065	2.079	2.094	2.111	2.110	2.103	2.081
54				2.077		2.079		2.112			2.099	
162	2.045	2.060	2.060	2.082	2.094	2.082	2.091	2.113	2.112	2.108		
486	2.050											
						C-13						
2	2.062	2.081	2.089	2.104	2.108	2.115	2.108	2.137	2.139	2.136	2.133	2.132
6						2.111					2.132	2.129
18	2.074	2.091	2.098	2.100	2.097	2.110	2.125	2.137	2.139	2.137	2.135	2.112
54				2.117		2.121		2.141			2.134	
162	2.079	2.096	2.104	2.120	2.128	2.125	2.128	2.141	2.140	2.136		
486	2.082											
						C-7						
2	2.082	2.098	2.111	2.123	2.128	2.131	2.145	2.161	2.167	2.171	2.169	2.170
6											2.170	2.143
18	2.092	2.110	2.117	2.133	2.137	2.141	2.158	2.165	2.168	2.172	2.171	2.172
54				2.133		2.149		2.171			2.171	
162	2.097	2.113	2.128	2.123	2.145	2.155	2.165	2.178	2.173	2.172		
486	2.098			2.141								

Density Data

HTT (°C):	1350	1500	1650	1800	1950	2100	2250	2400	2550	2700	2850	3000
HTt (min)	Density, g/cm³											
						C-1						
2	1.963	1.969	1.972	1.990	1.992	2.000	2.005	2.007	2.012	2.019	2.022	2.027
6											2.026	2.028
18	1.969	1.978	1.986	1.992	1.997	2.002	2.008	2.013	2.019	2.023	2.028	2.030
54				1.996				2.015				
162	1.973	1.983	1.994	1.998	2.004	2.008	2.014	2.018	2.023	2.028		
486	1.974				2.006							
						C-3						
2	1.890	1.894	1.900	1.902	1.908	1.912	1.914	1.925	1.936	1.949	1.965	1.990
6											1.979	1.996
18	1.892	1.898	1.902	1.906	1.909	1.913	1.921	1.935	1.952	1.969	1.990	2.001
54			1.902	1.906		1.917		1.943			1.998	
162	1.894	1.902	1.903	1.909	1.914	1.920	1.934	1.947	1.969	1.986		
486	1.893											
						C-4						
2		1.709	1.713	1.714	1.717	1.721	1.732	1.748	1.778	1.810	1.852	1.919
6											1.889	1.930
18		1.710	1.713	1.717	1.722	1.729	1.745	1.770	1.809	1.859	1.919	1.944
54				1.719		1.738		1.791			1.934	
162		1.714	1.718	1.717	1.727	1.746	1.774	1.804	1.857	1.909		
486				1.726								

Density Data

HTT (°C):	1350	1500	1650	1800	1950	2100	2250	2400	2550	2700	2850	3000
HTt (min)						Density, g/cm³						
						C-8						
2			1.425	1.420	1.434	1.442	1.457	1.473	1.499	1.532	1.577	1.663
6											1.629	1.711
18			1.426	1.433	1.440	1.451	1.472	1.500	1.537	1.588	1.665	1.761
54			1.428	1.435		1.460		1.513			1.706	
162			1.431	1.440	1.451	1.470	1.495	1.529	1.581	1.646		
						C-6						
2		1.407	1.408	1.410	1.416	1.423	1.435	1.451	1.467	1.484	1.510	1.546
6											1.529	1.560
18		1.407	1.411	1.416	1.425	1.434	1.448	1.466	1.485	1.510	1.545	1.585
54		1.407		1.418		1.440		1.475			1.563	
162		1.410	1.415	1.422	1.433	1.446	1.465	1.483	1.508	1.537		
						C-5						
2		1.573	1.575	1.577	1.579	1.582	1.593	1.605	1.620	1.638	1.661	1.692
6											1.676	1.712
18		1.575	1.577	1.579	1.584	1.591	1.603	1.617	1.635	1.658	1.693	1.737
54				1.581		1.594		1.625			1.713	
162		1.576	1.579	1.582	1.589	1.599	1.616	1.634	1.655	1.685		

Density Data

HTT (°C):	1350	1500	1650	1800	1950	2100	2250	2400	2550	2700	2850	3000
HTt (min)						Density, g/cm³						
						C-9						
2			1.468	1.471	1.475	1.482	1.491	1.502	1.515	1.534	1.546	1.573
6											1.559	1.580
18			1.470	1.474	1.479	1.486	1.497	1.511	1.527	1.548	1.572	1.590
54						1.491		1.419			1.579	
162			1.472	1.474	1.487	1.497	1.516	1.522	1.544	1.568		
						C-11						
2						2.099	2.100	2.102	2.104	2.107		
6												
18						2.098	2.101	2.102	2.106	2.112	2.114	2.118
54						2.101		2.104				
162						2.100	2.102	2.105		2.112		
						C-10						
2						1.691	1.712	1.709	1.710	1.716	1.718	1.721
6												
18						1.695	1.705	1.712	1.719	1.720	1.722	1.724
54						1.693		1.709				
162						1.698	1.707	1.721	1.721	1.722		

Diamagnetic Susceptibility Data

HTT (°C):	1350	1500	1650	1800	1950	2100	2250	2400	2550	2700	2850	3000
HTt (min)						$\overline{\chi}$ (-10^{-6} emu/g)						
						C-12						
2	1.72	2.21	2.77	3.41	4.14	5.38	6.72	7.30	6.93	6.63	6.66	6.63
6	1.83	2.31	2.89	3.57	4.45	5.83	7.16	7.06	6.81	6.66	6.67	6.69
18	1.96	2.39	3.02	3.91	4.86	6.32	7.30	6.86	6.69	6.67	6.68	6.70
54	2.01	2.49	3.23	4.17	5.32	6.79	7.15	6.79	6.67	6.64	6.72	
162	2.07	2.64	3.50	4.43	5.79	7.14	6.95	6.73	6.64	6.66		
486	2.10	2.75	3.71	4.94	6.28							
						C-13						
2	1.65	2.17	2.69	3.34	4.05	5.27	6.72	7.26	6.99	6.71	6.70	6.66
6	1.74	2.26	2.84	3.53	4.44	5.83	7.09	7.12	6.89	6.76	6.73	6.72
18	1.85	2.32	2.99	3.84	4.84	6.32	7.31	6.93	6.77	6.72	6.68	6.75
54	1.91	2.44	3.18	4.13	5.33	6.76	7.19	6.85	6.76	6.59	6.69	
162	1.98	2.59	3.43	4.46	5.76	7.09	7.05	6.81	6.72			
486	2.07	2.72	3.64	4.89	6.26							
						C-7						
2	1.53	2.06	2.69	3.29	4.02	5.25	6.58	7.28	7.05	6.78	6.77	6.79
6	1.69	2.18	2.83	3.54	4.44	5.82	7.03	7.22	7.00	6.82	6.76	6.74
18	1.79	2.29	2.99	3.85	4.87	6.30	7.20	6.96	6.80	6.75	6.74	6.76
54	1.86	2.38	3.15	4.10	5.22	6.80	7.11	6.90	6.86	6.78	6.69	
162	1.93	2.51	3.39	4.38	5.78	7.07	6.99	6.85	6.84	6.77		
486	2.01	2.65	3.66	4.82	6.19							

Diamagnetic Susceptibility Data

HTT (°C):	1350	1500	1650	1800	1950	2100	2550	2400	2550	2700	2850	3000
HTt (min)					$\bar{\chi}$ (-10^{-6} emu/g)							
						C-1						
2	1.56	1.89	2.35	2.87	3.46	4.41	5.47	6.27	6.81	6.88	6.95	6.94
6	1.64	1.98	2.49	3.03	3.74	4.76	5.84	6.51	6.87	6.90	6.92	6.93
18	1.74	2.10	2.60	3.33	4.07	5.15	6.20	6.75	6.90	6.94	6.93	6.85
54	1.79	2.20	2.82	3.54	4.42	5.61	6.56	6.81	6.95	6.95	6.91	
162	1.84	2.32	3.02	3.84	4.83	6.03	6.75	6.87	6.94	6.91		
486	1.97	2.43	3.21	4.25	5.29							
						C-3						
2	1.63	1.91	2.35	2.81	3.31	4.15	5.03	5.75	6.44	6.79	7.13	7.17
6	1.66	2.01	2.46	2.96	3.52	4.39	5.27	6.02	6.70	7.04	7.12	7.12
18	1.76	2.10	2.57	3.19	3.80	4.72	5.60	6.32	6.84	7.08	7.16	7.08
54	1.81	2.18	2.75	3.35	4.10	5.12	6.04	6.57	7.00	7.15	7.18	
162	1.90	2.34	2.92	3.61	4.49	5.39	6.33	6.80	7.06	7.14		
486	1.95	2.44	3.12	3.97	4.82							
						C-4						
2	1.77	1.89	2.30	2.65	3.13	3.76	4.39	4.90	5.77	6.33	6.86	7.17
6	1.78	1.98	2.38	2.80	3.28	3.92	4.61	5.25	6.05	6.52	7.09	7.20
18	1.81	2.10	2.47	2.98	3.50	4.18	4.85	5.59	6.31	6.82	7.20	7.20
54	1.84	2.17	2.61	3.15	3.70	4.38	5.18	5.92	6.58	6.99	7.22	
162	1.89	2.27	2.83	3.34	3.95	4.72	5.51	6.20	6.80	7.07		
486	2.03	2.38	2.95	3.55	4.19							

Diamagnetic Susceptibility Data

HTT (°C):	1350	1500	1650	1800	1950	2100	2250	2400	2550	2700	2850	3000
HTt (min)						$\bar{x}$ (-10^{-6} emu/g)						
						C-8						
2			2.53	2.74	3.19	3.57	4.00	4.37	4.81	5.25	5.76	6.50
6			2.58	2.88	3.34	3.74	4.12	4.55	5.03	5.58	6.27	6.65
18			2.68	3.02	3.43	3.85	4.29	4.82	5.28	5.85	6.49	6.78
54			2.79	3.18	3.50	4.01	4.43	4.93	5.53	6.06	6.57	
162			2.88	3.25	3.67	4.13	4.72	5.16	5.78	6.32		
						C-5						
2		2.22	2.49	2.79	3.24	3.69	4.20	4.66	5.05	5.47	5.95	6.49
6		2.31	2.61	2.93	3.39	3.88	4.41	4.79	5.30	5.64	6.18	6.62
18		2.40	2.77	3.09	3.56	4.00	4.59	5.04	5.45	5.93	6.41	6.73
54		2.47	2.85	3.21	3.71	4.28	4.79	5.23	5.71	6.08	6.59	
162		2.52	2.96	3.35	3.87	4.43	4.91	5.39	5.88	6.25		
486		2.60										
						C-6						
2		2.58	2.80	3.02	3.39	3.88	4.20	4.57	4.99	5.25	5.59	6.10
6		2.62	2.87	3.16	3.55	3.95	4.37	4.74	5.09	5.50	5.87	6.22
18		2.67	2.98	3.34	3.71	4.12	4.50	4.88	5.29	5.62	6.12	6.41
54		2.75	3.10	3.42	3.88	4.26	4.69	5.05	5.47	5.72	6.21	
162		2.82	3.17	3.48	3.94	4.39	4.89	5.18	5.62	5.97		
486		2.89	3.27	3.70	4.10							

Diamagnetic Susceptibility Data

HTT (°C):	1350	1500	1650	1800	1950	2100	2250	2400	2550	2700	2850	3000
HTt (min)					$\overline{X}$	(-10^{-6} emu/g)						
						C-9						
2			3.05	3.26	3.65	4.17	4.67	5.17	5.55	5.84	6.16	6.61
6			3.11	3.44	3.88	4.39	4.83	5.27	5.71	6.10	6.41	6.68
18			3.18	3.58	4.02	4.64	5.05	5.53	5.96	6.20	6.59	6.77
54			3.35	3.74	4.25	4.82	5.29	5.71	6.04	6.34	6.70	
162			3.48	3.88	4.44	5.01	5.52	5.85	6.20	6.43		
486			3.58	4.14	4.64							
						C-10						
2						6.54	6.91	7.08	7.41	7.47	7.61	7.78
6						6.61	6.96	7.23	7.49	7.52	7.65	7.83
18						6.88	7.15	7.32	7.49	7.63	7.75	7.85
54						6.94	7.23	7.38	7.59	7.65	7.78	
162						7.00	7.30	7.45	7.64	7.75		
						C-11						
2						8.30	8.46	8.58	8.53	8.10	7.69	7.35
6						8.27	8.52	8.54	8.42	7.97	7.47	7.27
18						8.35	8.64	8.47	8.09	7.58	7.30	7.13
54						8.52	8.51	8.31	7.91	7.44	7.20	
162						8.54	8.45	8.10	7.74	7.33		

X-Ray Diffraction Data

HTT (°C):	1500	1800	2100	2400	2700	3000	1500	1800	2100	2400	2700	3000
Specimen			$\bar{d}$ (Å)						L_a (Å)			
C-12	3.44	3.43	3.42	3.40	3.39	3.38	48	62	82	a		
C-13	3.44	3.43	3.41	3.39	3.38	3.38	48	62	75	a		
C-7	3.43	3.42	3.41	3.39	3.38	3.38	47	64	72	a		
C-1	3.45	3.44	3.43	3.41	3.40	3.39	43	58	69	69[a]		
C-3	3.45	3.44	3.43	3.41	3.40	3.39	43	58	65	69	62[a]	
C-4	3.45	3.45	3.44	3.43	3.42	3.40	41	54	62	69	72	a
C-8		3.45	3.44	3.43	3.42	3.39		53	58	59	66	66[a]
C-6	3.45	3.45	3.44	3.43	3.42	3.41	47	60	65	64	64	64
C-5	3.45	3.44	3.43	3.42	3.41	3.40	45	54	58	64	64	65
C-9		3.43	3.42	3.42	3.41	3.40		56	60	64	66	72
C-11			3.41	3.39	3.38	3.38			96	a		
C-10			3.42	3.42	3.42	3.42			82	87	87	87

[a]Incipient splitting of (10) profile.

INTERNAL DISTRIBUTION

(3) Central Research Library
ORNL – Y-12 Technical Library
Document Reference Section
(10) Laboratory Records Department
Laboratory Records, ORNL RC
ORNL Patent Office
G. M. Adamson, Jr.
(10) R. L. Beatty
E. S. Bomar
R. A. Bradley
A. J. Caputo
J. H. Coobs
W. H. Cook
D. Costanzo
J. E. Cunningham
W. P. Eatherly
R. B. Evans III
J. S. Faulkner
J. I. Federer
R. L. Hamner
(3) M. R. Hill
F. J. Homan
O. J. Horne
J. D. Jenkins
D. R. Johnson
M. J. Kania
(38) P. R. Kasten
C. R. Kennedy
W. J. Lackey
T. B. Lindemer
E. L. Long, Jr.
A. L. Lotts
A. P. Malinauskas
G. B. Marrow (Y-12)
M. T. Morgan
K. J. Notz
A. R. Olsen
W. H. Pechin
C. B. Pollock (Y-12)
J M Robbins
J. L. Scott
J. D. Sease
D. P. Stinton
V. J. Tennery
K. H. Valentine
G. W. Weber
T. N. Washburn
J. R. Weir, Jr.
C. S. Yust
Advisory Committee:
W. C. Leslie (consultant)
John Moteff (consultant)
Hayne Palmour III (consultant)
J. W. Prados (consultant)
N. E. Promisel (consultant)
G. V. Smith (consultant)
D. F. Stein (consultant)

EXTERNAL DISTRIBUTION

Fiber Materials, Inc., Biddeford, ME 04005

J. L. Cook

General Atomic Company, P.O. Box 81608, San Diego, CA 92138

J. C. Bokros
T. D. Gulden
J. L. Kaae
C. B. Scott
D. W. Stevens

Los Alamos Scientific Laboratory, Los Alamos, NM 87544

R. J. Bard
P. Wagner

Sandia Laboratories, Albuquerque, NM 87115

B. Granoff

Super-Temp Company, Sante Fe Springs, CA 90670

W. V. Kotlensky

University of Washington, Dept. of Mining, Metallurgical, and Ceramic Engineering, Seattle, WA 98105

(5) D. B. Fischbach
J. I. Mueller

U.S. Energy Research and Development Administration, Washington, DC 20545

N. Haberman, RRD-GF
Kermit Laughon, RRD-GA
W. S. Schieb, RRD-GP
E. A. Womack, RRD-G

USERDA, Oak Ridge Operations Office, P.O. Box E, Oak Ridge, TN 37830

R. L. Egli
Research and Technical Support Division

USERDA Technical Information Center, Office of Information Services, P.O. Box 62, Oak Ridge, TN 37830

(2) Manager

☆U. S. GOVERNMENT PRINTING OFFICE: 1975-748-189/23